CROSS β STRUCTURE IN FIBRILS OF

FEATHER KERATIN AND OF INSULIN

by

Michael John Burke

A Dissertation Submitted to the

Graduate Faculty in Partial Fulfillment of

The Requirements for the Degree of

DOCTOR OF PHILOSOPHY

Major Subject: Biophysics

Approved:

In Charge of Major Work

Head of Major Department

Dean of Graduate College

Iowa State University
Ames, Iowa

1969

TABLE OF CONTENTS

INTRODUCTION

Among the extended or β configurations of fibrous proteins and poly-
peptides, one may distinguish between parallel and antiparallel β struc-
ture, depending upon whether the adjacent polar chains are oriented in
the same or opposite direction, and between the normal and cross-β struc-
ture, depending upon whether the chains are oriented parallel or perpen-
dicular to the long axis of the fiber. The principal concern of this
thesis is with the formation and characterization of cross-β structures
of parallel or antiparallel habit.

The cross-β structure naturally occurs in the silk of green lace-
wing fly, Chrysopa flava (Parker and Rudall 1957, Geddes et al. 1968)
and possibly also in bacterial flagella (Astbury et al. 1955). It is gen-
erally found in fibrillar structures and consists of a parallel or anti-
parallel β structure having protein chains oriented perpendicular to the
long axis of the fibrils which compose the fibrillar structure. Although
this structure is somewhat rare in nature, it is quite common in denatured
proteins and many polypeptides when shear stress by extrusion or stretching
is applied. Astbury et al. (1935) first found it in the proteins of poached
and stretched egg-albumin. It is also found in casein, hemoglobulin, zein,
edestin (Senti et al. 1943) and insulin fibrils (Rudall 1950, Ambrose and
Elliott 1951). Normal β structure proteins occur when a similar treatment
is applied to ovalbumin (Senti et al. 1943, Palmer and Galvin 1943),
β-lactoglobulin (Senti et al. 1943), myosin (Astbury and Dickinson 1935),
edestin (Astbury et al. 1935) and arachin (Astbury 1945).

The original interest in β structure protein fibrils was generated

by the textile industry but with the advent of commerically available synthetic polypeptides like nylon and other synthetic polymers this interest abated. The only successful fabric to come out of this research was Ardil from the peanut globulin, arachin (Astbury 1945). Interest in cross-β structure insulin fibrils remained because of insulin's physiological and medical importance. The most significant finding involving insulin fibrils was that the process generating them could be reversed by moderate variation of pH, and biologically active crystalline insulin could be obtained (Waugh 1957).

The cross-β structure in polypeptides is discussed in some detail by Bradbury et al. (1960). In general, they found that polypeptides of low molecular weight, when stretched, formed cross-β structures. Polypeptides working best had a degree of polymerization of approximately 20 residues per molecule.

The purpose of this study was to determine in detail the structure of two fibrillar structures which are generated from two distinctly different proteins, insulin and soluble feather keratin. Fibrillar insulin was known to contain significant amounts of cross-β structure. The structure of feather keratin fibrils was unknown. It was thought that if these two distinctly different proteins could generate similar fibrillar structures, this process might be generalized to many other dissimilar proteins. The biological and physiological implications arising from a large number of proteins capable of reversibly forming fibrils in environments similar to those in the cell are unlimited.

The chemical and physical properties of fibrillar feather keratin

and fibrillar insulin will be discussed later. First it will be necessary
to describe in some detail the infrared and ultraviolet optical properties
of the peptide group for they were used extensively in this study.

Infrared absorption spectroscopy is one of the more useful diagnostic
tools for the elucidation of the secondary structure of proteins and poly-
peptides. The most sensitive absorption band for this purpose appears to
be the amide I band of the peptide group. The position and shape of this
band is significantly different in the α-helix, β structure and random
coil conformations and is useful to detect their presence (Bamford et al.
1956)(Table 1). Miyazawa (1960) predicted that the parallel and antiparal-
lel β structures could also be distinguished using this method. He pro-
posed that the weak band observed at 1690 cm^{-1} in the antiparallel β
structures of silk and polyglycine I was a component of the amide I band.
He treated this predicted splitting of the amide I band as arising from
first order perturbations in a weakly coupled oscillator model. The
vibrations causing the absorption band were assumed localized and only
nearest neighbor interactions were considered. The general relationship
he derived is given as equation 1. Here $\nu(\partial\partial')$ and ν_0 are the observed

$$\nu(\partial\partial') = \nu_0 + \sum_k D_k \cos(k\partial) + \sum_l D_l \cos(l\partial') \qquad \text{(Eq. 1)}$$

frequency and unperturbed frequency respectively. The second and third
terms are due to intra- and interchain vibrational interactions respec-
tively, ∂ is the phase angle between adjacent group motions in the chain
and the coefficients D_k involve the potential and kinetic energy interac-
tions between the kth neighbors in the chain; ∂' and D_l pertain to the
interactions through interchain hydrogen bonds and have meanings similar

Table 1. The infrared absorption spectra of the amide I band of basic protein structures

Structure	ν(max)	Dichroism	Intensity
random coil	1656 cm^{-1}	none	strong
α-helix	1650 cm^{-1}	//	strong
	1652 cm^{-1}	⊥	medium
β structure	1685 cm^{-1}	//	weak
	1632 cm^{-1}	⊥	strong

to those of ∂ and D_k respectively.

The antiparallel β structure has a unit cell which contains four peptide groups, two groups in one chain and two groups in the adjacent chain. Group theory predicts that each absorption band associated with the amide chromophore will be split into four bands, one of which is inactive. The phase angles ∂ and ∂' of the motions in the various groups must be either 0 or π . The frequencies of the four bands must therefore be those given by equations 2,3,4 and 5. Here $\nu_\perp$ and $\nu_{\parallel}$ indicate bands

$$\nu_{\parallel} (00) = \nu_0 + D_1 + D_1' \qquad \text{inactive} \qquad \text{(Eq. 2)}$$

$$\nu_\perp (\pi0) = \nu_0 + D_1 - D_1' \qquad \text{active} \qquad \text{(Eq. 3)}$$

$$\nu_{\parallel} (0\pi) = \nu_0 - D_1 + D_1' \qquad \text{active} \qquad \text{(Eq. 4)}$$

$$\nu_\perp (\pi\pi) = \nu_0 - D_1 - D_1' \qquad \text{active} \qquad \text{(Eq. 5)}$$

active for light polarized so that the electric vector is perpendicular and parallel to the chain direction respectively.

The parallel β structure has a unit cell which contains two peptide groups, both in the same chain. Group theory predicts that each absorption band of the amide chromophores will be split into two bands. The

phase angle ∂ must be 0 or π. The phase angle ∂' involving the relative motions of vibrations in nearest neighbor groups in different unit cells must be 0. The frequencies of the two bands must then be those given by equations 6 and 7.

$$\nu_{\parallel}(00) = \nu_o + D_1 + D_1' \qquad \text{(Eq. 6)}$$

$$\nu_{\perp}(\pi 0) = \nu_o - D_1 + D_1' \qquad \text{(Eq. 7)}$$

For nylon 66 which is a β-like structure where the chromophores are separated by five carbon atoms, the frequency of absorption of the amide I band is expected to depend only on interactions of groups in adjacent chains. The phase angle ∂ must be 0. The frequency of the absorption band must then be given by equation 8.

$$\nu(\text{nylon } 66) = \nu_o + D_1' \qquad \text{(Eq. 8)}$$

Miyazawa and Blout (1961) assumed that the 1685 cm^{-1} band and the 1632 cm^{-1} band in the spectra of the antiparallel β structures of silk and polyglycine I were the $\nu_{\parallel}(0\pi)$ and the $\nu_{\perp}(\pi 0)$ bands respectively. They also determined the absorption maximum for nylon 66 to be at 1640 cm^{-1}. Using equations 4, 3 and 8 and frequencies assigned to the $\nu_{\parallel}(0\pi)$, $\nu_{\perp}(\pi 0)$ and $\nu(\text{nylon } 66)$, they solved for ν_o, D_1 and D_1'. Then using equations 6 and 7, they predicted the absorption spectrum of the parallel β structure. By this procedure they showed that the 1690 cm^{-1} band observed in β structures is due to antiparallel β structure only. This conclusion was further supported by Bradbury and Elliott (1963), who showed that $\nu_{\parallel}(0\pi)$ progressively shifted to lower frequencies in the series from polyglycine (nylon 2) to nylon 10. D_1' is expected to remain uncharged in this series of compounds and D_1 is expected to become smaller (Table

2.) In nylon 10, D_1 is equal to 0 and $v_o + D_1'$ correctly predict the absorption maximum of $v_{||}$ (0π). This is all consistent with Miyazawa's treatment.

Table 2. Infrared spectral properties of a series of nylon compounds

Polymer	$v_\perp$ (π0)	$v_{||}$ (0π)	v_o^a	D_1
nylon 2	1632 cm^{-1}	1686 cm^{-1}	1659 cm^{-1}	16 cm^{-1}
nylon 4	1640 cm^{-1}	1670 cm^{-1}	1655 cm^{-1}	4 cm^{-1}
nylon 6	1641 cm^{-1}	1667 cm^{-1}	1654.5 cm^{-1}	1.5 cm^{-1}
nylon 8	1641 cm^{-1}	1663 cm^{-1}	1652 cm^{-1}	0 cm^{-1}
nylon 10	1642 cm^{-1}	1664 cm^{-1}	1653 cm^{-1}	0 cm^{-1}

[a] D_1' was assumed to be equal to -11 cm^{-1}.

In practice no β structures other than the antiparallel β structured silk have been shown to possess either pure parallel or pure antiparallel β structure (Marsh, Corey and Pauling 1955). A weak band near 1690 cm^{-1} is present in the infrared spectra of many synthetic polypeptides and indicates the presence of at least a fractional amount of antiparallel β structure. Because this 1690 cm^{-1} band is weak and close to strong bands from random coil at 1660 cm^{-1} and from β structure at 1632 cm^{-1}, it is sometimes difficult to uncover and its absence can not be construed to imply the presence of pure parallel β structure.

Ultraviolet absorption and dispersion depend in an additive fashion on the properties of the chromophores comprising any molecule. There

is some dependence of these properties on molecular geometry; however, it is an effect of secondary importance. ORD and CD of chromophores having planes or centers of inversion are not intrinsic in a chromophore but are extrinsically induced in chromophores by local asymmetric molecular environments. From this it is evident that optical properties fall into two classes, in one they depend on the chromophore itself and in the other they depend on the chromophore's environment and, therefore, on molecular geometry. This discussion will concern the latter class.

The macroscopic properties molar rotation ([m']) and molar dichroism ($\Delta\varepsilon$) are directly related to the molecular optical parameter rotational strength (R_A) which is in turn related to the molecular electronic and magnetic transition dipole moments, μ_{OA} and m_{AO} respectively (Equation 9).

$$R_A = \mathrm{Im}\ \mu_{OA} \cdot m_{AO}$$

$$= \frac{2.303\ mc}{4\pi e^2 N_0} \int_A \Delta\varepsilon\, d\nu \simeq \frac{hc(\nu_A^2 - \nu^2)}{48 N_0 \nu^2}\ [m_A']$$

(Eq. 9)

Here m and e are the electron mass and charge, c is the velocity of light, N_0 is Avogadro's number and ν is frequency. The subscripts A and OA designate the $0 \rightarrow A$ molecular transition. Im signifies imaginary part. In molecules with points or planes of symmetry, it is necessary that the dot product of μ_{OA} and m_{AO} vanish. Because of this, these molecules are not optically active even though μ_{OA} and m_{AO} might have finite values. In many asymmetric molecules having symmetric chromophores optical activity is observed. In order to explain this observation, it is necessary to devise a method for the asymmetric molecule to perturb the symmetric chromophore in such a way that μ_{OA} is not perpendicular to m_{AO} and their

dot products will not vanish. The amide chromophore will be discussed before discussing methods of perturbation.

There are a number of absorption bands of the amide chromophore in polypeptides which will be of interest here. The characteristics of the amide group absorption spectrum above 150 nm are summarized in Figure 1 (Gratzer 1967). These are : one n → π* transition at approximately 210 nm, two π → π* transitions near 190 nm and 165 nm and one n → σ* transition near 150 nm. For each transition in an isolated group with a point or plane of inversion the transition must either be electrically allowed and magnetically forbidden ($\mu_{oa} \neq 0$ or $m_{ao} = 0$) or be magnetically allowed and electrically forbidden ($\mu_{oa} = 0$ and $m_{ao} \neq 0$)(Eyring et al. 1944). The lower case subscripts indicate the group transition o → a in group i as opposed to molecular transitions discussed previously. Of these transitions the n → π* transition is experimentally magnetically allowed, while the π_1 → π* and π_2 → π* transitions are electrically allowed.

Tinoco (1962) used first order perturbation theory to derive a general equation for optical activity in polymers. For magnetically allowed transitions like the n → π* transition, the general equation reduces to equation 10. Here R_A is the rotational strength of molecular transition A in a molecule with N identical groups. The μ's and m's are as defined previously. The states of the groups are labelled with subscript o (ground state) and a,b,--- (excited states). Thus, μ_{ioa} would be the electric dipole moment for the transition o → a in group i, while μ_{iaa} is the permanent electric dipole moment of the ith group in the excited state a. The factors $V_{ioa;job}$ etc. are the coulombic
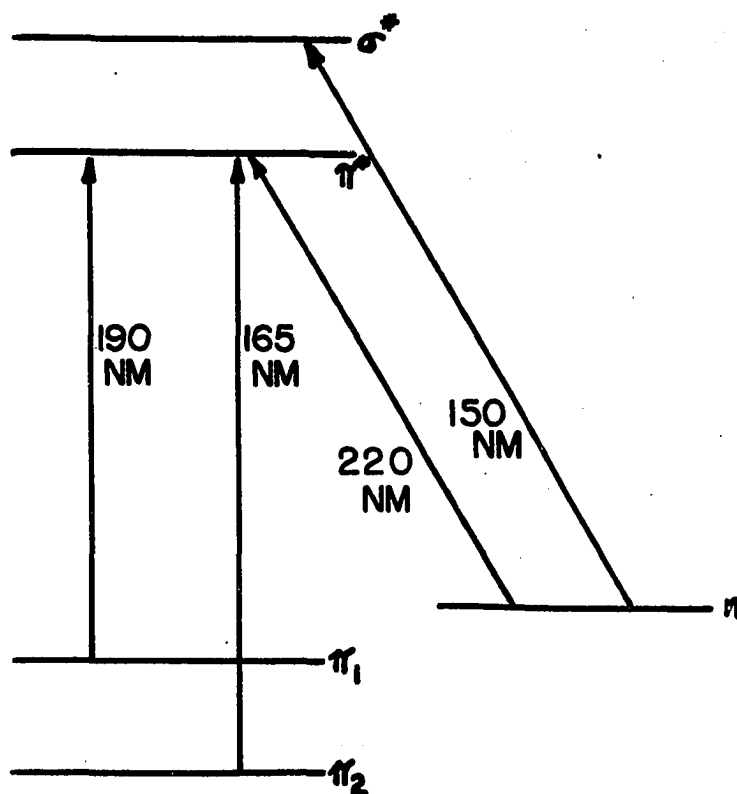
Figure 1. The electronic transitions above 150 nm in the absorption spectrum of the amide chromophore

$$R_A = -\sum_{i=1}^{N} \left[2 \sum_{j \neq i} \sum_{b \neq a} \frac{\text{Im } V_{ioa;job} \; \mu_{job} \cdot m_{ioa} \; \nu_b}{h(\nu_b^2 - \nu_a^2)} \right. \qquad \text{(a)} \qquad \text{(Eq. 10)}$$

$$+ \sum_{j \neq i} \sum_{b \neq a} \frac{\text{Im } V_{iab;joo} \; \mu_{iob} \cdot m_{iao}}{h(\nu_b - \nu_a)} \qquad \text{(b)}$$

$$+ \sum_{j \neq i} \sum_{b \neq a} \frac{\text{Im } V_{iob;joo} \; \mu_{iab} \cdot m_{iao}}{h\nu_b} \qquad \text{(c)}$$

$$+ \sum_{j \neq i} \frac{\text{Im } V_{ioa;joo} \; (\mu_{iaa} - \mu_{ioo}) \cdot m_{iao}}{h\nu_a} \left. \right] \qquad \text{(d)}$$

potential energies due to the interactions of transition charge densities in residue i with those in residue j, while $V_{ioa;joo}$ refers to the interaction of the transition charge density in group i with the permanent charge density in residue j. The frequencies ν_a and ν_b are respectively the frequencies of the transitions o → a and o → b. The b, c and d terms in equation 10 comprise the Condon or one electron mechanism for the generation of optical activity (Condon et al. 1937). In the Condon mechanism, two transitions on the same chromophore, one magnetic, the other electric are mixed by the perturbing field of the remaining asymmetric molecule. In effect this perturbing field partially breaks down the symmetry of the chromophore. The potential energies (V's) in these terms depend on the symmetry of the chromophore group itself (Schellman 1968, Schellman and Oriel 1962, Schellman 1966, Litman and Schellman 1964). The peptide group is a quadripole with C_{2v} symmetry having the axis of rotation along the C=O direction. The potential energy for the interaction of the quadripole chromophore with monopole perturbing atoms has the form in equation 11. Here X_i, Y_i and R_i are the x, y and radial coor-

$$\left.\begin{array}{c} V_{iab;joo} \\ V_{iob;joo} \\ V_{ioa;joo} \end{array}\right\} \quad = \quad F\left(\sum_i \frac{q_i X_i Y_i}{R_i^5}\right) \qquad \text{(Eq. 11)}$$

dinates of the perturbing atom i with the charge q_i. Because of the nature of this potential energy term, three requirements are necessary to generate optical activity from the Condon mechanism: 1) The quadripole must be rigid with respect to the nearest perturbing atoms, 2) there must be a low effective dielectric constant between the chromophore and the perturbing atoms and 3) the perturbing atoms must give an asymmetric field (Litman and Schellman 1964). The charge on any perturbing atom is weighted by R^{-5}, and therefore, only atoms near the chromophore contribute to the rotational strength. The first term in equation 10 is not included in the Condon mechanism although its contribution to the rotational strength might be significant. This term is the m-μ mechanism and is discussed by Schellman (1968) and Woody and Tinoco (1967). It involves the mixing of two transitions, one magnetic on one group and the other electric on another group by the perturbing field of the asymmetric molecule.

Before discussing the electrically allowed transitions in polymers like the $\pi_1 \rightarrow \pi^*$ transition, the phenomenon of exciton splitting must be discussed. When electrically allowed transitions in a polymer or crystal are degenerate, a phenomen known as exciton splitting occurs. In crystals Davydav (1962) showed that light is not absorbed by a single degenerate group, but that the excitation is distributed over many degenerate groups in a crystal. By first order perturbation theory it can be shown that N polymer energy levels occur, each level corresponding to one of the

N groups of the polymer. The relative intensity of each of the energy

levels is determined by the geometry of the degenerate groups in the

polymer (Tinoco et al. 1963). The frequency and oscillator strength

calculated for the exciton bands of a number of polypeptide structures

are given in Figure 2.

The general equation of Tinoco (1962) reduces to equation 12 for

electrically allowed transitions. In this equation the primes indicate

$$R_A = - \sum_{i=1}^{N} [\, 2\pi/c \sum_{j \neq i} \sum_{b \neq a} \frac{V'_{ioa;job} \nu'_a \nu'_b (R_j - R_i) \cdot \mu'_{job} \times \mu'_{ioa}}{h(\nu'^2_b - \nu'^2_a)} \quad \text{(a)} \tag{Eq. 12}$$

$$+ 2 \sum_{j \neq i} \sum_{b \neq a} \frac{\text{Im } V'_{ioa;job} \nu'_a \mu'_{ioa} \cdot m'_{jbo}}{h(\nu'^2_b - \nu'^2_a)}] \quad \text{(b)}$$

that the groups considered are in the static field of the polymer and not

isolated as were the groups considered previously. The a term in equation

12 comprises the Kirkwood dipole-coupling mechanism (Kirkwood 1937).

It involves the interactions between electrically allowed transitions in

different groups i and j separated by the vector $(R_j - R_i)$. The potential

energy (V) in this term is due to the interactions of dipoles and takes

the form in equation 13 (Schellman 1968). The b term in equation 12 is

$$V_{ioa;job} = F \left(\frac{\mu_1 \cdot \mu_2}{R^3} - \frac{3[\mu_1 \cdot (R_j - R_i)][\mu_2 \cdot (R_j - R_i)]}{R^5} \right) \tag{Eq. 13}$$

similar to the a term in equation 10 which was discussed previously.

The rotational strengths for the $\pi_1 \rightarrow \pi^*$ and $n \rightarrow \pi^*$ transitions of

the amide chromophore of polypeptides can and have been calculated using

considerations similar to these. Calculations of this type generally

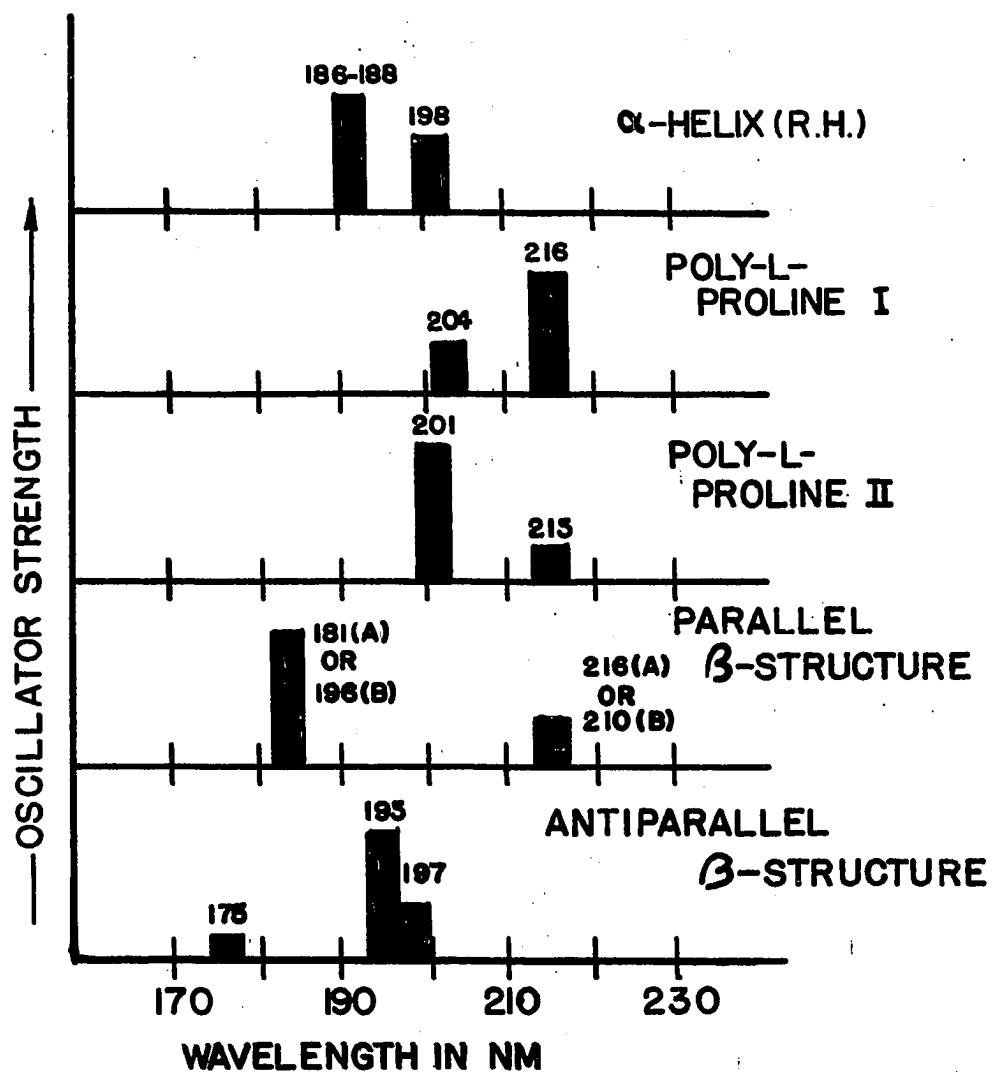suffer from lack of detailed knowledge concerning the wave functions

Figure 2. The frequency and oscillator strength calculated for the exciton bands of a number of polypeptide structures

and are therefore most useful in predicting sign and approximate position of cotton effects. The predictions of rotational strength should be reliable within an order of magnitude. Calculations of rotational strength have been made for the right and left handed α-helix as well as the 3_{10} helix by Woody and Tinoco (1967), Schellman and Oriel (1962) and Vaurnakis et al. (1968), for the poly-L-proline I and II helices by Pysh (1967) and for the parallel and antiparallel β structure by Pysh (1966) (Table 3). It is easily seen from this data that it would be difficult to distinguish between α-helix and 3_{10} helix or between parallel and antiparallel β structure on the basis of the theoretical predictions. However, with this information distinction between right and left handed α-helix or 3_{10} helix can be made as well as between the I and II forms of poly-L-proline.

Table 3. Rotational strengths in Debye-Bohr magnetons calculated for the $n \to \pi^*$ and $\pi_1 \to \pi^*$ transitions in polypeptides

Structure	Transitions calculated				Transitions observed			
	$R_{n \to \pi^*}$	$\lambda(nm)$	$R_{\pi_1 \to \pi^*}$	$\lambda(nm)$	$R_{n \to \pi^*}$	$\lambda(nm)$	$R_{\pi_1 \to \pi^*}$	$\lambda(nm)$
α-helix right handed	-0.028[a]	220	-5.230[a]	186.1	-0.160[d]	222	0.870[d]	198
	-0.031[b]	220	6.400[a]	188.4			-0.310[d]	205
	-0.140[c]	220	-1.170[a]	197.5				
α-helix left handed	0.003[a]	220						
	0.031[b]	220						
3₁₀ helix right handed[a]	-0.017	220	-8.830	185.1				
			9.460	186.1				
			-0.630	197.6				
3₁₀ helix left handed[a]	0.006	220						
poly-L-proline I	-0.022[d]	220	-1.720[d]	204	-0.018[e]	232	-0.190[e]	200
			1.720[d]	216			-0.300[e]	216
poly-L-proline II	0.000[d]	220	-0.410[d]	201	0.000[e]	---	-0.360[e]	206
			0.020[d]	215			0.054[e]	221
β structure parallel	-0.023[f]	220	0.230[f]	181				
			-0.076[f]	216				
β structure antiparallel	-0.035[f]	220	-0.027[f]	175	-0.160[g]	218	0.210[g]	195
			0.057[f]	195 & 197			-0.160[g]	218

[a]Woody and Tinoco (1967).
[b]Schellman and Oriel (1962).
[c]Vaurnakis et al. (1968).
[d]Pysh (1967).
[e]Bovey and Hood (1967).
[f]Pysh (1966).
[g]Iizuka and Yang (1966), Sarkar and Doty (1966), Yang (1967).

MATERIALS AND METHODS

Feather Keratin Fibrils

The feathers used in this study were the mature primary flight
and tail feathers obtained from turkeys. The feathers were washed
with water to remove dirt and debris and allowed to dry. The calamus
(quill) of the dried feather was scraped to remove the disoriented outer
layer and the tip and the blade of the feather trimmed from the calamus.
The resulting portion was split open and the interior scraped to remove
the pulp caps. The scraped feather was then extracted with hot ben-
zene in soxhlet apparatus for 24 hours and then allowed to dry at
room temperature.

Peracetic acid used for the oxidation of the feather was prepared
by the method of Greenspan (1947), modified for the use of 30% hydro-
gen peroxide. The pH of the peracetic acid was adjusted in the cold
to 4.5 by the addition of concentrated sodium hydroxide. The proce-
dure used for oxidation of the keratin is similar to that used by
Hail (1964). The feather was oxidized in the above solution for between
15 and 24 hours at 4°C. At the completion of the oxidation period, the
remaining oxidizing agent was removed by washing the feather parts
exhaustively using distilled water. The feather was then dispersed
in solution by placing the oxidized feather in distilled water and ele-
vating the pH to 10.5 with sodium hydroxide. The solution was main-
tained at pH 10.5 for up to two hours and then dialysed 24 hours against
distilled water to remove inorganic compounds and small peptides.
The oxidized feather keratin (OxFK) solution was then centrifuged for

four hours at 144,000 × g to remove any large or insoluble protein.

The procedure used for reduction and alkylation of feather was similar to that used by Harrap and Woods (1964 a). The feather was reduced in a 0.2 molar mercaptoethanol solution at pH 11.0. The feather composed about 2% of the weight of the solution. The reaction proceeded under an atomsphere of nitrogen at 4°C for between 24 and 48 hours. At the completion of the reduction period, the solution was clarified by centrifugation and the supernatant obtained was titrated with a 0.6 to 1.0 molar iodoacetic acid which had been adjusted to pH 6. During the titration, the pH of the solution was maintained at pH 9.5, and the titration was continued until the nitroprusside test was negative. The reaction was always completed in 15 minutes. Sodium sulphite was then added to destroy the excess of iodoacetate, and the reaction products were removed by dialysis against distilled water at 4°C. The S-carboxy-methylated feather keratin (SCMFK) was then concentrated by pressure filtration and centrifuged for four hours at 144,000 × g to remove any large or insoluble protein.

Fibril formation occurred under numerous conditions of temperature, concentration, pH and ionic strength. It occurred most rapidly at or near room temperature in concentrated solutions (1 or 2%) when the pH was slightly higher than that at which precipitation occurred. The pH's generally used were pH 4.5 for OxFK and pH 6.0 for SCMFK. The SCMFK preparations gelled readily while a period of several days was required for gel formation in OxFK. The fibrils were separated from the solution by centrifugation at 105,000 × g for four hours,

suspended in distilled water and recentrifuged. Repeating this final suspension and centrifugation several times produced pure feather keratin fibrils as evidenced by the lack of slow sedimenting components in the fibril solutions.

Insulin Fibrils

Samples of crystalline insulin were obtained from Calbiochem. A method suggested by Waugh (1944) was used for the conversion of native to fibrillar insulin. The pH of a 1% solution of insulin was adjusted to between pH 1.5 and 2.0 with hydrochloric acid and about 10 ml was placed in a sealed glass test tube. The tubes were heated in a waterbath to between 80° and 100°C until a clear gel was formed. The time required for gelling was between 2 and 10 minutes depending on the exact temperature and pH. The sample was then cooled and frozen rapidly by immersion in a dry ice-acetone solution, thawed under running tap water, and reheated (80° to 100°C) for approximately two minutes. The process of freezing and reheating was repeated until a firm gel formed which was usually after three or four times. Total conversion of native to fibrillar insulin was possible by this procedure and sedimentation velocity experiments with the fibrillar solution showed no slow sedimenting components.

Diamides

Samples of crystalline acetyl-glycine-N-methyl amide (AGMA), acetyl-L-alanine-N-methyl amide (AAMA), acetyl-L-leucine-N-methyl amide (ALMA) and noncrystalline acetyl-L-lysine-N-methyl amide (ALyMA) were obtained

from the Cyclo Chemical Corp. and were used without further purification.

Other Materials

All other chemicals were analytical grade reagents and were not further purified.

Electron Microscopy

Copper grids, 200 or 400 mesh, were coated with formvar films and subsequently coated with carbon by vacuum evaporation. A dilute solution of the fibrils in distilled water was deposited on the above grids with a fine-bore pipette and allowed to stand several seconds before removal of the liquid with the edge of a strip of filter paper. This process sometimes was repeated several times. As the drop receded, fibrils remained on the grid surface.

For negatively stained specimens, the above staining procedure was performed before the grids had completely dried. Uranyl formate at a concentration of 1% in distilled water was used. The staining procedure was always repeated several times.

For shadowed specimens, the shadowing was performed by evaporating platinum carbon pellets (Ladd Research Industries) in a vacuum evaporator (Illini Consultants) in which a prepared grid was placed. Evaporation was usually done at a distance of 10 cm from the grid and the tangent of the angle between the plane of the grid and the trajectory of the vaporized platinum was either 0.10 or 0.25.

Specimen grids were examined with an RCA-EMU-3F electron microscope. The objective aperture was operated at an accelerating voltage of 100 KV for negatively stained samples and 50 KV for shadowed samples. The

instrumental magnification was always near 30,000X as determined by periodic calabration. All measurements quoted were made on the original plates with a Nikon Profile Projector Model 6-C.

X-ray Diffraction

Feather keratin and insulin fibrils were studied as rod and disc specimens. Rod specimens were prepared by suspending a drop of an aqueous fibril solution between the end of two approximately 1 mm diameter glass rods separated by from 1 to 3 mm. The ends of the rods were fire polished. After allowing several hours for drying rod specimens 1 to 3 mm long and 0.1 mm in diameter were obtained. The fibrils were oriented parallel to the main axis of the rod. These specimens were generally mounted perpendicular to the x-ray beam; however, whenever particular meridional diffractions were to be studied, the rod was tilted away from this perpendicular position by the Bragg angle of the diffraction involved. Disc specimens were prepared in cylindrical capillary tubes, of about 1 mm diameter, by filling a short segment of the capillary with an aqueous fibril solution and allowing several days for drying. After the drying period, thin cylindrical discs 0.1 mm thick and 1 mm in diameter were obtained. The fibrils were oriented in the plane of the discs. They were always mounted with the x-ray beam in their plane.

Bundles of fine needle-like diamide crystals were made by numerous mechanical techniques and mounted in the same way as rod specimens.

Nickel filtered copper $K\alpha$ radiation from a General Electric XRD-5 x-ray unit was used throughout this study. Flat film cameras which could be evacuated or could be maintained in a helium atmosphere were

used at specimen to film distances near 3, 5 or 10 cm.

Infrared Measurements

Infrared (IR) and infrared dichroism (IRD) spectra were obtained at room temperature on a Beckman IR4 recording spectrophotometer which was modified for dichroism measurements with a beam condenser and polarizer. Some IR measurements were also made with a Beckman IR12 recording spectrophotometer. Solid samples of feather keratin fibrils, insulin fibrils and crystalline diamides were oriented by stroking viscous fibril solutions or Nujol suspended diamide crystals on calcium fluoride windows with a fine brush. The fibrils and crystals oriented with their long axis parallel to the direction of stroking. The IR spectra of diamide solutions were made in Beckman standard liquid cells with sodium chloride windows and path lengths of 0.1 mm and 1.0 mm or in IR quartz cuvettes having path lengths of 1 mm and 10 mm. The spectrophotometer was always used in the double beam mode and standard Beckman liquid cells were used in matched pairs.

Near IR spectra were obtained at room temperature with a Cary 14 recording spectrophotometer using a matched pair of 5 cm path length quartz cuvettes.

Optical Activity

Optical rotatory dispersion (ORD) and circular dichroism (CD) spectra were obtained at room temperature on either a Jasco recording dichrograph (CD-ORD-UV5) or a Jasco recording polarimeter which had been modified for the measurement of CD (model ORD/UV5). Some CD measurements were also made with a modified Roussel-Jouan dichrograph (Foss and McCar-

ville 1965). Most of the ORD and CD spectra of proteins were made with a 1 mm path length quartz cuvette which showed no strain birefringence. Because of interference with ORD and CD measurements by the strong flow induced birefringence normal insulin fibrils produced, fibrils were frozen and thawed prior to the recording of these data. The freezing technique was found to reduce fibril length thus eliminating the birefringence, but had no effect on the ORD at 230 nm. The CD and ORD spectra of diamides were made in a number of quartz cuvettes and in teflon cells having quartz end windows attached by silicone grease. Path lengths between 0.05 and 10 mm were used.

Ultraviolet Measurements

Absorption determinations and spectra were obtained at room temperature with a Cary 15 recording spectrophotometer. For recording spectra in the far ultraviolet several special precautions were necessary. The instrument which was flushed with nitrogen was operated in the double beam mode using two carefully matched cuvettes having 1 mm path lengths. In fibrillar insulin solutions, some hydrochloric acid was present; however, its absorbance was never larger than 20% of that of the fibrils and should have cancelled with the same concentration of hydrochloric acid in the solvent. Dust was eliminated from the solutions by centrifugation. Even though dust is eliminated from solutions and solvents, light scattering due to protein occurs. This was corrected by plotting the logarithm of the absorption spectra of the protein and fitting it to the logarithm of K/λ^5 (K is a constant and λ is wavelength) at wavelengths removed from absorption bands. This curve is then extrapolated

under the protein absorption spectra and subtracted from it. This correction never accounted for more than 5% of the absorbance at 200 nm.

Hydrodynamic Measurements

Viscosity measurements were made using a Cannon-Ubbelohde semi-micro dilution viscometer size 150. The viscometer was immersed in a constant temperature bath at 25°C and flow times were measured with an auto viscometer (Hewlett and Packard Models 5901B and 5901A respectively). The solution and solvent densities were determined with a 10 ml specific gravity bottle.

Sedimentation velocity measurements were made with a Spinco Model E analytical ultracentrifuge using an An-D rotor and double sector synthetic boundary cell. The centrifuge was operated at 60,000 rpm and the temperature was regulated near 20°C. The data were recorded on Kodak Metallographic Plates using the schlieren optical system. The photographic data were measured with a Nikon Profile Projector Model 6-C.

Diffusion coefficients were measured with a Spinco Model E analytical ultracentrifuge using an An-J rotor and a double sector synthetic boundary cell. The centrifuge was operated at 4000 rpm or slower and the temperature was regulated near 20°C. The data were recorded on Kodak Type II G spectroscopic plates using the Rayleigh interference optical system.

Concentration and Error Determination

Concentrations were generally determined by dry weight measurement. Exceptions to this were in the absorption study on native insulin and insulin fibrils in which concentrations were compared using biuret color,

and in the sedimentation velocity and diffusion studies where concentrations were determined by schlieren peak area and interference fringe numbers respectively.

Error bars in spectra represent instrumental noise and are not related to the ability to reproduce spectra. All other errors are given as probable error.

RESULTS AND DISCUSSION

Feather Keratin

Low molecular weight derivatives

OxFK and SCMFK preparations contain four fractions. Each fraction has different elution properties with respect to Sephadex G-100 column chromatography (Figures 3 and 4). In the order of their elution, the four fractions are polymer, trimer, dimer and monomer. Monomer is in the greatest abundance and is presumably the basic constituent of native feather keratin. It has a molecular weight of 10^4 g/mole and from hydrodynamic and optical rotation studies appears to be a random coil in aqueous solution (Rougvie 1954, Woodin 1954, Schor and Krimm 1961, Harrap and Woods 1964 b). The ORD of aqueous monomer above 200 nm has a single rotational trough at 210 nm (Figure 5). This is expected for the random coil in aqueous solution. It is interesting that the ORD's of feather keratin monomer and soluble aqueous silk, both of which are thought to be random coils, are similar (Iizuka and Yang 1966). The ORD of random coil synthetic polypeptides has a much deeper trough at 210 nm than silk or feather keratin monomer (Blout et al. 1962, Sarkar and Doty 1966, Holzwarth and Doty 1965).

The dimer and trimer fractions are abundant in OxFK preparations. The dimer is presumably composed of two monomers which have one or more cystines in common. It has a molecular weight of 2×10^4 g/mole, and on the basis of hydrodynamic investigation appears to be a random coil in aqueous solution (Hail 1964). The ORD of aqueous dimer is, within experimental error, identical to that of monomer (Figure 5). This also

Figure 3. The Sephadex G-100 column chromatography of a S-carboxy-
methylated preparation of feather keratin

Sephadex columns (2 X 100 cm) were prepared. The columns
were equilibrated and eluted with pH 7.0 phosphate buffer
having an ionic strength of 0.15. Ten ml samples were applied.

Figure 4. The Sephadex G-100 column chromatography of an oxidized pre-
paration of feather keratin

See Figure 3 for details.
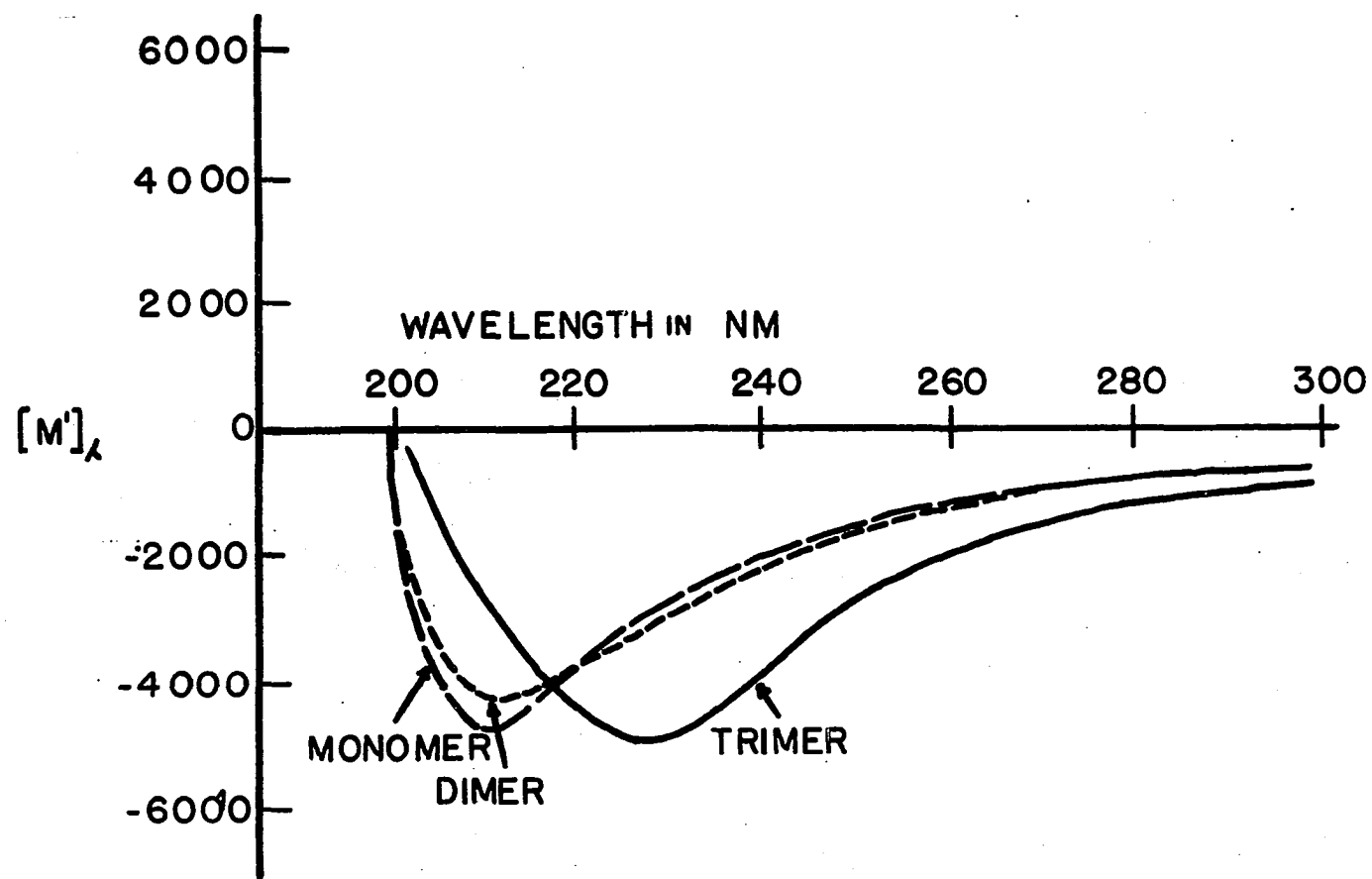
SCM FEATHER KERATIN

OXIDIZED FEATHER KERATIN
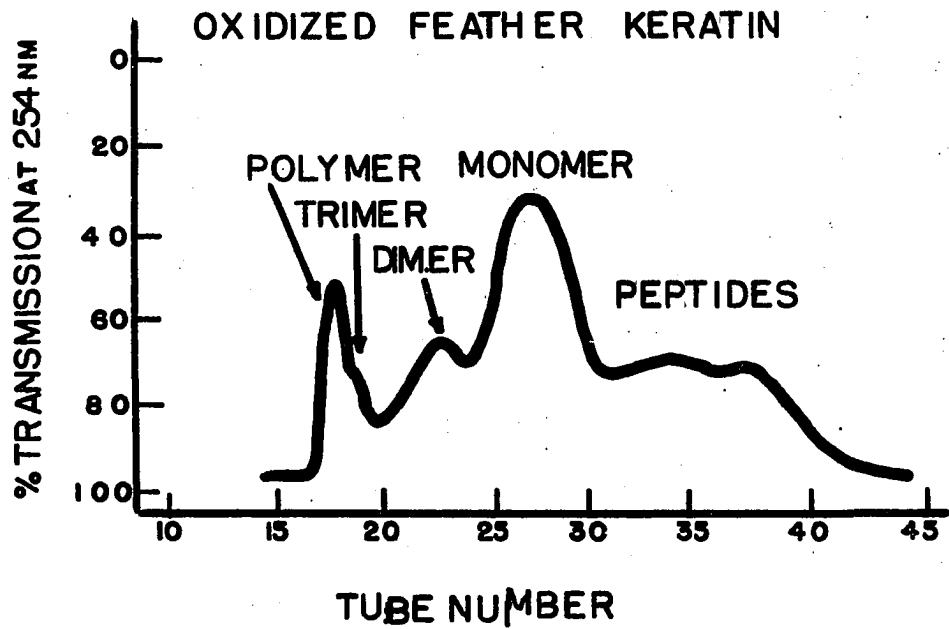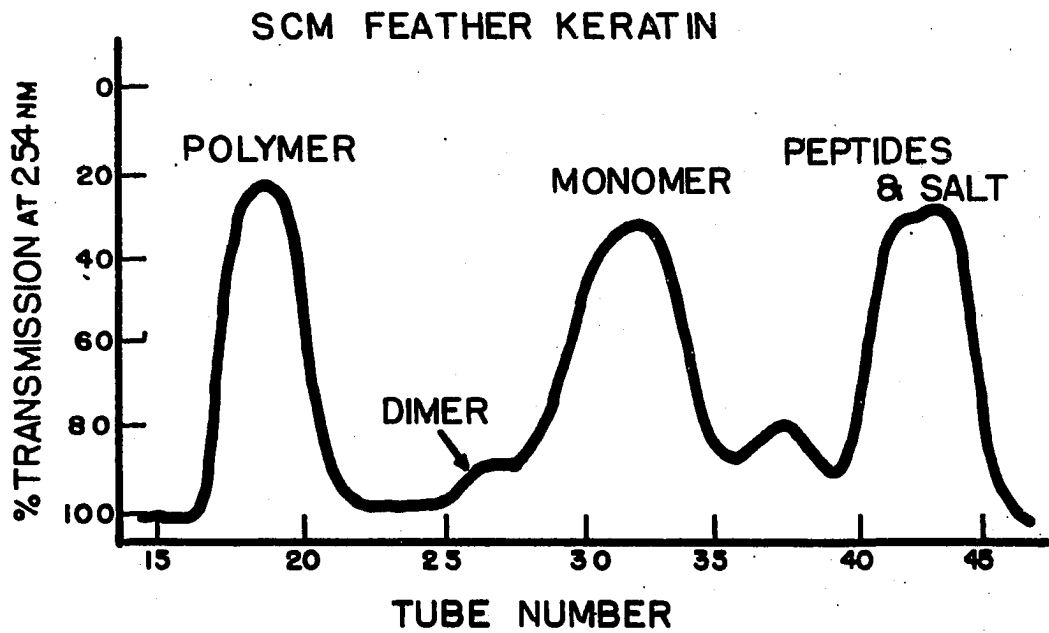
Figure 5. The optical rotatory dispersion of aqueous monomer, dimer and trimer

indicates random coil conformation.

The trimer fraction has not been completely characterized. The trimer molecule is presumably composed of three covalently associated monomeric molecules. Its elution properties on G-100 Sephadex indicate that it is more similar to a 3×10^4 molecular weight random coil than a globular structure of the same molecular weight. The ORD of aqueous trimer has a broad trough centered at approximately 230 nm (Figure 5). The presence of a rotational trough near 230 nm indicates an n $\rightarrow$ π^* electronic transition in the peptide group and is sufficient evidence for nonrandom coil protein conformations in aqueous solvents. Because the crossover point of the trimer ORD is not above 220 nm, it is expected that the trimer is predominately random coil with some regions of struc-tured protein. Another possibility is that the trimer molecule is to-tally random coil and is mixed with polymer impurities not separable with G-100 Sephadex chromatography. The polymer fraction is present in SCMFK and OxFK preparations. It consists of a continuum of high molecular weight derivatives. Electron microscopic investigation of the polymer fraction has revealed no distinct repeating structures. The ORD of aqueous polymer has only a single rotational trough above 200 nm which is centered at 232 nm and has a crossover at 225 nm. Based on ORD, it appears that the polymer fraction consists primarily of struc-tured protein.

The preparation and electron microscopy of fibrillar feather keratin

At the proper conditions of pH and ionic strength, the aqueous mixture of the fractions of OxFK or SCMFK preparations form a gel.

Gelation is due to the formation of a fibrillar derivative from any of the soluble fractions or a combination thereof. The fibril formation which accompanies gelation does not occur in solutions of purified monomer fraction. The SCMFK fractions gel more readily than the OxFK fractions which show gel formation only after a period of several days. The polymerization process is reversed by urea and guanidine hydrochloride as well as concentrated formic acid. The fibrils are easily separated from the low molecular weight fractions by centrifugation.

Under investigation with the electron microscope, the fibrils appear to be long rod-like structures which have uniform cross sections (Figure 6). The width and height of the fibrils were experimentally measured using negative staining with uranyl formate for the width and shadowing with platinum carbon for height. Negative staining experiments with samples of both OxFK and SCMFK preparations of fibrils indicated a fibril width which was between 70 and 100 Å (Figure 6). The width was difficult to determine due to the absence of clearly defined fibril boundaries produced by the uranyl formate. Close inspection of the negatively stained fibrils showed faintly stained cross striations separated by about 50 Å (Figure 8). Platinum carbon shadowing experiments on samples of the fibrils indicated a somewhat smaller fibril height of 60 Å (Figure 7). The height was computed by comparing the shadows cast by tobacco mosaic virus with those cast by the fibrils. The results of these experiments indicate that the fibrils might have somewhat elliptical or rectangular cross sections.

Filshie et al. (1964) reported finding fibrils formed from feather keratin which were composed of two or three filaments twisted around

Figure 6. Oxidized feather keratin fibrils negatively stained with
uranyl formate

Figure 7. Oxidized feather keratin fibrils shadowed with platinum
carbon

A distance of 1000 Å is represented in the lower left hand
corner by a bar. The tangent of the shadowing angle was 0.1.
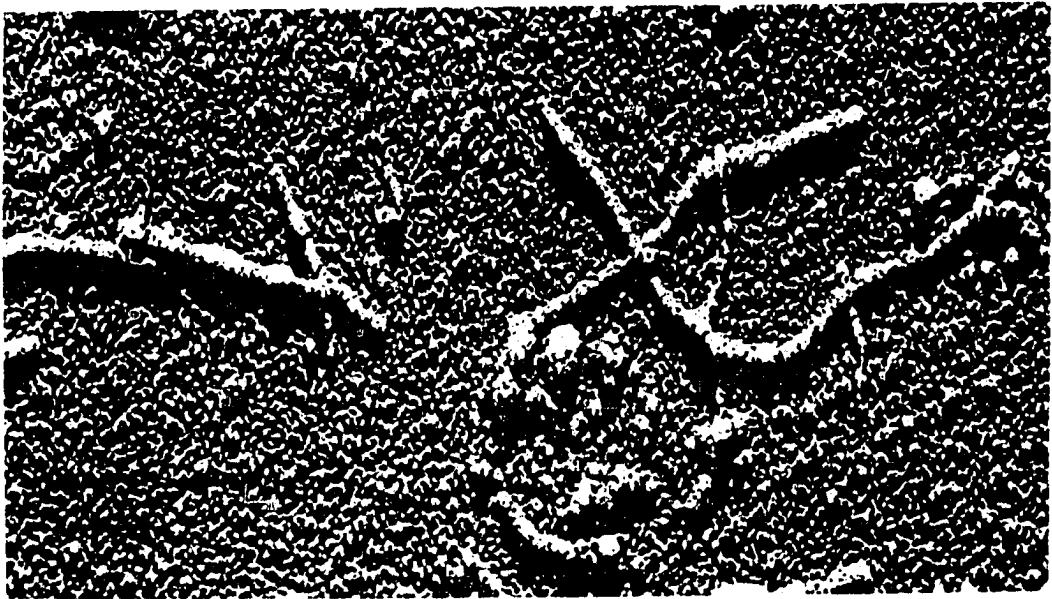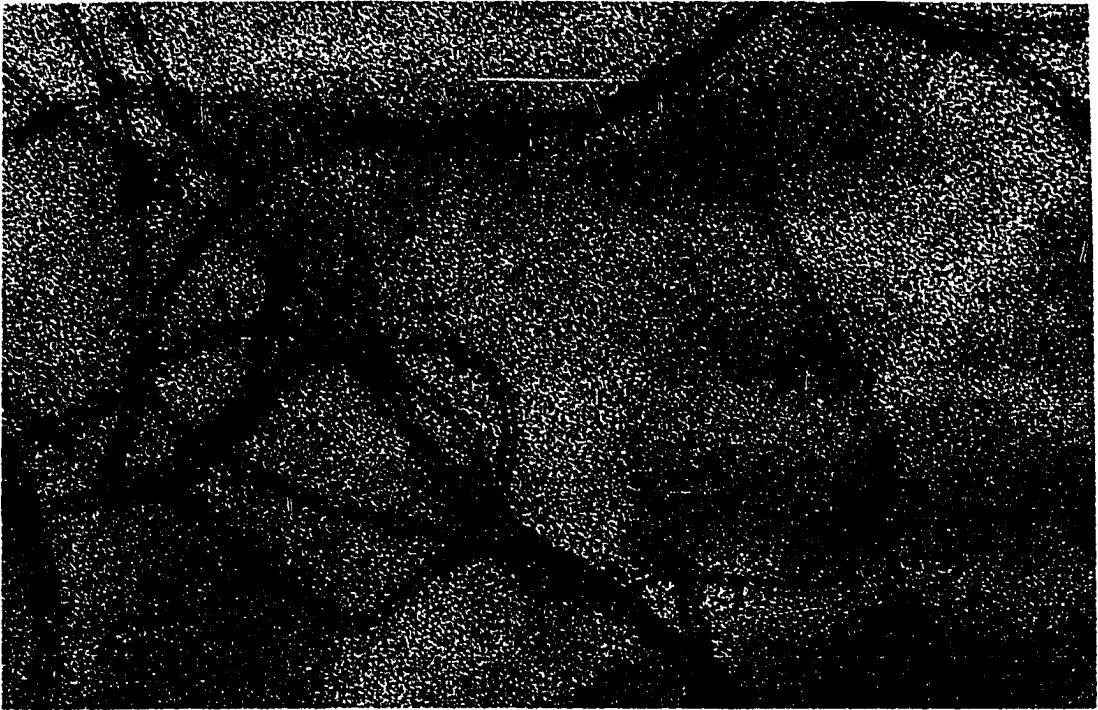
each other which appeared as twisted ribbons. Examples of this phenome-
non clearly indicate the presence of two fibrils per ribbon (Figure 9).
The occurrence of ribbon-like structure, although common, was not the
norm. Filshie et al. (1964) suggested that the fibrils might be similar
to the microfibrils found in native feather keratin. From the data
which follows their suggestion is not plausible.

X-ray diffraction studies of feather keratin fibrils

The rod and disc methods of x-ray specimen preparation have been
described in a previous section. To make clear the interpretation of the
x-ray results, a brief discussion of the orientation of fibrils in such
specimens and the resulting nature of the diffraction pattern is provided
here.

In rod specimens the fibrils are positioned so that their longitu-
dinal axes are parallel to the long axis of the rod. The x-ray diffraction
pattern generated by the specimens are rotation patterns where the axis
of rotation is the longitudinal axis of the fibrils. Along the vertical
axis of such a pattern will be found diffractions related to axial peri-
odicities of the fibril. Diffractions on the horizontal axis will be
related to lateral structure.

In disc specimens the fibrils are positioned so that their longi-
tudinal axes are in the plane of the disc. For convenience, all patterns
of disc preparations are presented so that axial diffractions of fibrils
are again vertical. The nature of specimen orientation is now such
that all in-plane periodicities, axial as well as transverse, will provide
intensity along this pattern direction. Diffractions related to peri-

Figure 8. Oxidized feather keratin fibrils negatively stained with
            uranyl formate

Figure 9. S-carboxy-methylated feather keratin fibrils

            In the upper micrograph two fibrils which are twisted around
            each other appear as a twisted ribbon.
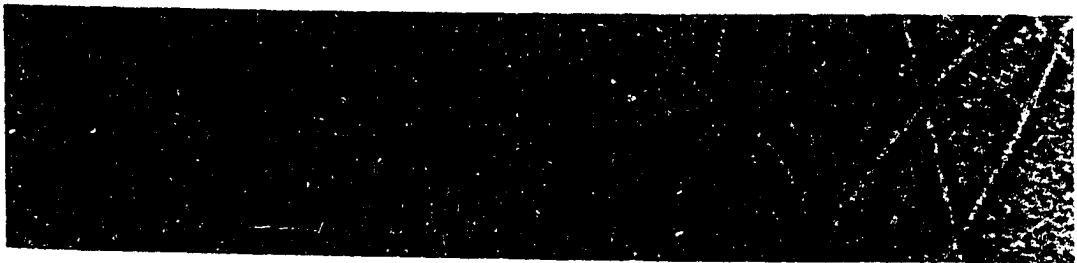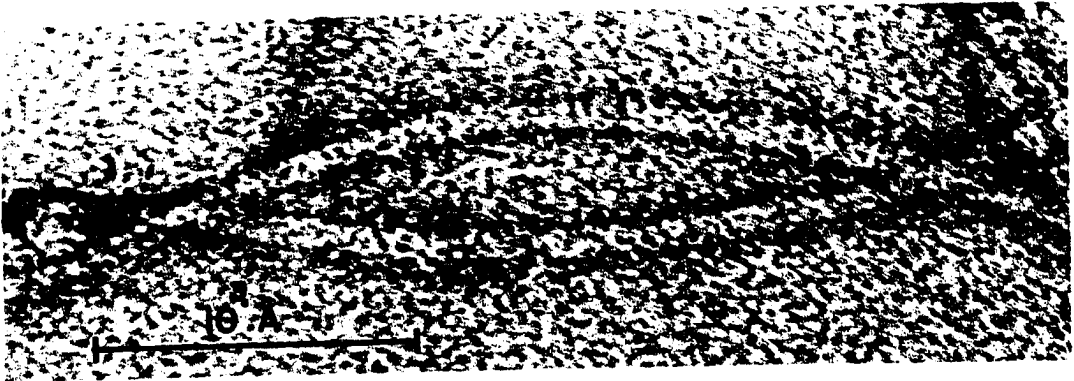
odicities perpendicular to the plane of the disc will be found along the horizontal axis of the pattern and will concern only transverse fibrillar structure.

The low angle x-ray diffraction pattern of a disc specimen of oxidized fibrils is shown in Figure 10. In the rod specimen (not shown), three discrete low angle diffractions are on the equator and none are on the meridian. The equatorial diffractions represent spacings of 69, 35±5 and 23±3 Å. These spacings which must involve the transverse dimensions of the fibrils are the first, second and third orders of 69 Å. The 69 Å spacing probably represents the average separations between fibril centers in the rod preparation. The diffuseness of the diffractions indicates poor fibril packing.

In the disc specimens, there are three discrete low angle diffractions on the equator and one on the meridian. The equatorial diffractions represent spacings of 58, 36 and 23 Å. The meridional diffraction represents a spacing of 90 Å. In the disc specimens, equatorial diffractions must involve the transverse dimensions of the fibrils. The cross sectional dimensions obtained are in fair agreement with those for rod specimens. As pointed out earlier, fibril meridional diffractions in disc specimens may be related to either axial or transverse fibrillar periodicities. Evidence for axial periodicities should be found also on the meridian of rod patterns. Since this is not true for the 90 Å diffraction, one must conclude that it refers to a transverse spacing and that this transverse dimension of the fibrils is preferably oriented in the plane of the disc.

The conclusion then reached is that the fibril centers are separated

by 90 Å in one direction and 58 Å in the other. Again the diffuseness of these low angle diffractions indicates poor fibril packing. The 69 Å spacing observed in rod specimens is probably a composite or an average of the 58 and 90 Å spacings.

A low angle x-ray diffraction investigation of the SCMFK fibrils was not undertaken in detail. Electron microscopic investigation of the SCMFK fibrils showed no difference between the SCMFK and OxFk fibrils.

Because fibrillar dimensions are not necessarily related to intra-fibrillar spacings, the low angle x-ray diffraction pattern need not be related to the wide angle pattern. In this treatment the low and wide angle diffraction patterns are treated independently. The wide angle x-ray diffraction patterns of disc and rod specimens of OxFK and SCMFK fibrils are shown in Figures 11 and 12. The rod and disc diffraction patterns showed no significant differences.

The most striking feature of the x-ray diffraction patterns of the OxFK and SCMFK fibrils is a strong sharp meridional diffraction representing approximately a 4.7 Å spacing. Typically the 4.7 Å spacing is the separation between hydrogen bonded chains in the β structure. When the 4.7 Å spacing is on the meridian, as it is here, it indicates a β structure where the protein backbone chains lie normal to the long axis of the fibrils. Configurations of this type are referred to as cross-β structures. Table 4 contains a list of the other spacings and Miller indices assigned to them. These spacings are indexed to an orthogonal pseudo unit cell having the dimensions given in Table 5. All of the equatorial diffractions were diffuse and therefore, their interpretation is subject to error. Furthermore, the 14 and 10 Å spacings indicated

Figure 10. The low angle x-ray diffraction pattern of a disc specimen
of oxidized feather keratin fibrils

The intermediate angle diffractions are shown best on the
left pattern. The low angle diffractions are shown on the
right pattern.

Figure 11. The wide angle x-ray diffraction pattern of a disc specimen
of oxidized feather keratin fibrils

Figure 12. The wide angle x-ray diffraction pattern of a rod specimen
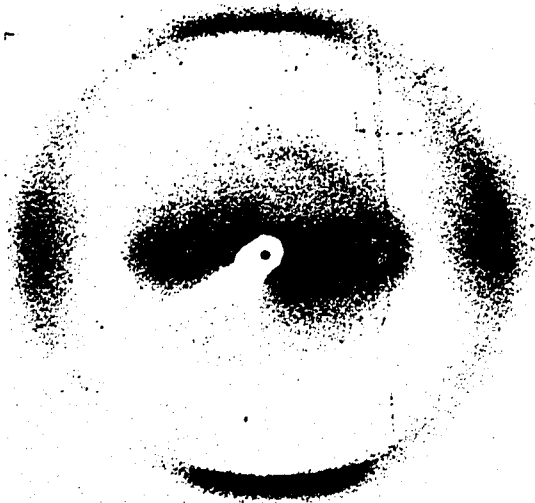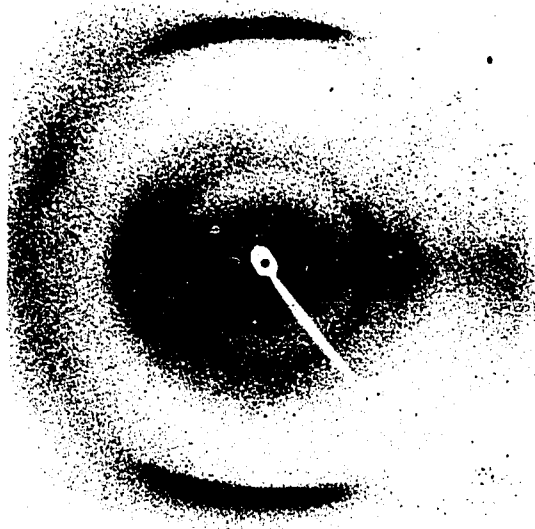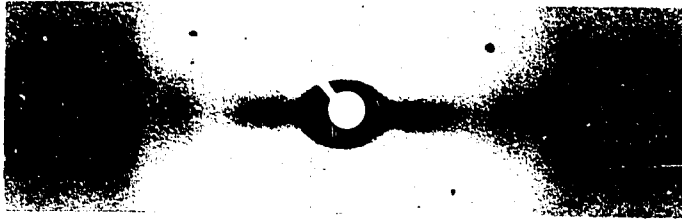of S-carboxy-methylated feather keratin fibrils

Table 4. The wide angle x-ray diffraction data for S-carboxy-methylated and oxidized feather keratin fibrils oriented by the rod and disc methods

Miller indices h k l	Spacings observed[a] (Å)		Spacings calculated (Å)
S-carboxy-methylated fibrils			
0 1 0	13.8	m	13.8
0 0 2	9.74±0.09	vs	9.74
0 1 2	7.95±0.10	m	7.95
0 1 4	4.52±0.10	w	4.59
0 2 4	3.85±0.03	w	3.98
0 4 3	3.05	m	3.05
1 0 0	4.70	vs	4.70
1 1 0	4.48	s	4.45
1 0 1			4.57
1 0 4			3.38
1 0 3	3.59	m	3.81
2 0 0	2.349	m	2.350
Oxidized fibrils			
0 1 0	14.4	m	14.4
0 0 1	9.9	vs	9.9
0 1 1			8.16
0 2 0	7.53	md	7.20
1 0 0	4.67	vs	4.67
1 0 1	4.51	s	4.55
1 1 0			4.45
2 0 0	2.364	m	2.335
2 0 2	2.178	w	2.133

[a]The intensity is indicated after the spacing by vs = very strong, s = strong, m = medium, w = weak and d = diffuse.

by the intermediate angle diffractions are subject to error because of possible contributions to them by lattice related to the fibril dimensions. It is interesting that the fifth order of the 69 Å fibril dimension is near 14 Å and that the seventh order is near 10 Å. For these

Table 5. The dimensions of the orthogonal pseudo unit cell of S-carboxy-
          methylated and oxidized feather keratin fibrils

Side	Dimension	
	S-carboxy-methylated fibrils ($\mathring{A}$)	Oxidized fibrils ($\mathring{A}$)
a	4.70	4.67
b	13.8	14.4
c	19.5	9.9

reasons, the b and c dimensions of the pseudo unit cell of Table 5 might
be off by as much as 1 $\mathring{A}$.

Two β structures were proposed by Pauling and Corey (1951) after
a systematic survey of proteins in which the arrangement of the amide
groups were restricted to certain orientations. The structures were
the parallel and antiparallel chain pleated sheets. The fiber axis
identity distance calculated for the parallel β structure was 6.5 $\mathring{A}$
and that for the antiparallel β structure was 7.0 $\mathring{A}$. The lateral dis-
placement in the hydrogen bond direction between equivalent parallel
chains was 4.85 $\mathring{A}$ in the parallel β structure and between equivalent
chains of the antiparallel β structure was 9.50 $\mathring{A}$.

Several antiparallel cross-β structures have been subjected to
detailed x-ray diffraction analysis (Arnott et al. 1967, Geddes et al.
1968). All of these structures with the exception of poly-L-alanine
have diffraction patterns which agree with the antiparallel β structure
proposed by Pauling and Corey (1951). In poly-L-alanine there is no

diffraction requiring a 9.5 Å spacing in the hydrogen bond direction; however, the diffraction pattern fits in all other respects to the anti-parallel β structures. Arnott suggested that the absence of a 9.5 Å spacing in the hydrogen bond direction was due to a statistical displacement of peptide chains in which nearest neighbor chains in the side chain direction are displaced randomly by ± one half of the 4.7 Å spacing in the hydrogen bond direction. This explanation cannot be invoked with the fibrils. β structures which are predominately parallel chain pleated sheets have not been reported.

In the orthogonal pseudo unit cell proposed for the fibrils, the 14 Å spacing is twice the fiber axis identity period. The 14 Å spacing is not reliable in the feather keratin fibrils, and therefore, cannot be used to distinguish between parallel and antiparallel β structure. The 10 Å spacing is the side chain identity period and is not relevant to this discussion. This leaves the lateral displacement identity period with which to make distinction between β structures. This hydrogen bond spacing indicates that the OxFK and SCMFK fibrils have parallel cross-β structures.

It is difficult to relate the low and wide angle x-ray diffraction data with the available diffraction patterns. However, the evidence available indicates that the 90 Å fibril width and the 10 Å side chain identity period are in the same direction. In specimens oriented by the disc method the low angle meridional diffractions, which correspond to the spacings in the same direction as the 90 Å spacing, should be ring-like with greatest intensity on the equator. The equatorial dif-

fraction corresponding to the 58 Å spacing and the higher angle diffractions corresponding to spacings in that same direction should have little or no meridional intensity. The reflection corresponding to the 10 Å side chain spacing appears most ring-like and therefore, is most likely to be in the same direction as the 90 Å spacing. The 14 Å chain spacing likewise appears to be in the same direction as the 58 Å spacing.

Infrared studies of feather keratin fibrils

The amide I IR absorption band of the peptide group in polypeptides is quite sensitive to secondary structure. This absorption originates from molecular vibrations of the four atoms of the carbonyl stretching vibration. Various perturbations due to hydrogen bonding and other interactions split this absorption band in a predictable fashion enabling the distinction between the parallel and antiparallel β structure (Miyazawa 1960, Bradbury and Elliott 1963). The amide I band of the parallel and antiparallel β structure is at 1632 cm^{-1}. In the antiparallel β structure a component of the amide I band is predicted at or near 1690 cm^{-1}.

IRD spectra were made on solid samples of OxFK and SCMFK fibrils. Polarized IR radiation was passed normal and parallel to the oriented fibrils and their absorption spectrum was recorded as $A_{\perp}$ and $A_{\parallel}$ respectively (Figure 13). Table 6 lists the amide I and II frequencies of the fibrils and those theoretically predicted and experimentally observed with synthetic polypeptides. Although β structure is clearly indicated by the fibril absorption at 1632 cm^{-1} for the amide I band, no component at 1690 cm^{-1} could be detected. The presence of the overlapping absorption centered at 1660 cm^{-1} might obscure any weak band near 1690 cm^{-1}.
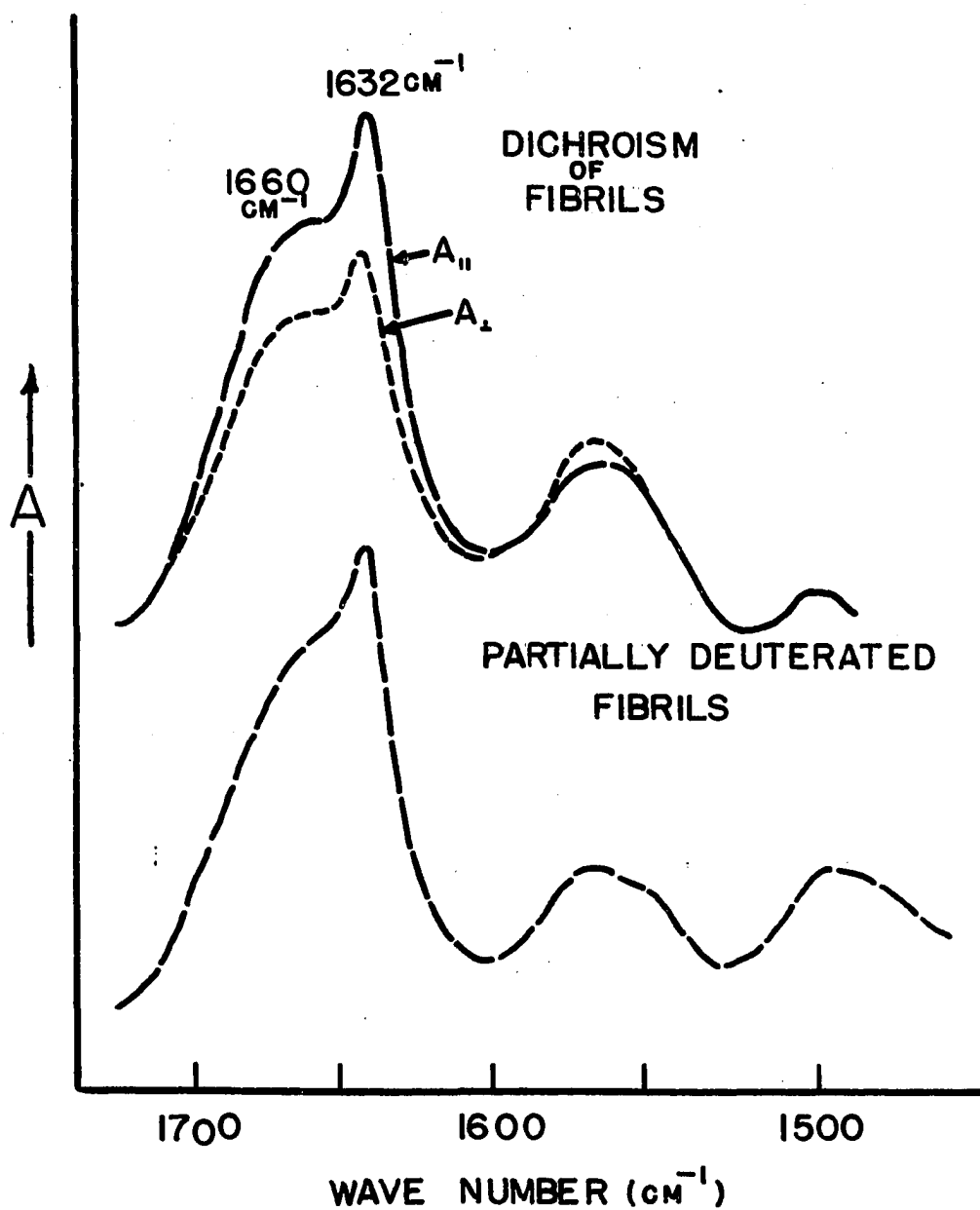
Figure 13. The infrared dichroism spectra and infrared spectra of oxidized feather keratin fibrils and partially deuterated oxidized feather keratin fibrils

Table 6. The amide I and II absorption bands for the feather keratin
fibrils and synthetic polypeptides

Material	Amide I^a (cm^{-1})	Amide II^a (cm^{-1})
OxFk fibrils	1632 s ll	1543 s ⊥
	1660 m	
SCMFK fibrils	1632 s ll	1540 s ⊥
	1660 m	1650
α-helix theoretical[b]	1650 $\nu_{//}$ (0)	1516 $\nu_{//}$ (0)
	1647 $\nu_{\perp}$ (2π/n)	1546 $\nu_{\perp}$ (2π/n)
α-helix experimental[c]	1650 s ll	1516 m ll
	1652 m⊥	1546 s ⊥
Antiparallel β structure theoretical[b]	1685 $\nu_{//}$ (0π)	1530 $\nu_{//}$ (0π)
	1668 $\nu_{\perp}$ (ππ)	1550 $\nu_{\perp}$ (ππ)
	1632 $\nu_{\perp}$ (π0)	1540 $\nu_{\perp}$ (π0)
Parallel β structure theoretical[b]	1648 $\nu_{//}$ (00)	1530 $\nu_{//}$ (00)
	1632 $\nu_{\perp}$ (π0)	1550 $\nu_{\perp}$ (π0)
β structure experimental Silk[d]	1701 m ll	1525 vs ll
	1657 m	1540 vw
	1632 vs⊥	
Poly-L-alanylglycine[d]	1702 vw⊥	1535 s ⊥
	1630 vs ll	
Poly-β-n-propyl-L-asparate[e]	1700 w ⊥	1530 m ⊥
	1632 vs ll	1532
Poly-γ-benzyl-L-glutamate[e]	1692 w ⊥	1525 m ⊥
	1623 s ll	
Poly-S-carbobenzoxy-L-cysteine[f]	1678 vw⊥	1503 m ⊥
	1641 vs ll	1547 w ⊥
Poly-S-carboxymethyl-L- cysteine[g]	1690 vw	1527 m
	1624 vs	
Random coil theoretical[b]	1658	1535
Random coil experimental[b]	1656 s	1535 s

^{a}The intensity and the dichroism of the absorption band appear after the absorption band; s, m and w indicate strong, medium and weak intensity and // and ⊥ indicate parallel and perpendicular dichroism.
[b]Miyazawa and Blout 1961.
[c]Bamford et al. 1956.
[d]Fraser et al. 1965.
[e]Bradbury et al. 1960.
[f]Elliott et al. 1964.
[g]Ikeda 1967.

In order to determine the origin of the 1660 cm^{-1} absorbance and to check the spectrum at 1690 cm^{-1}, vapor phase deuterium exchange experiments were performed (Figure 13). After treatment with deuterium vapor, the 1660 cm^{-1} absorbance shifted to lower frequencies leaving the other amide I absorption bands unaffected. This indicated the incorporation of deuterium into those peptide groups responsible for the 1660 cm^{-1} absorption. The rapidity with which the deuterium exchange took place suggests that random coil must be present in the preparation. This interpretation is in accord with the absorption at 1660 cm^{-1} by random coil synthetic polypeptides. Even with the shifting of the 1660 cm^{-1} band, a 1690 cm^{-1} amide I absorption could not be detected. Although this data cannot be used to show that a weak 1690 cm^{-1} absorption band does not exist, it can be used to show that a 1690 cm^{-1} band of moderate strength is nonexistent. If the 1690 cm^{-1} component of the amide I band of the fibrils were as strong as it is in the antiparallel β structure of silk, this IR technique would have uncovered it without difficulty. Because of the absence of a 1690 cm^{-1} band, it appears that the OxFK and SCMFK fibrils are parallel β structures.

The dichroism of the amide I and amide II absorption indicates that the hydrogen bonds are parallel to the long axis of the fibrils. This implies that the peptide chains are normal to the long axis of the fibrils and therefore, in a cross-β structure. These IR results are satisfied by parallel cross-β structured fibrils which have incorporated with them finite amounts of random coil protein.

Circular dichroism and optical rotatory dispersion of feather keratin fibrils

In order to further establish the secondary structure of the fibrils and to examine their structure in solution, the ORD and CD of an aqueous solution of fibrils were measured (Figure 14 and 15). These two UV optical properties, related by the Kronig-Kramer transform, are powerful tools in the elucidation of secondary protein structure. Experimental evidence indicates that the α-helix, random coil and β structure conformation of synthetic polypeptides can be distinguished by their optical properties. The CD of experimentally observed β structures has a negative dichroic band at 218 nm and a positive band at approximately 195 nm (Table 7). The ORD of β structures has a trough with minimum at 230 nm (Table 8).

The negative circular dichroism band at 218 nm obtained with OxFK and SCMFK fibrils indicates the presence of β structure. The magnitude of the ORD trough at 232 nm backs up this conclusion. Although these results indicate β structure, the particular type of β structure present is difficult to extract from ORD and CD measurements. Extensive theoretical studies involving a quantum mechanical analysis of the UV optical properties indicate that the parallel and antiparallel β structures should have significantly different ORD and CD (Pysh 1966, Rosenheck and Summer 1967). Unfortunately, attempts to predict the form of structure experimently observed using the theoretical approach lead to some ambiguities that render structure characterization questionable. In general, it can be said that if the dichroic bands at 218 nm and 196 nm, that are experimently observed in synthetic polypeptides, represent the
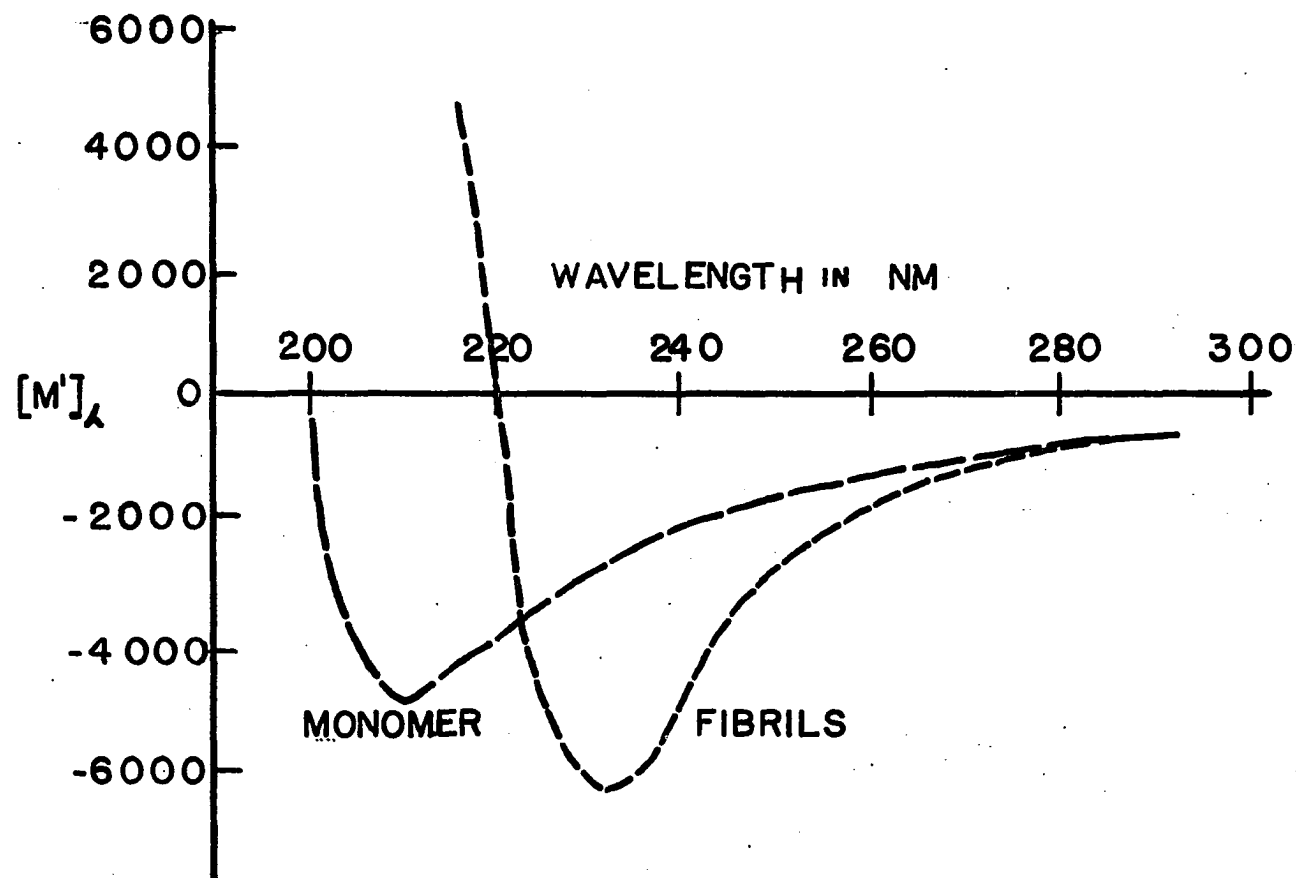
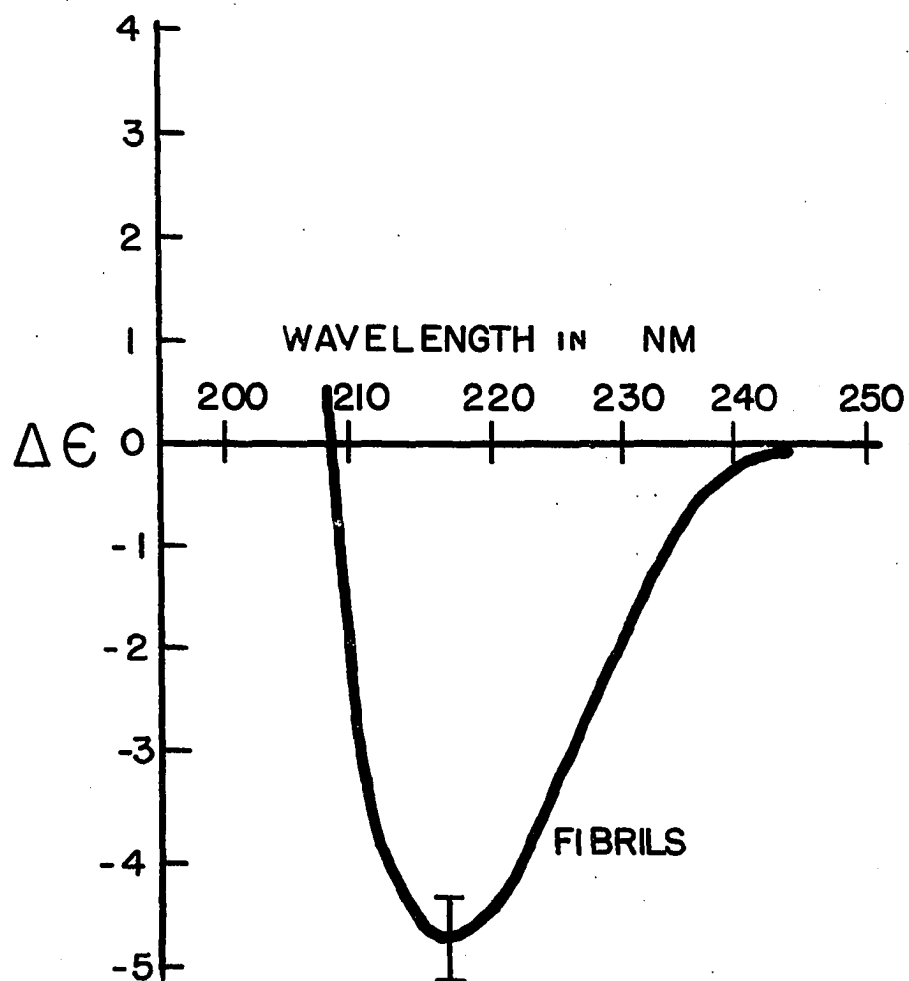Figure 14. The optical rotatory dispersion of oxidized feather keratin fibrils and monomer

Figure 15. The circular dichroism of oxidized feather keratin fibrils

Table 7. The circular dichroism of β structures and feather keratin fibrils

Material	Negative bands		Positive bands	
	λ(nm)	Δε	λ(nm)	Δε
Feather keratin	218	-5.7±0.7		
Poly-L-lysine in H_2O[a]	217	-5.85±0.85	195	8.5±1.2
Poly-L-lysine in H_2O[b]	218	-7.30		
Poly-L-lysine in SDS[c]	217	-3.5	197	12
Poly-L-lysine in SDS[b]	217	-2.7		
Silk fibroin in 93% methanol[d]	218	-3.0	197	10

[a]Townend et al. 1966.
[b]Sarkar and Doty 1966.
[c]Timasheff et al. 1967.
[d]Iizuka and Yang 1966.

antiparallel β structure, the parallel β structure will have dichroic bands at approximately the same frequency but of larger magnitudes than in the antiparallel β structure. If on the other hand, the experimentally observed bands represent the parallel β structure then the antiparallel β structure will have dichroic bands of smaller magnitudes. It appears that most β structure synthetic polypeptides, experimentally observed, have a mixture of parallel and antiparallel β structure. It can not be shown in these structures that either parallel or antiparallel β structure predominates.

In interpreting the magnitude of the CD bands at 218 nm and 195 nm, caution must be exercised. The rotational strengths of these two cotton

Table 8. The optical rotatory dispersion of β structures and feather keratin fibrils

Material	Trough		Peak	
	λ(nm)	[m']	λ(nm)	[m']
Feather keratin	232	-6190		
Poly-L-lysine[a]	230	-6300	204-5	+23000
Co-poly-L-lysine-L-tyrosine[a]	230	-6500	205	+21500
Poly-L-lysine[b]	230	-6220	205	+29200
Silk fibroin[c]	229-30	-5000	205	+24000

[a]Sarkar and Doty 1966.
[b]Davidson et al. 1966.
[c]Iizuka and Yang 1966.

effects in polypeptides depend strongly on the presence of sodium dodecyl sulfate (SDS) in the polypeptide solutions (Timasheff et al. 1967, Sarkar and Doty 1966). The effect of SDS is to reduce the rotational strength at 218 nm and increase it at 195 nm by a factor of two. This detergent presumably provides a nonpolar environment somewhat resembling that within globular proteins. These pleated sheets of synthetic polypeptides are assumed exposed to water when SDS is not present. This strong dependence of the optical properties of β structures on their environment makes the application of the theoretical results of Rosenheck and Summer (1967) and Pysh (1966) of no value in determining the type of structure present in the fibrils.

Simple comparison of the optical properties of the presumed antiparallel β structure of synthetic polypeptides and reconstituted silk

with the β structure of the fibrils shows many similarities. However, due to the uncertainity of the extent of β structure in all of these materials along with the effect that different β structure environments have, it does not necessarily follow that the fibril β structure is antiparallel.

Hydrodynamic properties of the feather keratin fibrils in guanidine hydrochloride

The fibril fraction forms from a solution containing a number of components, and therefore, the makeup of the fibrils is unknown. In order to determine the makeup of the fibrils, a detailed hydrodynamic investigation of the OxFK fibrils dissolved in guanidine hydrochloride was undertaken. This investigation involved the evaluation of sedimentation coefficient, diffusion coefficient and intrinsic viscosity (Figures 16, 17 and 18).

Extensive evidence presented by Tanford et al. (1967) shows that native globular proteins when dissolved in concentrated guanidine hydrochloride have the hydrodynamic properties of random coils. With random coils, hydrodynamic parameters such as intrinsic viscosity ([η]) and frictional coefficient (f) can be related directly to the number of amino acid residues per protein chain (σ) by equations 14 and 15 (Figures

$$f_o/\eta_o = 0.34\sigma^{0.5\,8} \qquad\qquad \text{(Eq. 14)}$$

$$[\eta] = 0.80\sigma^{0.6\,4} \qquad\qquad \text{(Eq. 15)}$$

19 and 20). The viscosity of the solvent is represented by η_o. In order to use these equations, it is necessary to establish that the fib-

Figure 16. The sedimentation velocity of oxidized keather keratin fibrils dissolved in 6 molar
guanidine hydrochloride

The centrifugations were performed in double sector synthetic boundary cells. The
concentration was determined by the area of the schlieren peaks.

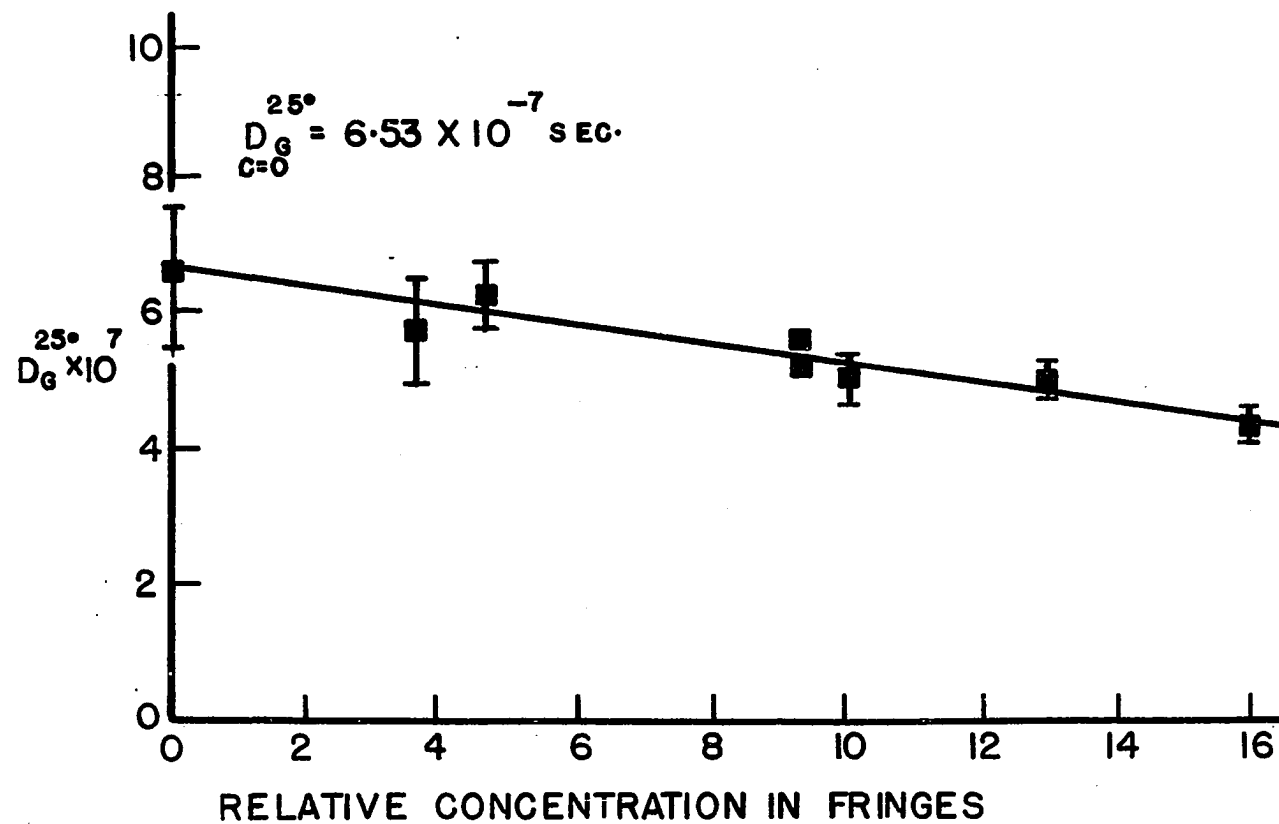$$S_G^{25°} = 0.483 \pm 0.084 \times 10^{-13} \text{ SEC}^{-1}$$
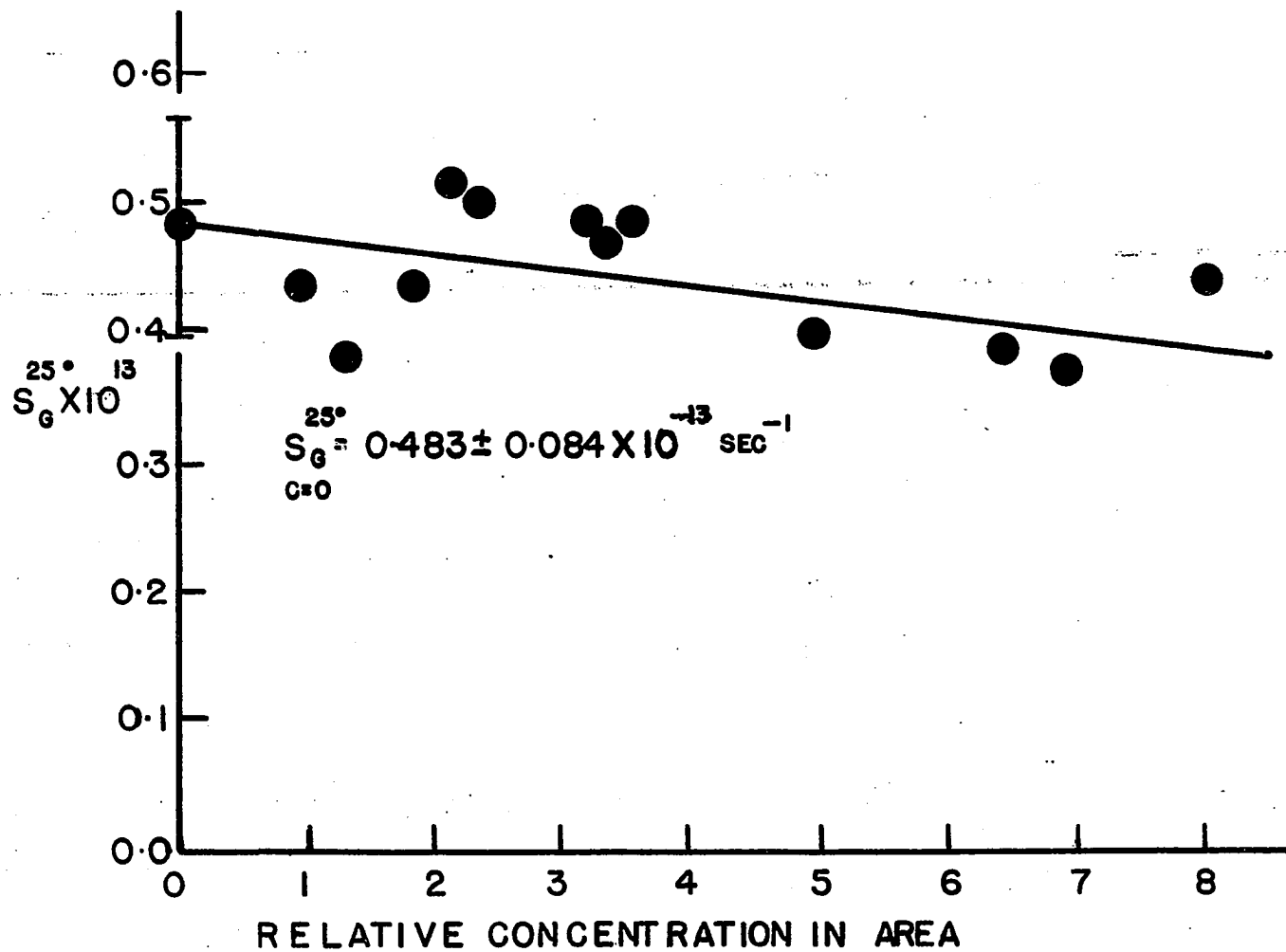
Figure 17. The diffusion coefficient of oxidized feather keratin fibrils dissolved in 6 molar guanidine hydrochloride
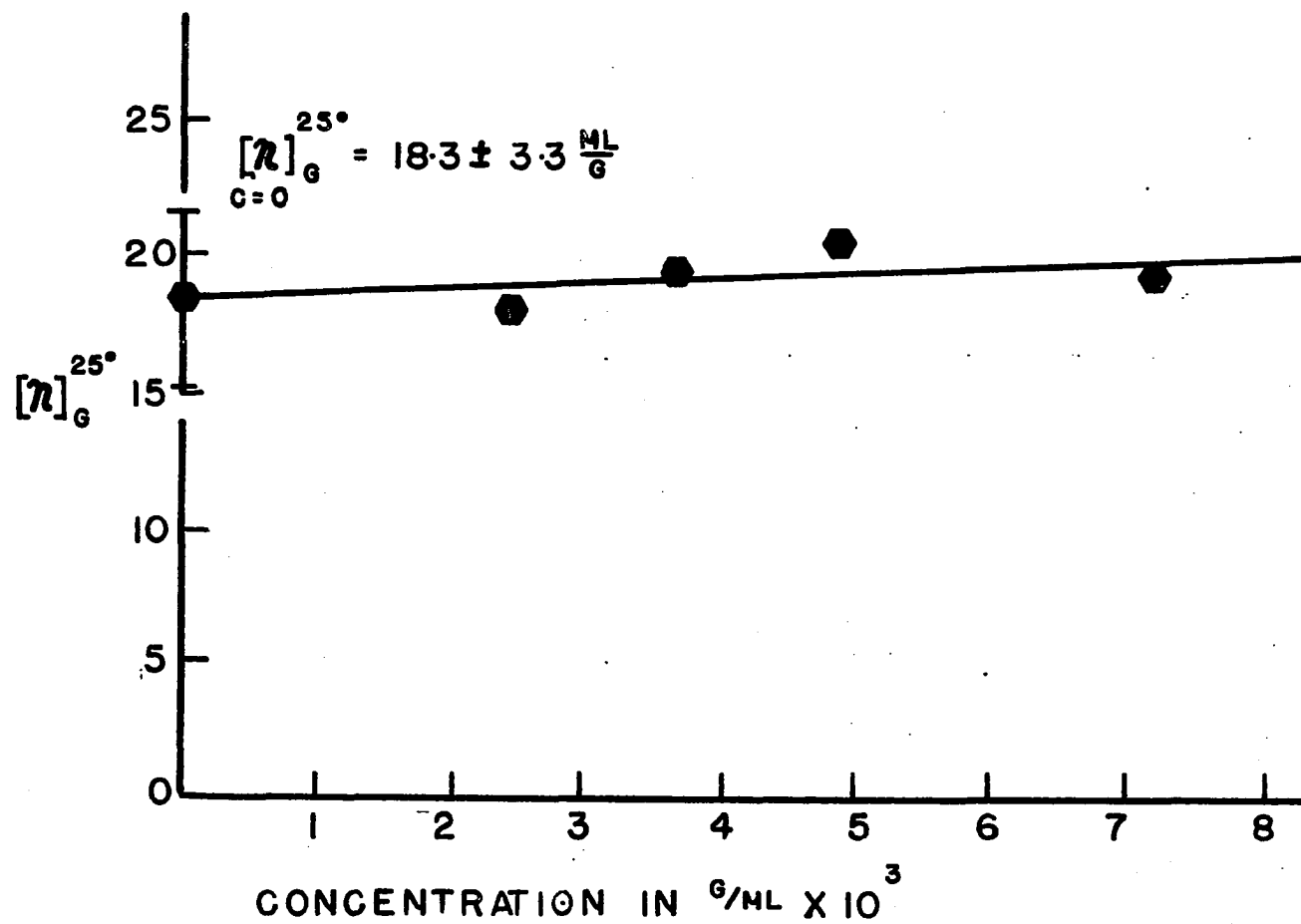
Figure 18. The intrinsic viscosity of oxidized feather keratin fibrils dissolved in 6 molar guanidine hydrochloride

Figure 19. The frictional coefficient as a function of protein chain length in 6 molar guanidine hydrochloride

This data was recalculated from sedimentation coefficients given by Tanford et al. (1967).

Figure 20. The intrinsic viscosity as a function of protein chain length in 6 molar guanidine hydrochloride

This data was taken directly from Tanford et al. (1967).

$f/n_{\circ} = 0.34 \, \sigma^{0.58}$

$[n] = 0.80 \, \sigma^{0.64}$
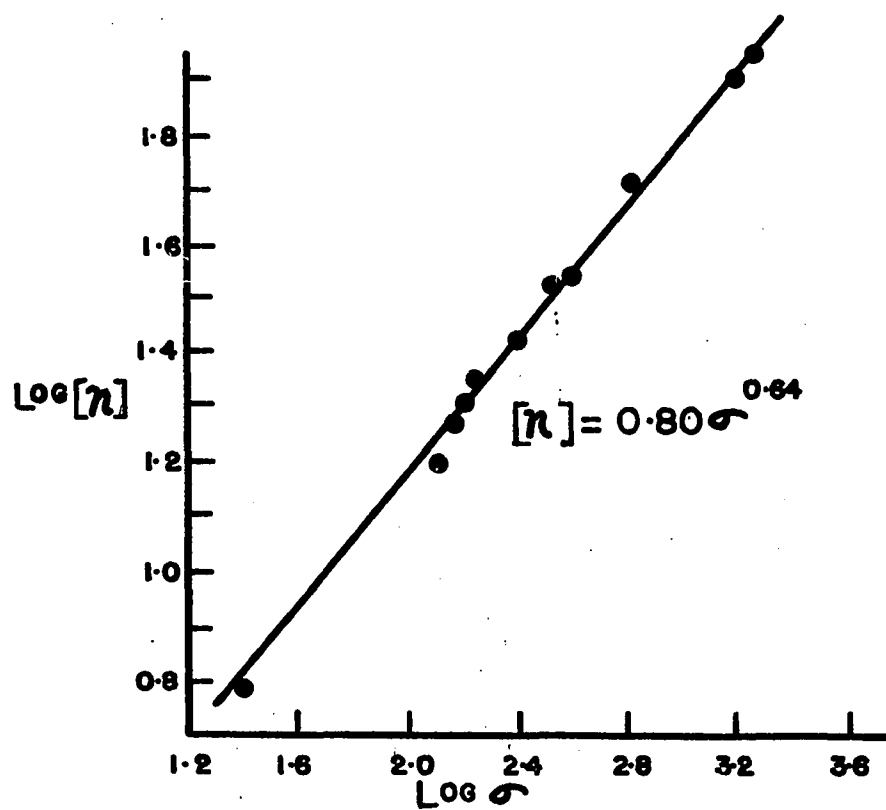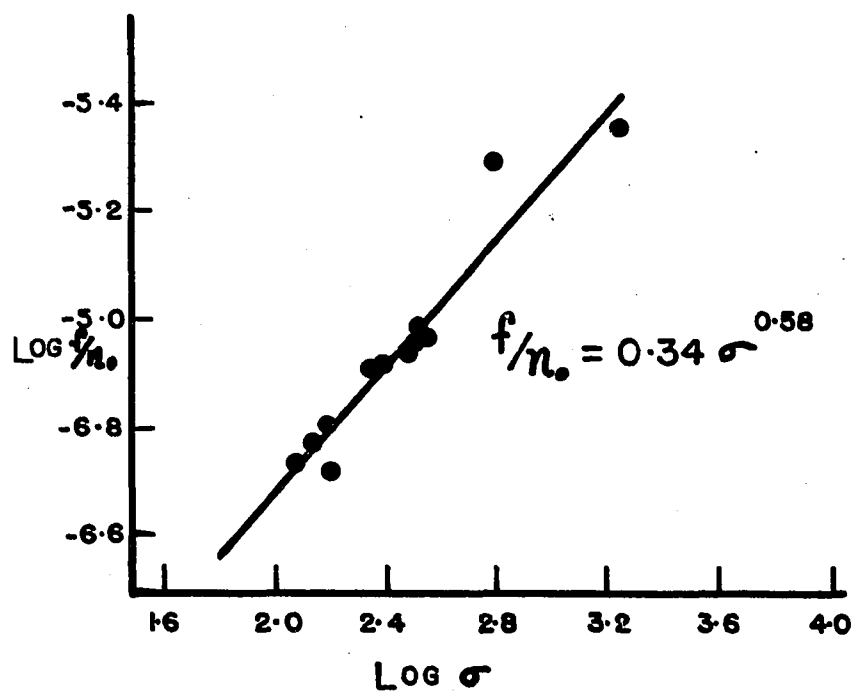
ril components are random coils in guanidine hydrochloride.

The random coil characteristics were established using the combined Flory-Fox (1951) and Mandelkern-Flory (1952) equations (Equation 16).

$$\Phi^{1/3}P^{-1} = \left(\frac{s[\eta]D^2 N_o^3 \eta_o}{R^2 T^2 (1-\overline{v}\rho)} \right)^{1/3}$$ (Eq. 16)

Here N_o is Avogadro's number, R is the universal gas constant, T is the absolute temperature, $\overline{v}$ is the partial specific volume, ρ is the density of the solvent and $\Phi^{1/3}P^{-1}$ is a universal constant. For random coils the theoretically predicted value for $\Phi^{1/3}P^{-1}$ is 2.45×10^6. The value obtained for the fibrillar component is 2.50×10^6, well within the experimental range found for random coils (Scheraga 1961). Therefore, equations 14 and 15 are valid for the fibrillar components.

The sedimentation velocity and diffusion coefficient are related to the frictional coefficient by equations 17 and 18. M, the molecular

$$s = M(1-\overline{v}\rho)/N_o f$$ (Eq. 17)

$$D = RT/N_o f$$ (Eq. 18)

weight, is related to the number of amino acid residues per chain (σ) and mean residue molecular weight (M_o) by equation 19. By combining

$$M = \sigma M_o$$ (Eq. 19)

equations 14, 17 and 19 with the sedimentation coefficient of Figure 16, the number of residues in the fibrillar components can be determined. The number of amino acid residues per component molecule is 93. Equations 14 and 18 and the diffusion coefficient of Figure 17 indicate 84 residues per molecule. The intrinsic viscosity indicates 130 residues per molecule. Based on the Svedberg equation (Equation 20), the diffu-

$$s/D = M(1-\overline{v}\rho)/RT$$ (Eq. 20)

sion coefficient and the sedimentation velocity, the molecular weight of the fibrillar components is 9500 g/mole. These results clearly indicate that the fibrils are composed of the monomer component which has approximately 100 residues per molecule and a molecular weight of 10^4 g/mole.

Proposed structures for feather keratin fibrils

Electron microscopy and low angle x-ray diffraction indicate that the fibrils have uniform transverse dimensions of 60 and 90 Å. The wide angle x-ray diffraction pattern and IRD of the fibrils show them to have a cross-β structure probably with the parallel chain pleated sheet of Pauling and Corey. These studies are in apparent disagreement with the optical properties of the fibrils which are similar to those of synthetic polypeptides reported to have the antiparallel chain pleated sheet. However, at this time little is known with regards to the optical properties of these two structures, and therefore, the significance of these properties must be left for future investigations. Relating the low and wide angle x-ray diffraction data, it appears that the protein chains are parallel to the 60 Å side of the fibrils.

The fact that all the feather keratin fibrils have the same transverse dimensions deserves some comment. In order for the fibrils to have a uniform cross section, it is necessary that their constituent monomer molecules be allowed by molecular constraints to fold in one and only one fashion. It is possible that the random coil monomer is solely responsible for these molecular constraints; however, the inability to obtain fibrils from pure monomer suggests that an initiating unit must be present. Once a fibril has been initiated its growth probably

involves the fibril end which duplicates the initiating unit.

Incorporating what is known of the fibril structure, two limiting methods of fibril growth from the initiator sight will be discussed. In the first method eight monomer molecules line up on the template which is 60 by 90 Å. The random coil portions of the remaining monomer molecules fold back onto themselves to give rise to an antiparallel β structure. Upon completion of the folding, the eight monomer molecules form a template identical to that to which they are associated. By repeating this process a fibril is formed (Figure 21). Only antiparallel β structures could be generated by this process.

In the second method of fibril growth, two monomer molecules become associated with the template. Both molecules then occupy one 4.7 Å thick layer. These two molecules regenerate the template and the process recycles (Figure 21). By this method either parallel or antiparallel chain pleated sheets can be generated.

Initiation may involve any one of the soluble products larger than monomer which may serve to increase the probability of formation of a stable nucleus for fibril growth.

Insulin Fibrils

Introduction

The globular protein insulin undergoes a reversible linear polymerization under favorable conditions to form submicroscopic fibrils. The chemistry of this transition has been studied extensively by Waugh (1957). There are two proposals for the structure of the fibrils. Koltun et al.
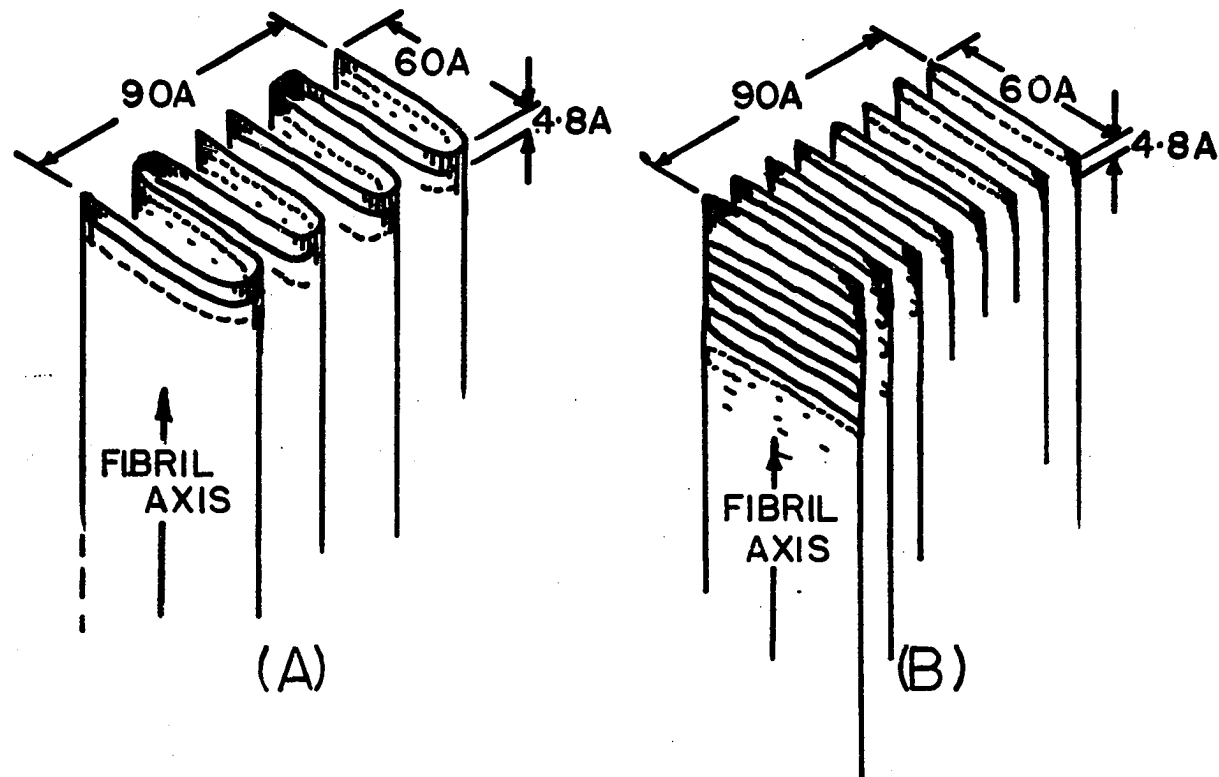
Figure 21.   Two possible models of the fibrillar structure of feather keratin fibrils

(1954) on the basis of a detailed x-ray diffraction analysis of the fib-
rils proposed that the fibrils are composed of a linear array of slightly
distorted globular insulin molecules. On the other hand, Ambrose and
Elliott (1951) proposed on the basis of IRD and a preliminary x-ray
diffraction analysis of the fibrils, that the fibrils are composed of
polypeptide chains in the β configuration laying perpendicular to the
fibril axis. Based on evidence from electron microscopy, x-ray diffrac-
tion, IRD, optical activity and optical density, a more precisely defined
structure is proposed. This structure is similar to that proposed by
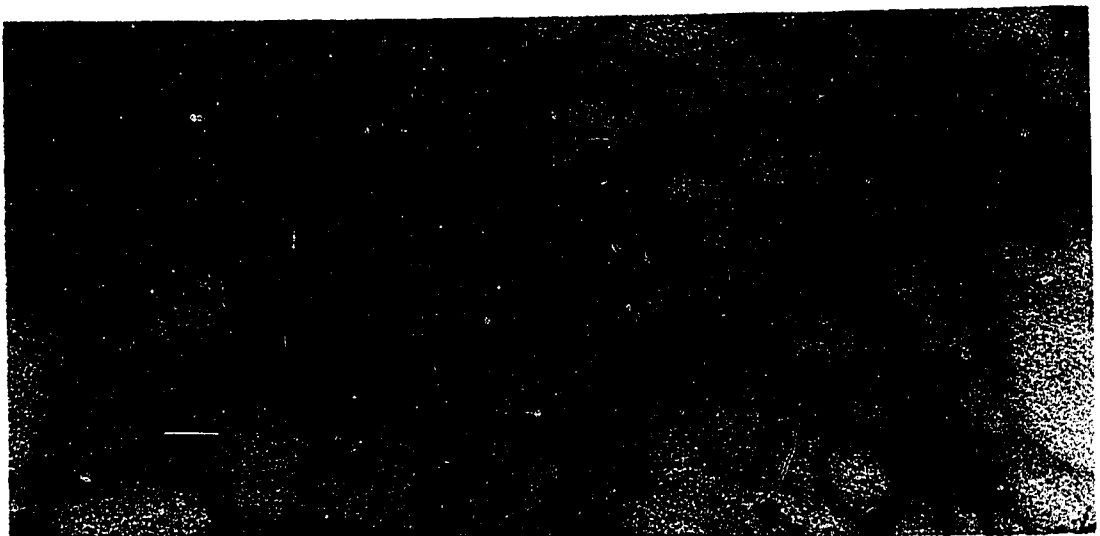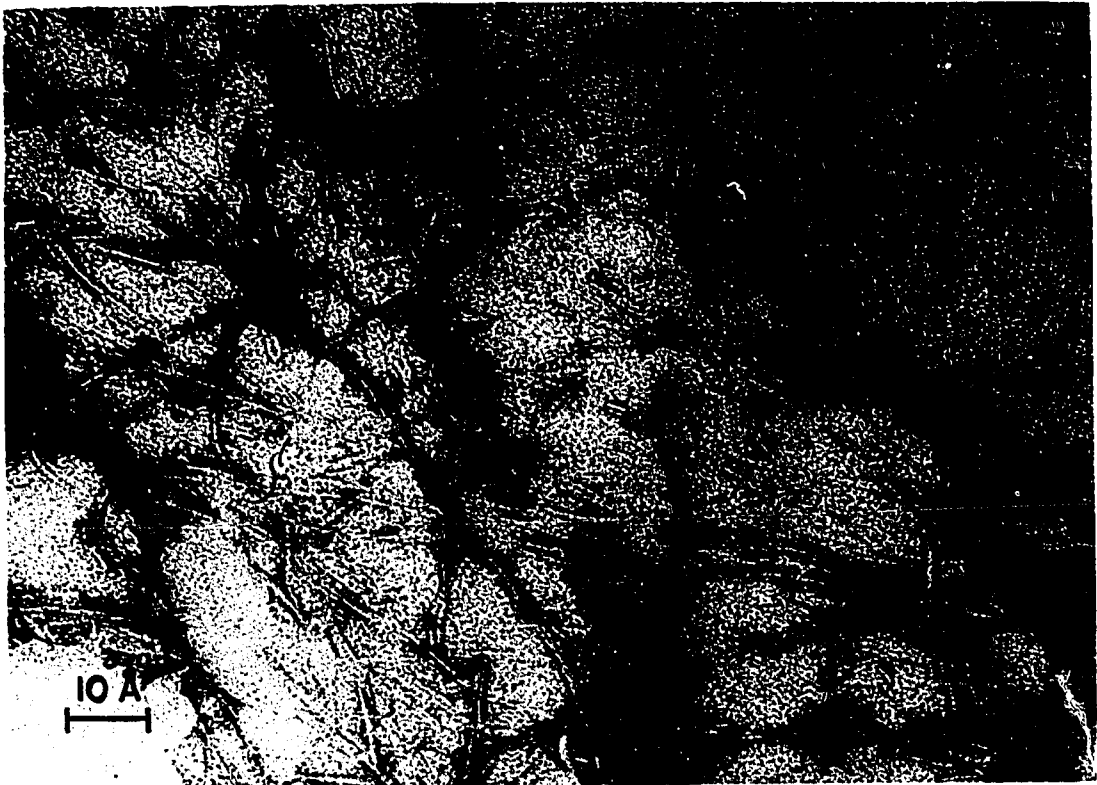Ambrose and Elliott.

Electron microscopy of fibrillar insulin

As seen in the electron microscope, insulin fibrils are long having
irregular diameters (Farrant and Mercer 1952, Kung and Tsao 1964).
Investigations of fibrils which were negatively stained with uranyl
formate show that the insulin fibrils observed are composed of bundles
of smaller laterally aggregated fibrils. These smaller fibrils which
have a cross sectional dimension of approximately 40 Å were more fre-
quently observed in fibril preparations which had been frozen prior to
negative staining (Figures 22 and 23). Freezing and thawing of insulin
fibrils causes partial disruption of the fibrils inducing drastic changes
in the viscosity of the fibril solution. Kung and Tsao (1964) who also
have found 40 Å diameter fibrils report that they are composed of two
25 to 30 Å diamter fibrils laterally associated. The micrographs on
which the Kung and Tsao proposal is based do not clearly show small
fibrillar components. In any case, they concluded that the structure

Figure 22.   Insulin fibrils negatively stained with uranyl formate

The laterally aggregated fibrils have widely varying diam-
eters, the smallest of which are 40 Å in diameter.

Figure 23.   Insulin fibrils negatively stained with uranyl formate

proposed by Ambrose and Elliott can not be accommodated by the smaller fibrils they observed.

X-ray diffraction studies of insulin fibrils

Two methods of specimen orientation have been found suitable for x-ray investigation of fibrils. They are the rod and disc methods described previously.

In this treatment of the x-ray diffraction pattern of insulin fibrils, the low and wide angle diffractions are treated independently. The low angle x-ray diffraction patterns of the rod and disc specimens of insulin fibrils are not significantly different, and therefore, only the diffraction pattern of the rod specimens will be described (Figure 24). In the rod specimen there are two discrete low angle diffractions on the equator and one on the meridian. The equatorial diffractions represent spacings of 30 and 15.3 $\overset{o}{A}$. These spacings which probably involve the cross sectional dimensions of the insulin fibrils are the first and second orders of 30 $\overset{o}{A}$. The 30 $\overset{o}{A}$ spacing probably is the average separation between fibril centers. The diffuseness of the diffractions indicates poor fibril packing.

These low angle results are in serious disagreement with those reported by Koltun et al. (1954). In that study the fibrils were oriented by stroking a film of the insulin gel. Their method of specimen orientation is expected to give results similar to the disc method described previously. In the Koltun diffraction pattern there were four low and intermediate angle diffractions on the equator and three intermediate angle diffractions on the meridian. The equatorial diffractions

Figure 24.   The x-ray diffraction pattern of a rod specimen of insulin
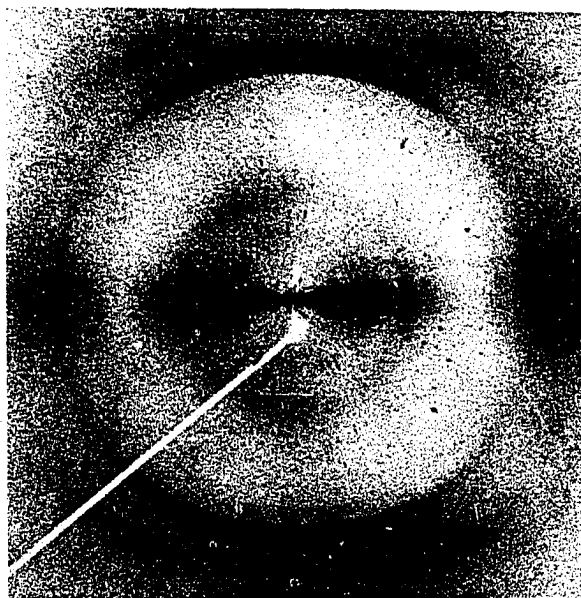   fibrils

Figure 24. The x-ray diffraction pattern of a rod specimen of insulin fibrils

represented spacings of 55, 30.8, 14.0 and 11.8 Å. The meridional diffractions represented spacings of 16.1, 12.0 and 8.2 Å. In the Koltun specimens, equatorial diffractions must have involved the transverse dimensions of the fibrils. Two of these diffractions, those representing the 30.8 and 14.0 Å spacings, are in fair agreement with the results from rod specimens. The other two equatorial diffractions have escaped detection in experiments specifically designed for their detection and, therefore, were probably artifacts. As pointed out earlier, fibril meridional diffractions in the disc or Koltun specimens may be related to either axial or transverse fibrillar periodicities. Evidence for axial periodicities should be found also on the meridian of rod specimens. Since this is not true, the intermediate angle meridional diffractions must refer to transverse spacings with this transverse direction preferably oriented in the plane of the specimen. It is possible that the meridional diffractions representing the 16.1 and 8.2 Å spacings are on the equator of rod specimens. No evidence for a diffraction representing a 12.0 Å spacing can be found in rod specimens (Table 9).

Koltun et al. (1954) proposed that the insulin fibrils were composed of a linear array of slightly distorted globular insulin molecules. His proposal depended on a 55 Å cross sectional spacing and the three longitudinal spacings of 16.1, 12.0 and 8.2 Å which order to 48 Å. In the low and intermediate angle x-ray diffraction patterns of rod and disc specimens, no evidence for these spacings was found on the meridian.

The wide angle x-ray diffraction pattern obtained with rod specimens of insulin fibrils is shown in Figure 24. The rod and disc diffrac-

Table 9. The x-ray diffraction data for insulin fibrils

Longitudinal spacings ($\overset{o}{A}$)		Lateral spacings ($\overset{o}{A}$)	
Koltun[a]	This study	Koltun[a]	This study
16.1		55	
12.0		30.8	30
8.2		14.0	15.3
4.79	4.73	11.8	
4.12		9.5	9.58
3.80	3.92	8.0	7.75
3.54	3.48	6.9	6.90
2.40	2.387	5.5	5.53
2.25	2.230		4.73
			4.07
		3.08	2.883
		2.77	

[a]Koltun et al. 1954.

tion patterns show no significant differences, and therefore, the diffraction patterns of only rod specimens will be discussed. The most striking feature of the x-ray diffraction patterns of insulin fibrils is the strong sharp meridional diffraction representing a 4.7 $\overset{o}{A}$ spacing. When the 4.7 $\overset{o}{A}$ spacing is on the meridian as it is here, it indicates a cross-β structure. Table 10 contains a list of the other spacings and Miller indices assigned to them. Comparison of these spacings with those for

Table 10. The wide angle x-ray diffraction data for insulin fibrils
oriented by the rod and disc methods

Miller indices h k l	Spacings observed[a] (Å)		Spacings calculated (Å)
0 0 1	9.58	m	9.58
0 1 1	7.75	md	7.87
0 2 0	6.90	wd	6.90
0 2 1	5.53	m	5.64
0 0 2			4.79
0 3 0	4.73	w	4.60
0 2 2	4.07	m	3.90
0 4 2	2.883	w	2.788
1 0 0	4.73	vs	4.73
1 1 1			4.04
1 2 0	3.92	s	3.90
1 2 1			3.60
1 0 2			3.59
1 2 1	3.48	w	3.35
2 0 0	2.387	m	2.365
2 2 0			2.256
2 2 1	2.230	m	2.192

[a]The intensity is indicated after the spacing by vs = very strong,
s = strong, m = medium, w = weak and d = diffuse.

feather keratin fibrils shows much in common. These spacings are indexed to an orthogonal pseudo unit cell having the dimensions given in Table 11. All the equatorial diffractions were diffuse and therefore, their interpretation is subject to error.

Two β structures were proposed by Pauling and Corey (1951), the parallel and antiparallel chain pleated sheets. In the orthogonal pseudo unit cell proposed for the insulin fibrils, the 13.8 $\overset{\circ}{A}$ spacing is twice the fibril axis identity period. This spacing is probably reliable only to about 0.5 $\overset{\circ}{A}$ and therefore, is not accurately enough determined to warrant its use in distinguishing between the parallel and antiparallel pleated sheets. The 9.58 $\overset{\circ}{A}$ spacing is the side chain identity period and can not be used to distinguish between the two β structures. This leaves the lateral displacement identity period with which to make the distinction between β structures. This hydrogen bond spacing indicates that insulin fibrils have parallel cross-β structure.

Table 11. The dimensions of the orthogonal pseudo unit cell of insulin fibrils

Side	Dimension ($\overset{\circ}{A}$)
a	4.73
b	13.8
c	9.58

Infrared studies of insulin fibrils

The amide I IR absorption band of the peptide group in polypeptides has been discussed in a previous section. IRD spectra were made on solid samples of the insulin fibrils and native insulin. Polarized IR radiation was passed normal and parallel to the oriented fibrils and their absorption spectrum was recorded as $A_\perp$ and $A_\parallel$ respectively (Figure 25). Table 6 and 12 list the amide I and II frequencies of the fibrils and those theoretically predicted and experimentally observed for synthetic polypeptides. Although β structure is clearly indicated by the fibril absorption at 1632 cm^{-1} for the amide I band, no component at 1690 cm^{-1} could be detected. The presence of an overlapping shoulder centered at 1740 cm^{-1} might obscure any weak band near 1690 cm^{-1}. This shoulder which is also present in the IR spectrum of native insulin films, probably originates from the many primary amides present in insulin. The weak shoulder at 1660 cm^{-1} could originate from β structure or non-hydrogen bound insulin in the fibrils or from native insulin. Although this data cannot be used to show that a weak 1690 cm^{-1} absorption band does not exist, it can be used to show that a 1690 cm^{-1} band of moderate strength is nonexistent. If the 1690 cm^{-1} component of the amide I band of the fibrils were nearly as strong as it is in the antiparallel β structure of silk, this IR spectra would have uncovered it without difficulty. Because of the absence of a 1690 cm^{-1} band, it appears that the insulin fibrils have a parallel β structure.

The dichroism of the amide I and II absorption bands indicate that the hydrogen bonds are parallel to the long axis of the fibrils. This implies that the peptide chains are normal to the long axis of the fib-

Figure 25.   The infrared dichroism spectra of fibrous insulin and the
             infrared spectra of native insulin

             The spectra labelled **||** and **⊥** represent the absorption spec-
             tra of light having its electric vector parallel and per-
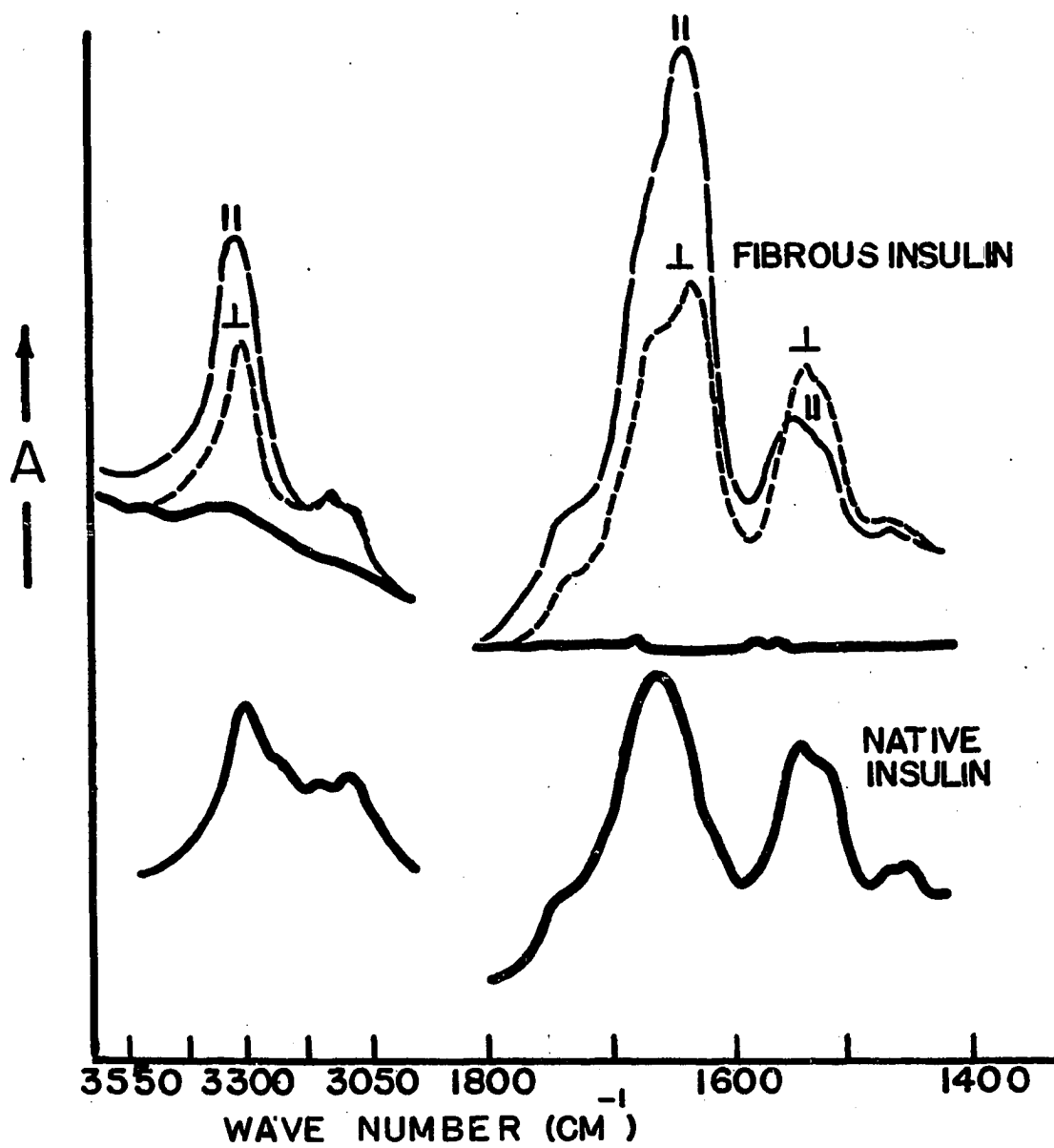   pendicular respectively to the long axis of the fibrils.

FIBROUS INSULIN

NATIVE INSULIN

WAVE NUMBER (CM⁻¹)

Table 12. The amide I and II absorption bands for insulin fibrils and native insulin

Material	Amide I[a] (cm^{-1})	Amide II[a] (cm^{-1})
Insulin fibrils	1633 s //	1545 m ⊥
	1730 w //	
Native Insulin	1660 s	1545 m
	1730 w	

[a]The intensity and the dichroism of the absorption band appears after the absorption band; s, m and w indicate strong, medium and weak intensity and // and ⊥ indicate parallel and perpendicular dichroism.

rils and therefore, in a cross-β structure. These IR results are satisfied by a relatively pure parallel cross-β structure fibril.

Ambrose and Elliott (1951) on the basis of IRD experiments similar to those above proposed that α structure globular insulin is converted to cross-β structure insulin fibrils. In their mechanism the native globular insulin molecule attaches to the fibril end, and the α structure in the native insulin is unfolded to β structure by being stretched across the fibril surface (Figure 26).

UV optical properties of insulin fibrils

In order to further establish the secondary structure of the fibrils and to examine their structure in solution, the ORD, CD and OD of aqueous solutions of the fibrils were measured. Experimental evidence indicates that the α-helix, random coil and β structure conformations of synthetic polypeptides can be distinguished by their optical properties. The CD of experimentally observed β structures has a negative dichroic

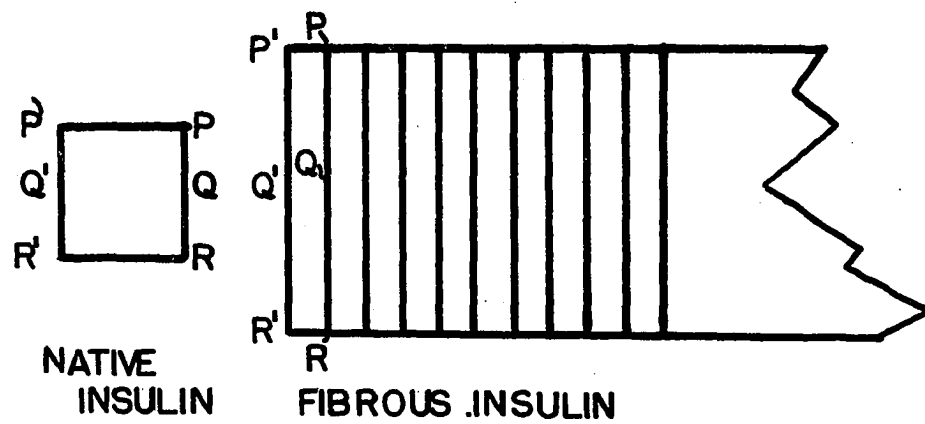Figure 26. The Ambrose and Elliott (1951) mechanism for the conversion of α structure native insulin to cross-β structure insulin fibrils

band at 218 nm and a positive band at approximately 195 nm (Table 7).
The ORD of β structures has a trough with a minimum at 230 nm (Table
8). The strongest band in the absorption spectrum of β structures is
centered at 195 nm with an extinction coefficient that is larger than
those found with the α-helix or random coil. There are large side chain
contributions to this extinction coefficient (Gratzer 1967). Side
chains have virtually no effect on the CD and ORD of polypeptides and
proteins.

The negative CD band at 218 nm and the positive band at 195 nm
obtained with insulin fibrils indicate the presence of β structure
(Figure 27). The differences in the CD spectra of fibrillar and native
insulin indicate that major conformational changes have taken place in
the conversion of native to fibrous insulin. The ORD of the insulin
fibrils also shows β structure; however, it is not significantly differ-
ent than the ORD of native insulin (Figure 28). This insensitivity of
ORD to major conformational alterations is expected from the CD of native
and fibrous insulin. The extinction coefficient of the insulin fibrils
at 195 nm is greater than with native insulin (Figure 29). This also
shows a major structural alteration in the conversion of globular insu-
lin to β structure fibrils. These results conclusively show that a major
conformational change occurs in insulin when the globular form is con-
verted to the fibril form. They also show that the insulin fibrils have
β structure. The particular type of β structure present is difficult
to extract from ORD and CD measurements. Extensive theoretical studies
involving a quantum mechanical analysis of the UV optical properties
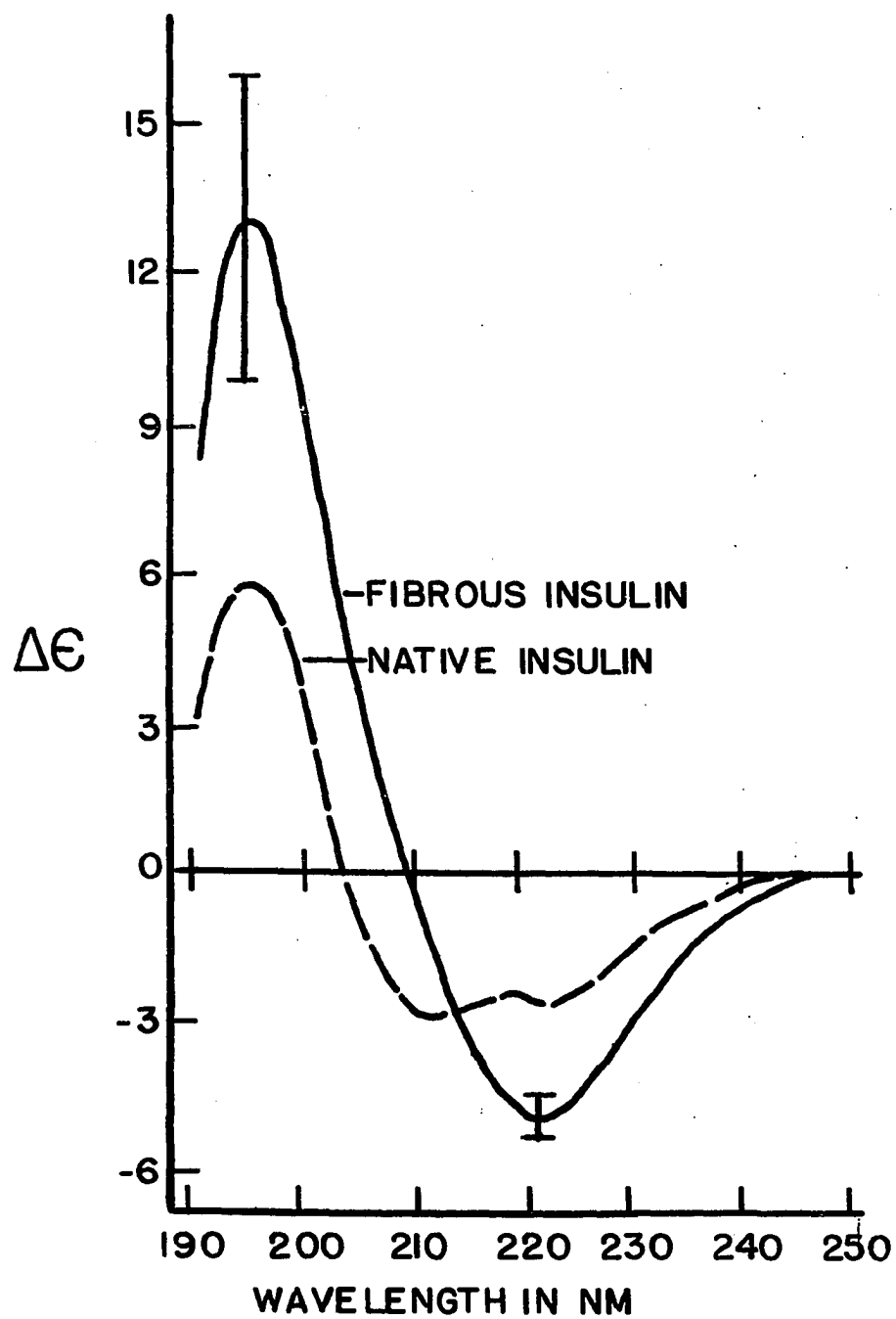have been discussed previously. Unfortunately, attempts to predict

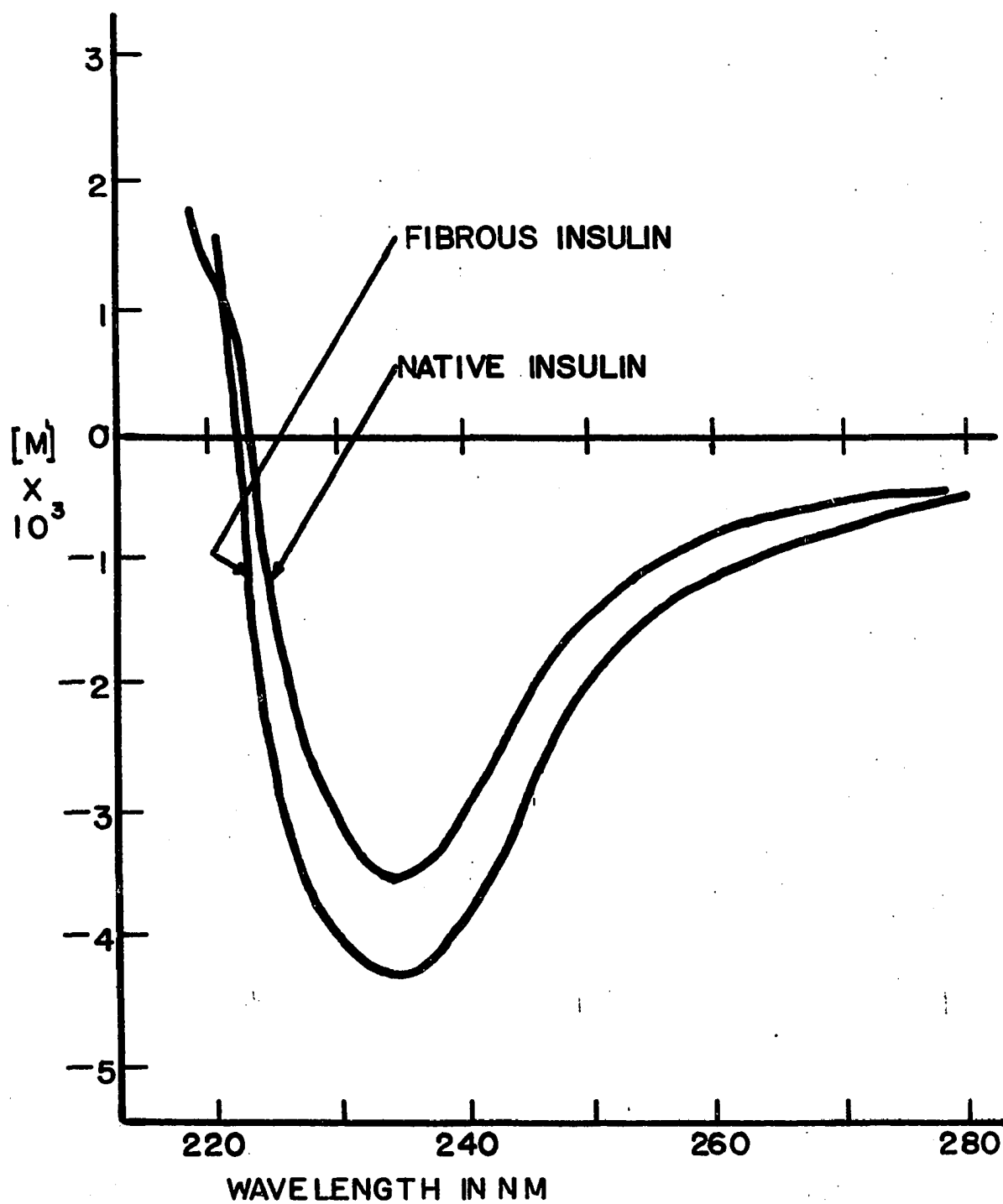Figure 27. The circular dichroism of insulin fibrils and native insulin

Figure 28. The optical rotatory dispersion of insulin fibrils and native insulin
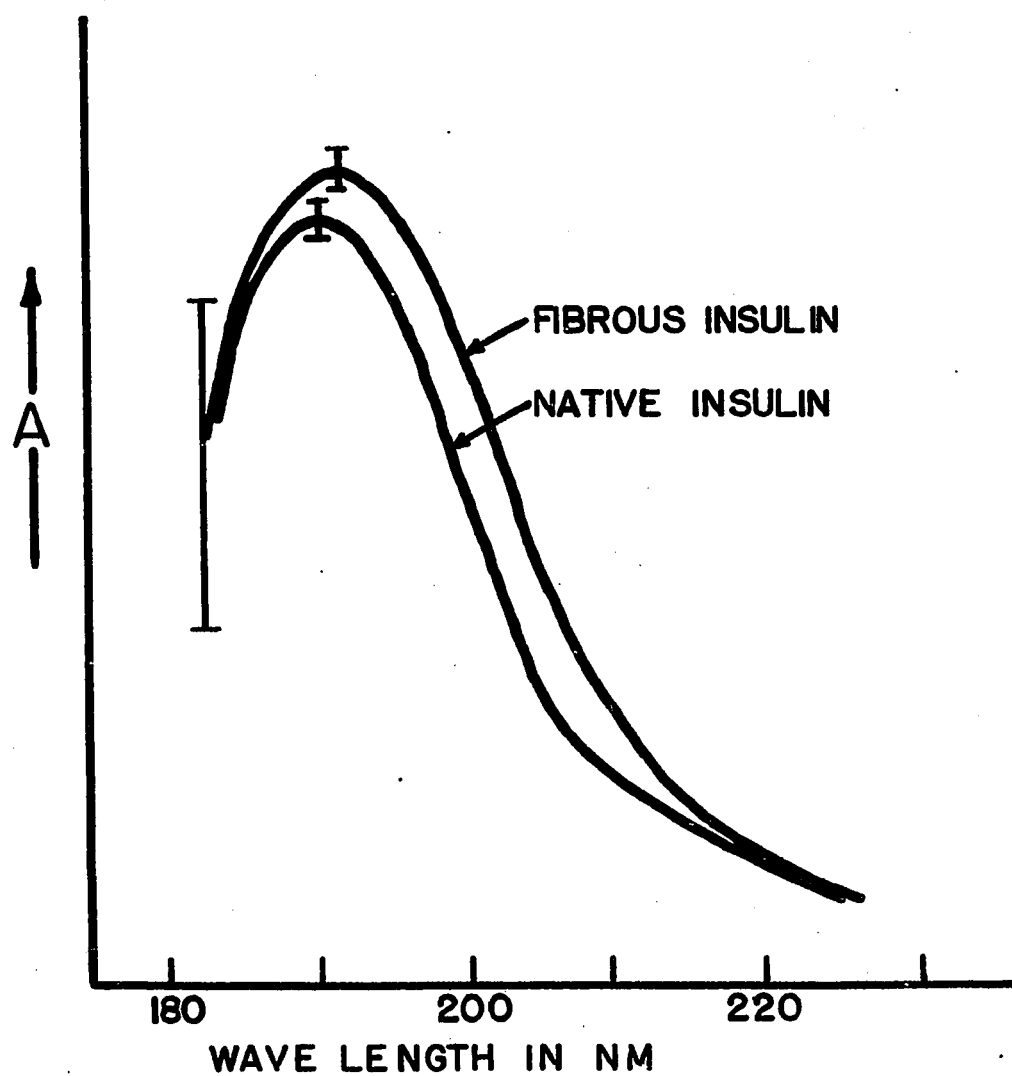
Figure 29. The absorption of insulin fibrils and native insulin

the form of β structure experimentally observed, using the theoretical approach, leads to some ambiguities that render β structure characterization questionable. Simple comparison of the optical properties of the antiparallel β structures of synthetic polypeptides and silk with the structure of the fibrils show many similarities. However, due to the uncertainty of the extent of antiparallel β structure in silk and polypeptides along with the effect that different β structure environments have on optical activity, it does not necessarily follow that the fibril structure of insulin is antiparallel.

Proposed structure for insulin fibrils

The electron microscopy and low and intermediate angle x-ray diffraction results of this study indicate that the fibrils have uniform cross sectional dimensions of approximately 30 to 40 Å. The wide angle x-ray diffraction pattern and IRD of the fibrils show them to have a cross-β structure probably with the parallel chain pleated sheet of Pauling and Corey. This evidence is almost identical with that obtained with OxFK and SCMFK fibrils. The optical activity of the fibrils is similar to that of synthetic polypeptides suggested to have the antiparallel chain pleated sheet of Pauling and Corey. However, at this time little is known of the optical properties of the parallel and antiparallel chain pleated sheets, and therefore, the significance of these properties must be left for future investigation. The optical properties including UV optical density show that rather drastic alterations of the structure of insulin accompany the conversion of the native to the fibrillar form.

Although there is some question as to whether the insulin fibrils

have parallel or antiparallel cross-β structure, there can be no doubt that the insulin and feather keratin fibrils have the same type of cross-β structure. In terms of the x-ray diffraction, IRD and ultraviolet optical activity, feather keratin and insulin fibrils are identical.

The primary structure of insulin was established by Sanger and coworkers more than 15 years ago (Sanger and Tuppy 1951, Sanger and Thompson 1953, Ryle et al. 1955). This primary structure which is not disrupted during fibril formation severely limits the number of possible ways in which insulin could form cross-β structure fibrils. There are two chains in insulin, one the A chain composed of 21 amino acid residues and the B chain composed of 30 amino acid residues. Two disulfide bridges connect the A and B chains and a third closes a small loop in the A chain (Figure 30). The restrictions induced in the insulin molecule by its disulfide bridges leave only several ways of arranging insulin in the cross-β structure fibrils.

In all of the arrangements that can generate cross-β structure fibrils, the insulin molecule lies in a plane normal to the fibril axis. Other arrangements of the insulin molecule do not allow the formation of significant amounts of β structure. Intermolecular hydrogen bonds between planes form β structure. Depending on the way in which the planes are oriented with respect to their neighbors, they generate either a mixture of parallel and antiparallel β structure with a significant amount of nonhydrogen bound insulin or all parallel β structure. Several examples of the combinations are given in Figure 31. From the point of view of molecular model studies and the experimental data, the most
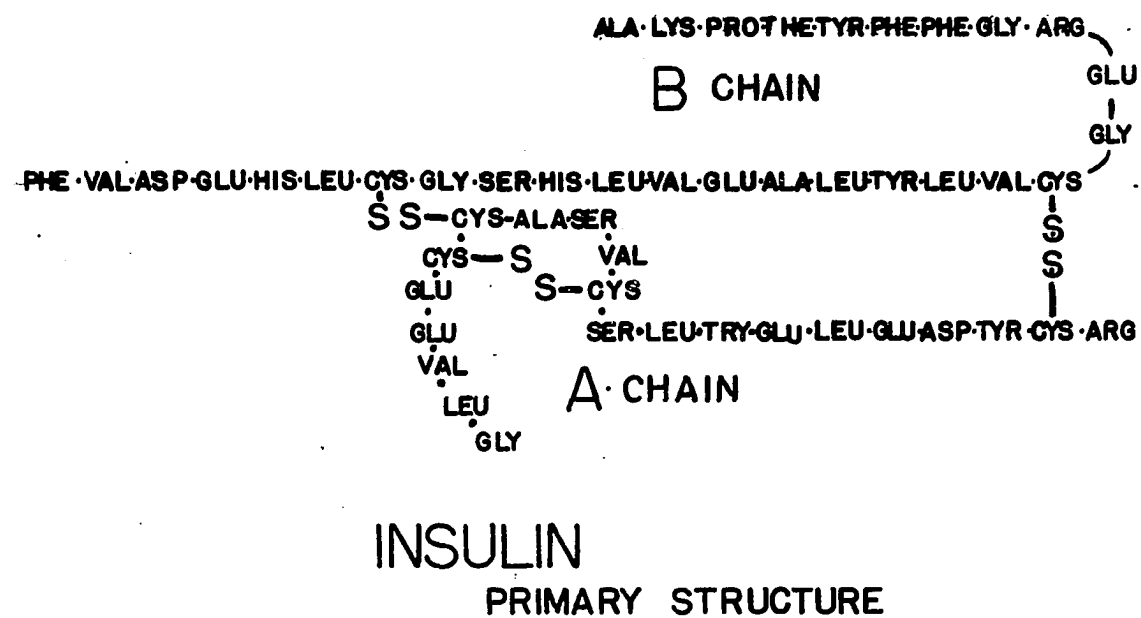
ALA·LYS·PRO·THE·TYR·PHE·PHE·GLY·ARG
GLU
GLY
B CHAIN

PHE·VAL·ASP·GLU·HIS·LEU·CYS·GLY·SER·HIS·LEU·VAL·GLU·ALA·LEU·TYR·LEU·VAL·CYS
S S—CYS-ALA·SER
CYS—S   VAL
GLU   S—CYS
GLU   SER·LEU·TRY·GLU·LEU·GLU·ASP·TYR·CYS·ARG
VAL
LEU   A·CHAIN
GLY

S
S

INSULIN
PRIMARY STRUCTURE

Figure 30. The primary structure of insulin

PARALLEL β STRUCTURE
ONLY

ANTIPARALLEL β
STRUCTURE &
RANDOM COIL

PARALLEL β STRUCTURE
& RANDOM
COIL
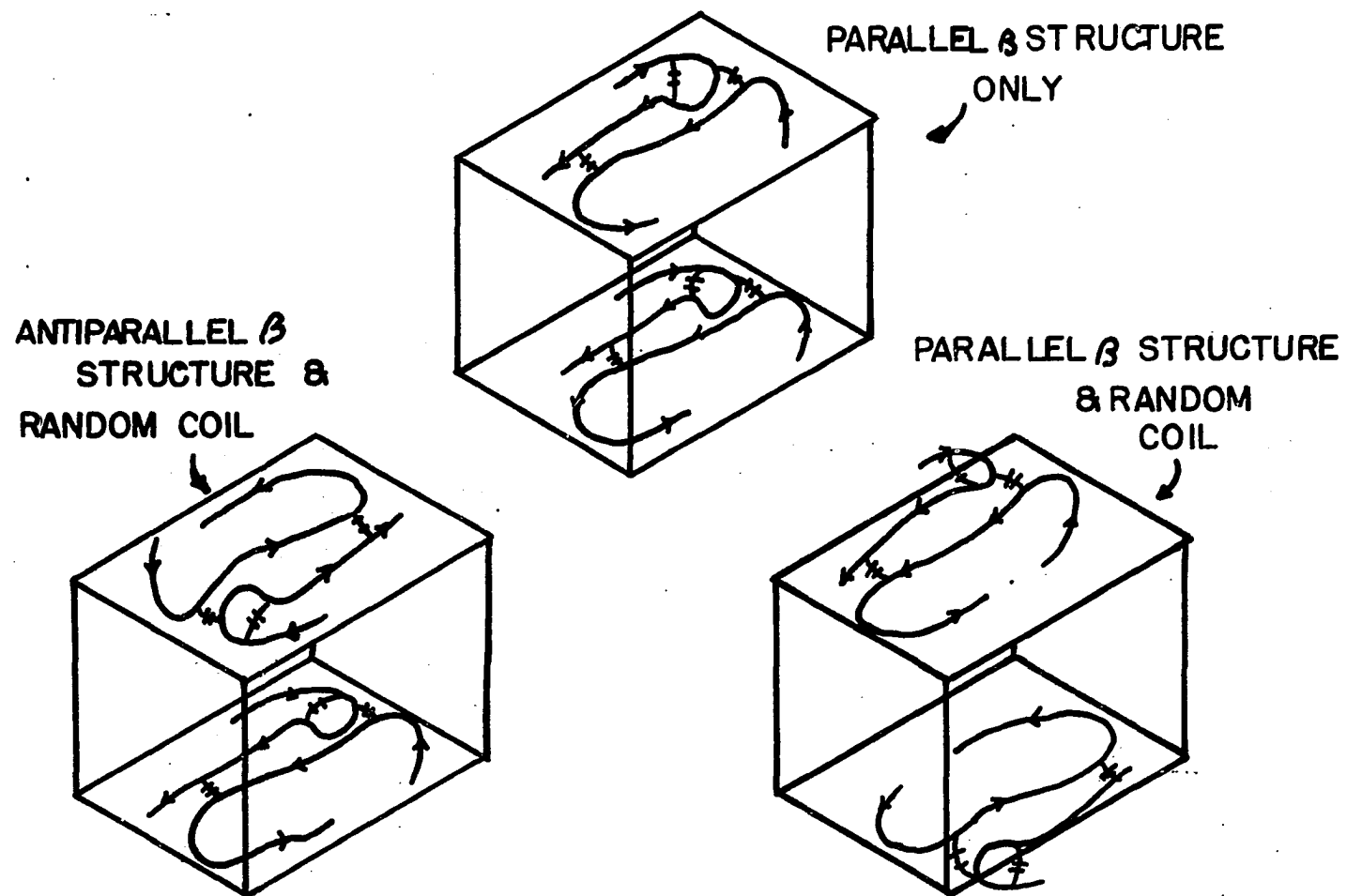
Figure 31.   Three ways of forming cross-β structure insulin fibrils

satisfactory structure is that where the planes are oriented so as to

generate a parallel cross-β structure. The parallel cross-β structure

insulin fits very nicely into a fibril with cross sectional dimensions

between 30 and 40 Å. Assuming the fibrils have a density of 1.4 g/cc,

it is possible to show that one insulin molecule will fill one 4.7 Å

thick layer which is 38 by 38 Å. The fibril probably has a structure

similar to that in Figure 32.

The initiation of fibril growth which occurs only at elevated tem-

peratures must involve first the disruption of the secondary structure

of globular insulin. Waugh (1957) has shown on the basis of kinetic

studies that the chance collision of at least three such molecules can

generate a fibril initiating unit. Once a fibril has been initiated,

its growth must involve the fibril end and the disrupted insulin mole-

cules in solution. Ambrose and Elliott (1951) suggested that once an

insulin molecule is in contact with the fibril end, the α structure

or globular structure of the disrupted insulin molecule is stretched

by hydrogen bond formation across the fibril surface.

<center>Diamides</center>

Introduction

There is some uncertainity about the type of β structure in feather

keratin and insulin fibrils. The fibrils have UV optical properties simi-

lar to those of polypeptides interpreted to have antiparallel β struc-

ture while the x-ray diffraction and IRD studies on the fibrils indicate

that they have parallel cross-β structure. This difficulty, which is

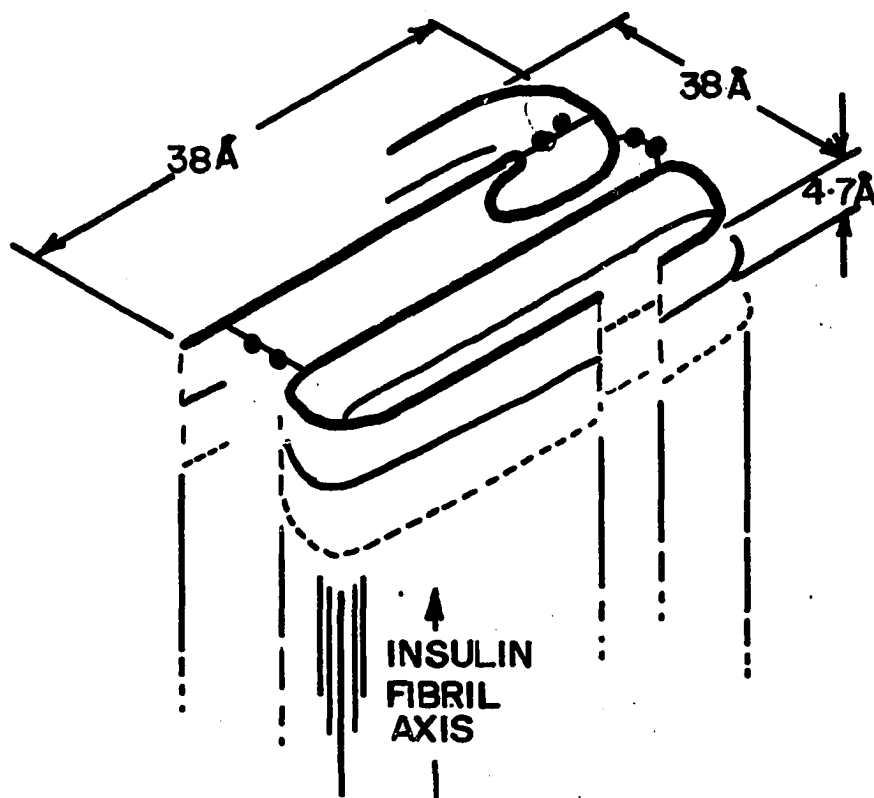related to the interpretation of UV optical activity, has been discussed

Figure 32. One possible model for the structure of insulin fibrils,
the parallel cross-β structure

in the previous sections. Based on theoretical considerations, significant differences in the optical properties of parallel and antiparallel chain pleated sheets are anticipated; however, it has not been possible to correlate these differences with experimental data because of the lack of demonstrably pure model systems of these types. To the contrary, there is evidence that β polypeptides contain mixtures of parallel and antiparallel β structure (Rosenheck and Summer 1967, Bradbury and Elliott 1963). In hopes of resolving the question of how the two types of β structure are related to optical activity observed in polypeptides, a detailed study of the optical activity of several model compounds was undertaken.

In order to be a valid structural and optical model for this study, the compound used must aggregate through hydrogen bonding to generate a parallel or antiparallel β structure. Also, the model compound must have peptide groups which have essentially the same molecular environment as peptide groups in β structure polypeptides. One group of compounds meeting these requirements is the diamide group. The diamides used in this study are acetyl-L-leucine-N-methyl amide (ALMA), acetyl-L-alanine-N-methyl amide (AAMA), acetyl-glycine-N-methyl amide (AGMA) and acetyl-L-lysine-N-methyl amide (ALyMA)(Figure 33).

Diamides have received a great deal of attention in the recent past. The reason for this attention is that diamides, like polypeptides, have two degrees of rotational freedom in their backbone. These are rotations about the bonds between the amide nitrogen and the α-carbon (ψ) and between the carbonyl group and the α-carbon (ϕ). ψ and ϕ have been described as a function of potential energy for various nonhydrogen

bound diamides and polypeptides (Leach et al. 1966, Ramachandran et al. 1963 and 1965, Brant et al. 1967). The calculations show that for diamides such as those above less than 20% of the ψ-ϕ values are energetically reasonable. Three conformational types exist for diamides and polypeptides; they are the right handed α-helix (ψ = 100-140, ϕ = 20-100), the left handed α-helix (ψ = 210-320, ϕ = 220-260) and the β structure (ψ = 240-360, ϕ = 0-150). IR spectra of some diamide solutions suggest the existence of a fourth diamide conformation which involves the formation of an intramolecular hydrogen bond (Figure 34)(Tsuboi et al. 1959). The considerations involving the conformational calculations do not take hydrogen bonding into account. It has been suggested that the diamide molecules associate through hydrogen bonding to make a β structure-like aggregate (Mizushima et al. 1954)(Figure 34). Although the diamide β structure is unlike the polypeptide structure in the direction of the peptide chain, it is similar in the hydrogen bond direction.

The ORD of diamides having fixed as well as variable ψ and ϕ angles was investigated by Schellman and Nielsen (1967). They found that the rotatory properties of the diamides, especially acetyl-L-alanine amide, were similar to those of polypeptides and proteins. In an analysis of the optical rotatory properties of acetyl-L-proline amide, they found that that diamide in dioxane formed an intramolecular hydrogen bond. This is in agreement with previous IR studies of Tsuboi et al. (1959). Detailed analyses of the rotatory properties of other diamides were unsuccessful.

Figure 33. The structure of acetyl-L-leucine-N-methyl amide (ALMA),
            acetyl-L-alanine-N-methyl amide (AAMA), acetyl-glycine-N-
            methyl amide (AGMA) and acetyl-L-lysine-N-methyl amide
            (ALyMA)

Figure 34. Four diamide conformations all of which allow the formation
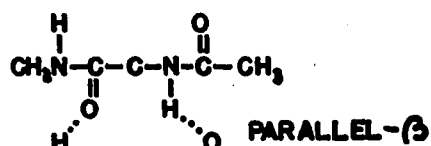   of inter- or intramolecular hydrogen bonds
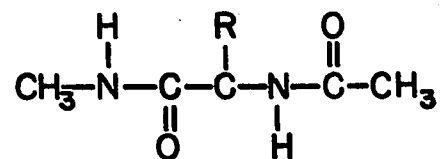
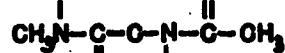ALMA R = $CH_2CH \cdot (CH_3)_2$
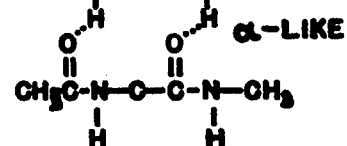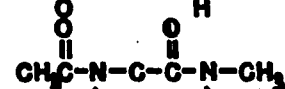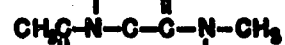
AGMA R = H

AAMA R = CH_3
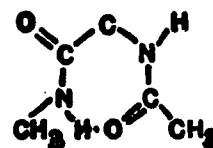
ALYMA R = $(CH_2)_4 \cdot NH_2$

PARALLEL-β

ANTIPARALLEL-β

α-LIKE

INTERMOLECULAR
HYDROGEN BONDING

INTRAMOLECULAR
HYDROGEN BONDING

Solid state properties

AGMA, ALMA and AAMA are crystalline in the solid state. The AGMA crystals are tabular and an analysis of their x-ray diffraction pattern shows them to have a triclinic unit cell having dimensions a = 17.6 Å, b = 4.8 Å and c = 4.8 Å and angles $\alpha \simeq 60$, $\beta \simeq 90$ and $\gamma \simeq 90$ (Moriwaki et al. 1959). Two AGMA molecules are required to fill the unit cell which is oriented with its long axis nearly perpendicular to the plane of the tabular crystals. The 4.8 Å spacings are related to the hydrogen bond and the side chain dimensions. The 17.6 Å spacing is related to the backbone dimension. The IR spectrum of unoriented crystalline AGMA has absorption bands near 1645 cm^{-1} (Amide I), 1560 cm^{-1} (Amide II) and 3300 cm^{-1} (NH stretching)(Figure 35)(Table 13). IRD of the crystals was not possible. From this data the conformation of the AGMA in the crystalline state can not be ascertained; however, it can be said that intramolecular hydrogen bonding is not present. AGMA having an intramolecular hydrogen bond can not be arranged within the above unit cell.

The ALMA crystals are needle-like when crystallized from all the organic solvents used and water. An analysis of the x-ray diffraction pattern of ALMA crystallized from chloroform shows it to have a monoclinic unit cell with dimensions a = 11.7 Å, b = 9.92 Å and c = 4.81 Å and angles $\alpha \simeq 90$, $\beta \simeq 90$ and $\gamma \simeq 88.9$. Two ALMA molecules are required to fill this unit cell which is oriented with the 4.81 Å dimension parallel to the long axis of the needle-like crystals. The x-ray diffraction pattern of ALMA crystallized from water indicates a significantly different unit cell (Figure 37). The crystals appear to be polymorphic

Table 13. The most prominent infrared absorption bands of the peptide group in crystalline AGMA, ALMA and AAMA

Absorption band	AGMA (cm^{-1})	ALMA[a] (cm^{-1})	AAMA[a] (cm^{-1})
Amide I (carbonyl stretching)	1645	1635 //	1670 $\perp$ 1640 //
Amide II (NH bending)	1560	1565 $\perp$ 1540 $\perp$	1575 $\perp$ 1560 $\perp$
NH stretching	3300	3300 //	3300 //

[a]// and $\perp$ indicate parallel and perpendicular respectively.

and their unit cell dimensions are not easily obtained; however, one thing the polymorphs have in common is a 4.80 Å dimension parallel to the long axis of the crystals. Also the unit cells of the various polymorphs are monoclinic or orthogonal. The IR spectrum of the crystalline ALMA has absorption bands near 1635 cm^{-1} (Amide I), 1540 and 1565 cm^{-1} (Amide II) and 3300 cm^{-1} (NH stretching)(Table 13). The positions of these IR absorption bands are not dependent on the method of crystallization. IRD of the crystals shows the amide I and NH stretching vibrations have parallel dichroism while the amide II bending vibration has perpendicular dichroism (Figure 36). Therefore, it appears that the hydrogen bonds are parallel to the long axis of the crystals and the 4.8 Å dimension is the hydrogen bond spacing. In order to place two ALMA molecules in the unit cell of the chloroform crystals, it is necessary that the ALMA molecules in the crystal be arranged in either a β-like structure or an α-helix-like structure (Figure 34). The sugges-

Figure 35. The amide I and II infrared absorption bands of unoriented
            crystalline AGMA

Figure 36. The infrared dichroism of the amide I and II absorption
            bands of oriented crystalline ALMA

            The spectra labelled $A_{\parallel}$ and $A_{\perp}$ represent the absorption
            spectra of light having its electric vector parallel and
            perpendicular respectively to the long axis of the crystals.

1645 cm^{-1}

ABSORBANCE
OF
AGMA

A

1700 1600 1500

1633 cm^{-1} DICHROISM
OF
ALMA

$A_{\parallel}$

$A_{\perp}$

$A_{\parallel} - A_{\perp}$

A

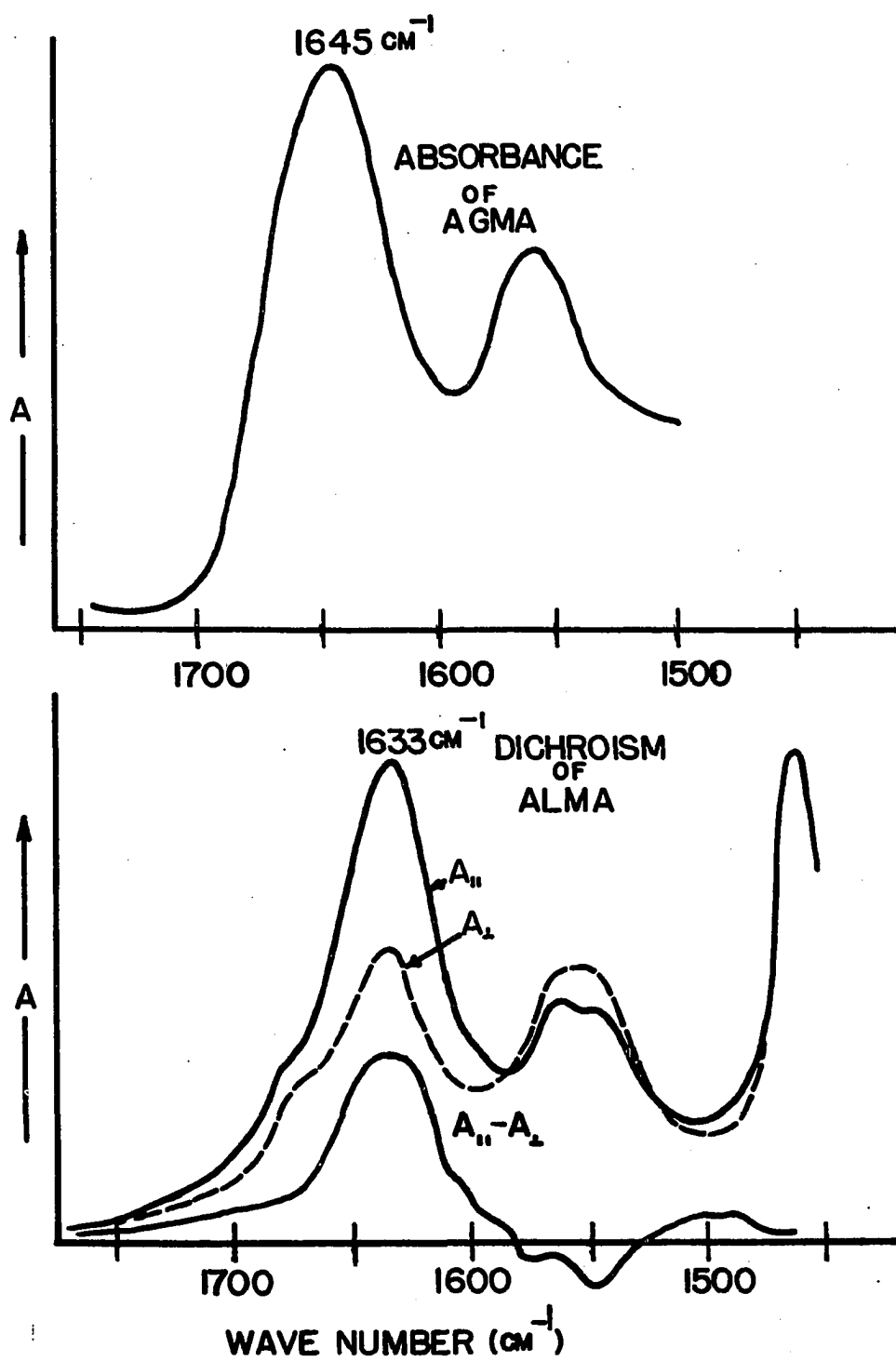1700 1600 1500
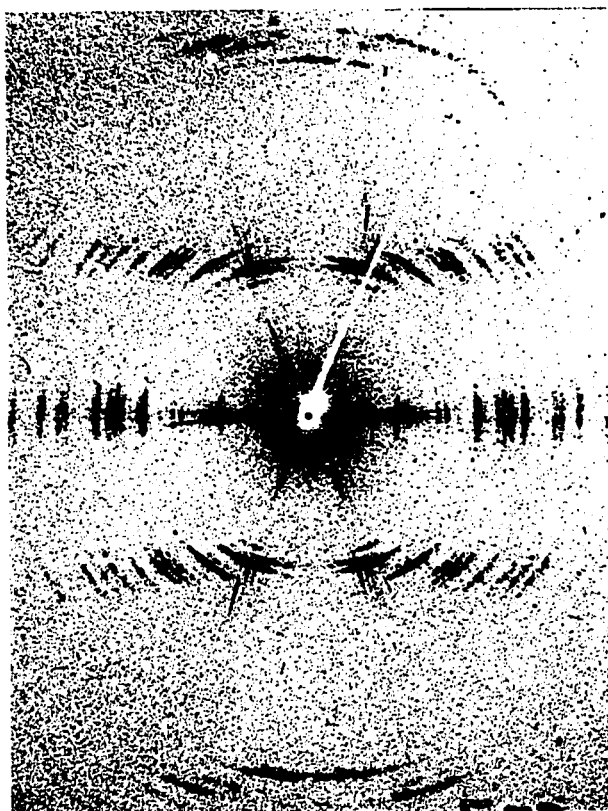
WAVE NUMBER (cm^{-1})

Figure 37. The x-ray diffraction pattern of acetyl-L-leucine-N-methyl
amide (ALMA) crystallized from water

The layer lines in the diffraction pattern indicate a 4.8 $\overset{\circ}{A}$
dimension parallel to the long axis of the crystals.

Figure 37. The x-ray diffraction pattern of acetyl-L-leucine-N-methyl amide (ALMA) crystallized from water

The layer lines in the diffraction pattern indicate a 4.8 Å dimension parallel to the long axis of the crystals.
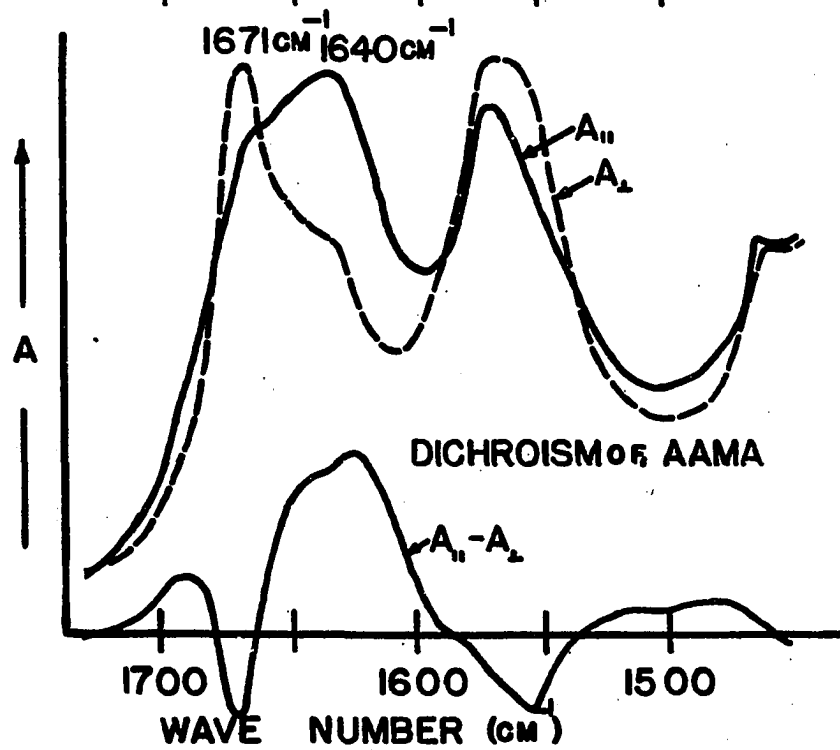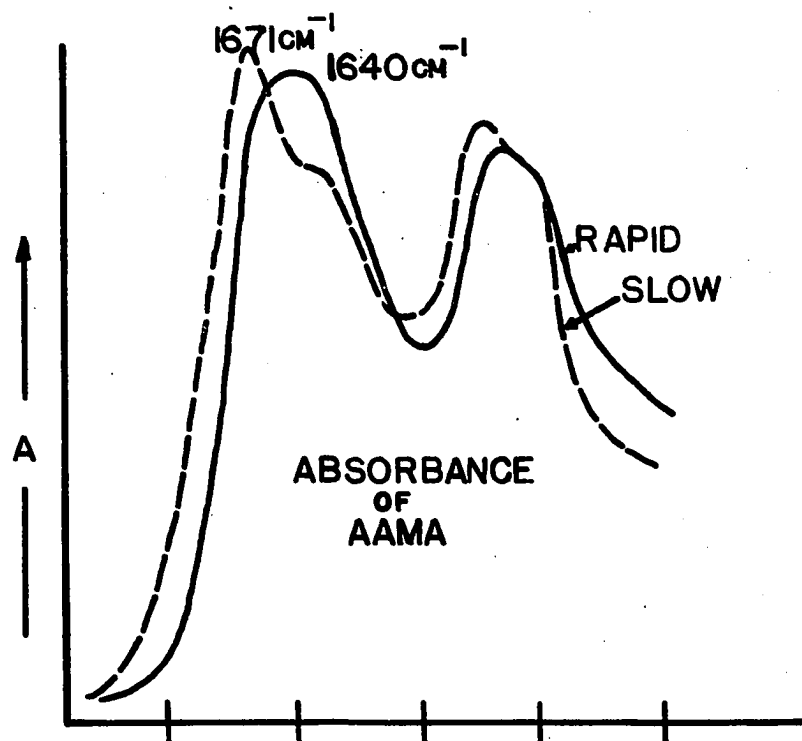
tion of parallel β structure conformation is particularly appealing due to similarities in the amide I bands of the crystalline ALMA and β structure polypeptides. Also from theoretical evidence the β-like structure diamide is energetically more favorable than the α-helix-like diamide in solution (Leach et al. 1966).

The AAMA crystals are needle-like when crystallized from all the organic solvents used and water. An analysis of the x-ray diffraction patterns (powder patterns) of AAMA showed no dependence on the method of crystallization. From this data the dimensions of the unit cell could not be ascertained. The IR spectrum of crystalline AAMA has absorption bands near 1670 and 1640 cm^{-1} (Amide I), 1575 and 1560 cm^{-1} (Amide II) and 3300 cm^{-1} (NH stretching)(Table 13). The relative strength of these absorption bands is strongly dependent on the rate of crystallization. In material crystallized rapidly, the amide I absorption maximum is at 1640 cm^{-1} with a shoulder at 1670 cm^{-1}. When crystallized slowly the amide I absorption maximum is at 1670 cm^{-1} with a shoulder at 1640 cm^{-1} (Figure 38). The IRD of the AAMA crystals shows the bands at 1640 cm^{-1}, 1560 cm^{-1} and 3300 cm^{-1} exhibit parallel dichroism while the bands at 1671 and 1575 cm^{-1} exhibit perpendicular dichroism (Figure 39). These IR results indicate that two significantly different forms of the AAMA are present. We have not been able to distinguish x-ray diffraction patterns of two crystalline forms indicating that one of the forms is not stable under the conditions of the x-ray diffraction experiemnt. The AAMA crystalline form having its amide I absorption at 1670 cm^{-1} must have a structural conformation radically different from those of the other diamides. The form absorbing at 1640 cm^{-1} probably has a struc-

Figure 38. The dependence of the infrared absorption spectrum of the
amide I and II bands of AAMA on rate of crystallization

Figure 39. The infrared dichroism of the amide I and II bands of oriented
crystalline AAMA

The spectrum labelled $A_{||}$ and $A_{\perp}$ represent the absorption
spectra of light having its electric vector parallel and
perpendicular respectively to the long axis of the crystals.

$1671cm^{-1}$ $1640cm^{-1}$

RAPID

SLOW

ABSORBANCE
OF
AAMA

$1671cm^{-1}$ $1640cm^{-1}$

$A_{||}$

$A_{\perp}$

DICHROISM OF AAMA

$A_{||} - A_{\perp}$

1700   1600   1500

WAVE   NUMBER (cm)

tural conformation similar to that of the crystalline ALMA and AGMA.

Solution studies

The IR absorption spectrum and UV optical rotation were measured for AGMA, ALMA, AAMA and ALyMA. These properties are surprisingly similar from one diamide to the next. AGMA when dissolved in dimethyl sulfoxide (DMSO) exhibits IR absorption bands at 1670 cm^{-1} (Amide I), 1554 cm^{-1} (Amide II) and 3320 and 3480 cm^{-1} (NH stretching)(Figure 40) (Table 14). The amide I band at 1670 cm^{-1} indicates that the carbonyl group is weakly or nonhydrogen bound as expected in DMSO. The NH stretching vibrations at 3320 and 3480 cm^{-1} indicate the presence of hydrogen bound and free amide hydrogens respectively. It is probable that DMSO forms hydrogen bonds with amide hydrogens. AGMA solutions are not optically active.

ALMA when dissolved in DMSO exhibits IR absorption bands at 1670, 1550, 3300 and 3500 cm^{-1} (Figure 40)(Table 14). The interpretation of these four absorption bands is identical to the interpretation for the similar bands in the AGMA-DMSO solution. The IR absorption spectrum of ALMA was investigated in a number of other organic solvents (Table 14). The IR spectrum in dioxane and DMSO are similar. In ethanol, octanol and hexane-octanol mixtures a shift in the amide I band to lower frequency indicates the formation of hydrogen bonds with the carbonyl group of the diamide. In these solvents the NH stretching vibration can not be observed. In chloroform and carbon tetrachloride a similar shift in the amide I band is observed, which can not be accounted for by hydrogen bonding to solvent. It must therefore, be attributed to inter- or
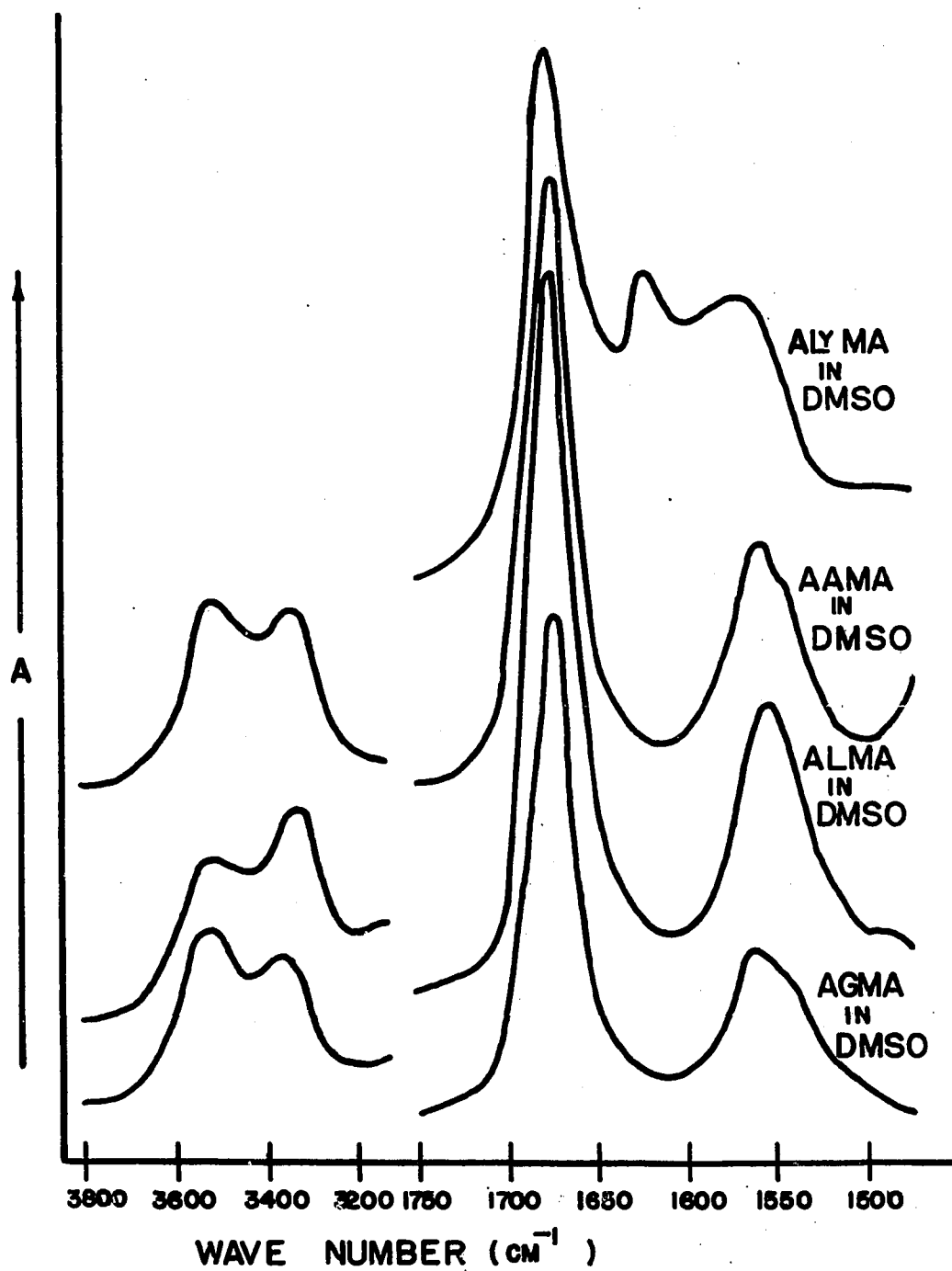
Figure 40. The infrared absorption of ALyMA, AAMA, ALMA and AGMA in
dimethyl sulfoxide

Table 14. The most prominent infrared absorption bands of the peptide groups of AGMA, ALMA, AAMA and ALyMA in solution

Solute and solvent	Amide I[a] (cm⁻¹)	Amide II[a] (cm⁻¹)	NH stretching[a] (cm⁻¹)	
AGMA in				
DMSO	1670 s	1554 m	3480 m	3320 m
ALMA in				
DMSO	1670 s	1550 m	3500 m	3300 m
1-4 Dioxane	1674 s	1540 m	6660 w[b]	6350 s[b]
Ethanol (100%)	1662 s	1565 m		
n-Octanol	1664 s	1550 m		
n-Octanol and Hexane	1664 s	1560 m		
Chloroform				
High concentration			3450 w	3350 m
Low concentration	1665 s		3450 m	3350 w
Carbon tetrachloride				
High concentration				3320 m
Low concentration	1650 s		3450 m	3350 m
AAMA in				
DMSO	1668 s	1550 m	3500 m	3320 m
n-Octanol	1665 s	1555 m		
Deuterochloroform				
High concentration			3450 w	3350 m
Low concentration	1665 s		3450 m	3350 w
ALyMA in				
DMSO	1670 s	1555 m	3480 m	3330 m
Ethanol (100%)	1660 s	1560 m		

[a]The symbols s, m and w indicate strong, medium and weak intensity.
[b]The first overtone of the NH stretching vibration.

intramolecular hydrogen bonds involving only the ALMA molecules. The NH stretching vibration at 3350 cm⁻¹ in chloroform at 3320 cm⁻¹ in carbon tetrachloride also indicate the presence of inter- or intramolecularly hydrogen bound ALMA. In order to distinguish between inter- and intramolecular bonding in the ALMA carbon tetrachloride and ALMA chloroform

solutions, the concentration dependence of hydrogen bonding was determined. In these two solvents the most sensitive IR absorption band to hydrogen bonding between amide groups is the NH stretching vibration. Absorption near 3350 cm^{-1} is from hydrogen bound amide hydrogens and near 3450 cm^{-1} is from free amide hydrogens. The specific absorption of these bands is strongly dependent on concentration (Figures 41 and 42), demonstrating formation of intermolecularly associated diamides. Due to the absorbance of dioxane and alcohols near 3300 cm^{-1} and the relative insensitivity of the amide I band to hydrogen bonding, similar experiments could not be carried out in the other solvents.

The ORD and CD of ALMA was determined in a number of organic solvents and water (Table 15)(Figure 43). The position and magnitude of the rotational trough is dependent upon the dielectric constant of the solvent. In low dielectric solvents like dioxane, the trough is at 238 nm with a molar rotation at the minimum $[m]_{238}$ of greater than 6650 while in 95% ethanol, it is at 230 nm with a minimum of 4000. This wavelength dependence is expected for an n → π* transition although this is not the only possible explanation. There is little or no concentration dependence exhibited by optical rotation in ethanol, dioxane or chloroform (Figures 44 and 45).

AAMA when dissolved in DMSO exhibits IR absorption bands at 1668, 1550, 3320 and 3500 cm^{-1} (Figure 40)(Table 14). The interpretation of these four bands is identical to the interpretation for the similar bands in AGMA-DMSO and ALMA-DMSO solutions. The IR absorption spectrum of AAMA was also investigated in octanol and deuterochloroform (Table 14).
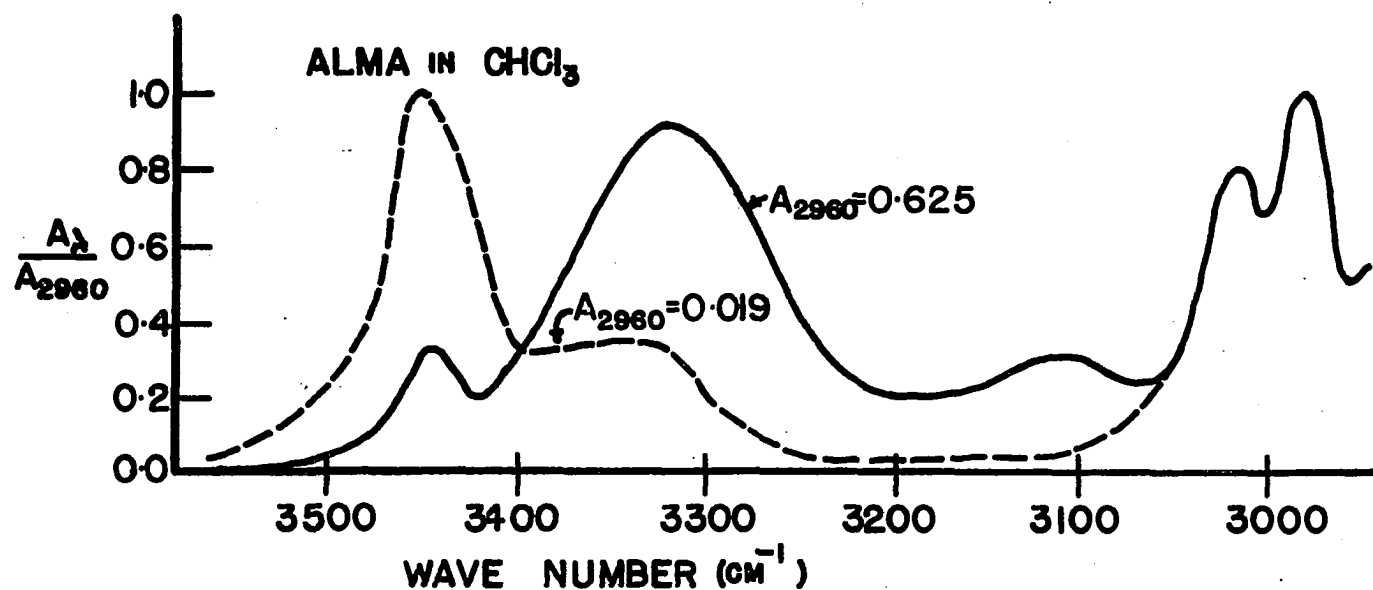
Figure 41. The concentration dependence of the infrared absorption bands near 3350 and 3450 cm^{-1}

Absorption at 3350 and 3450 cm^{-1} are due to hydrogen bound and free amide hydrogens respectively. Absorption at 2960 cm^{-1} was found to be a linear function of concentration.
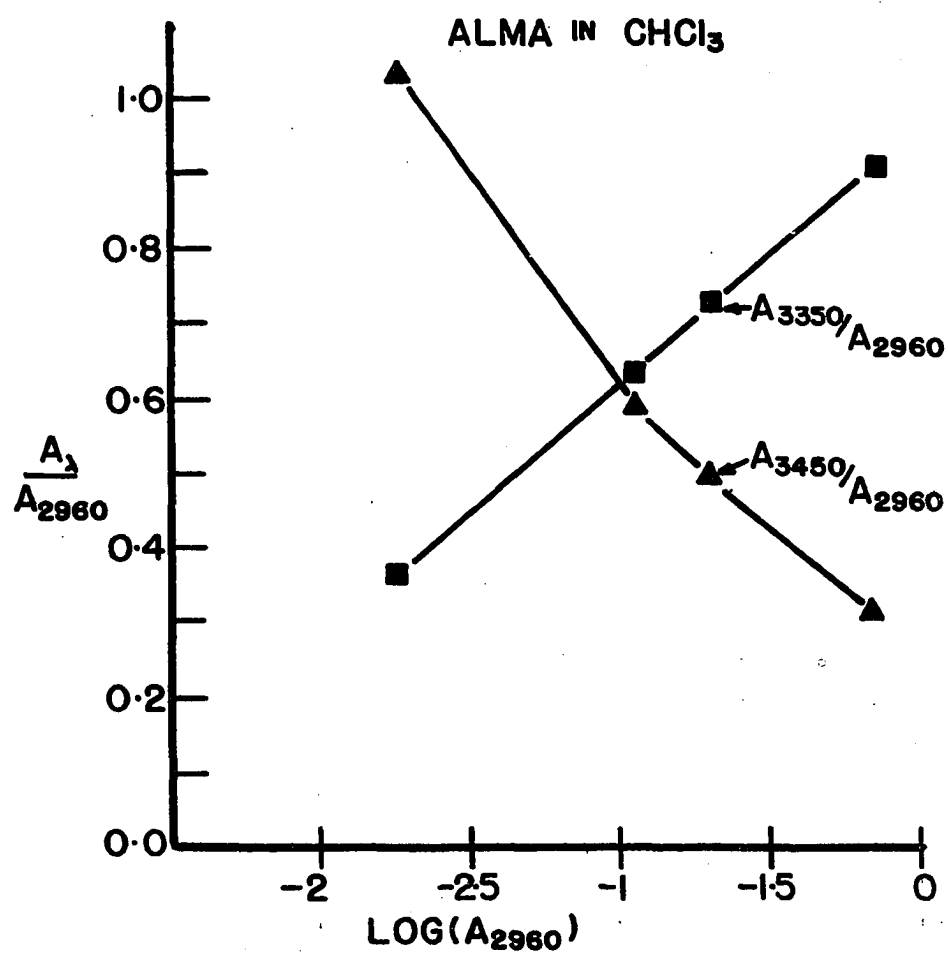
Figure 42. The concentration dependence of the infrared absorption bands near 3350 and 3450 cm^{-1}
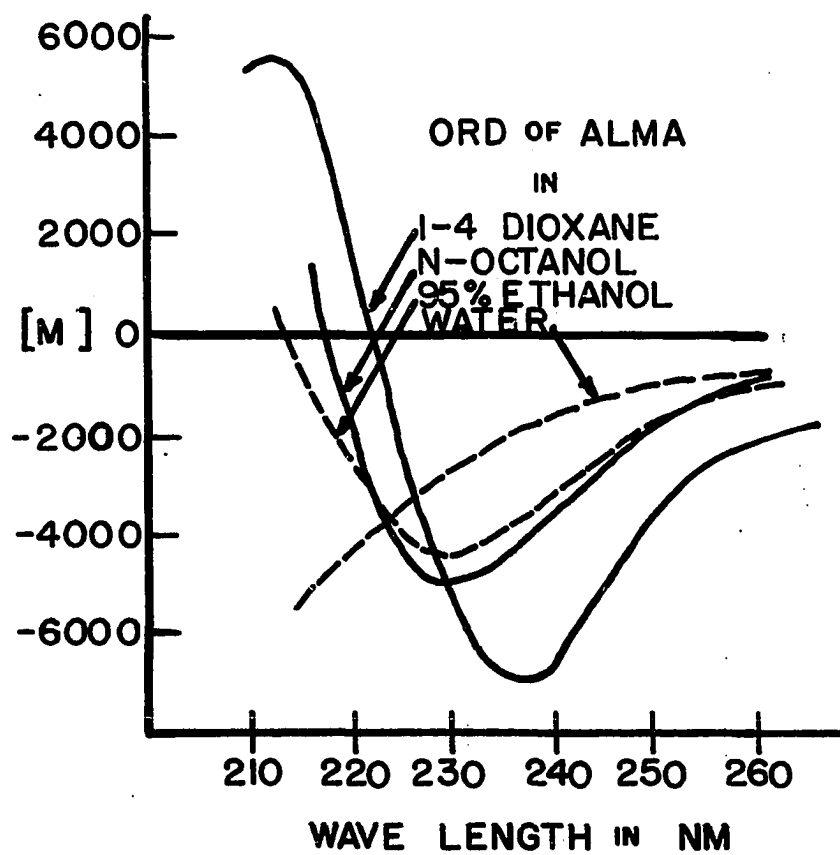
See Figure 41 for further details.

Figure 43. The optical rotatory dispersion of ALMA in a number of solvents

Figure 44. The concentration dependence of the minimum optical rotation
of ALMA in dioxane and ethanol

Figure 45. The concentration dependence of the minimum optical rotation
of ALMA in chloroform

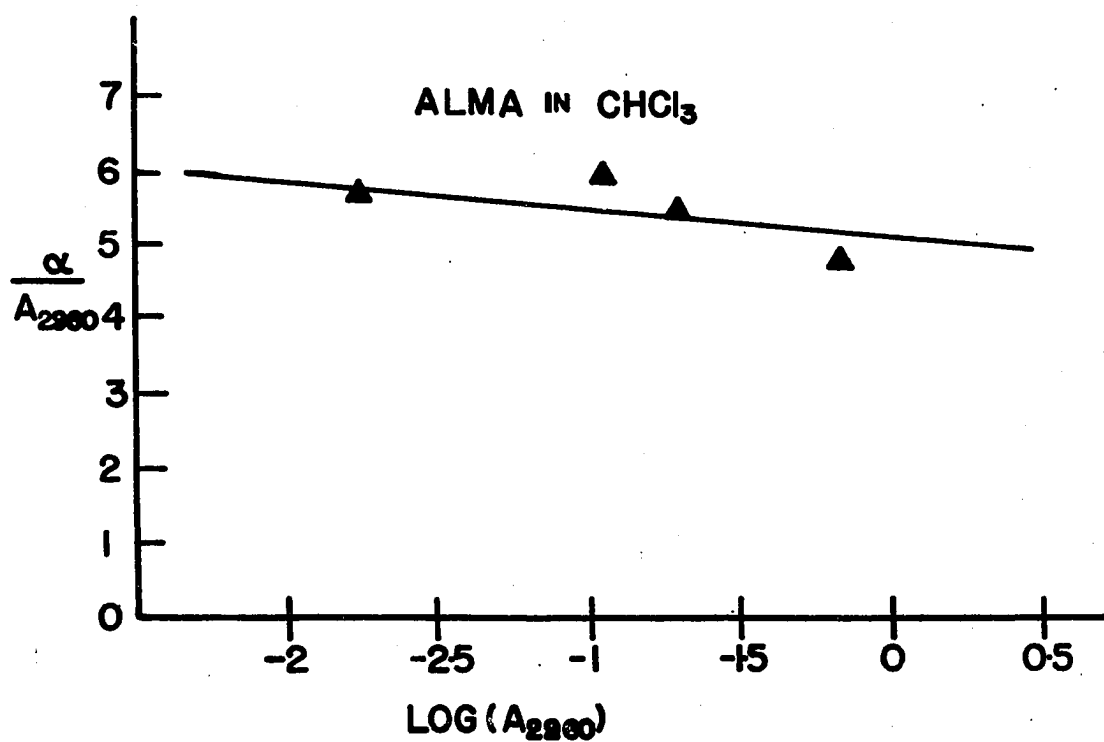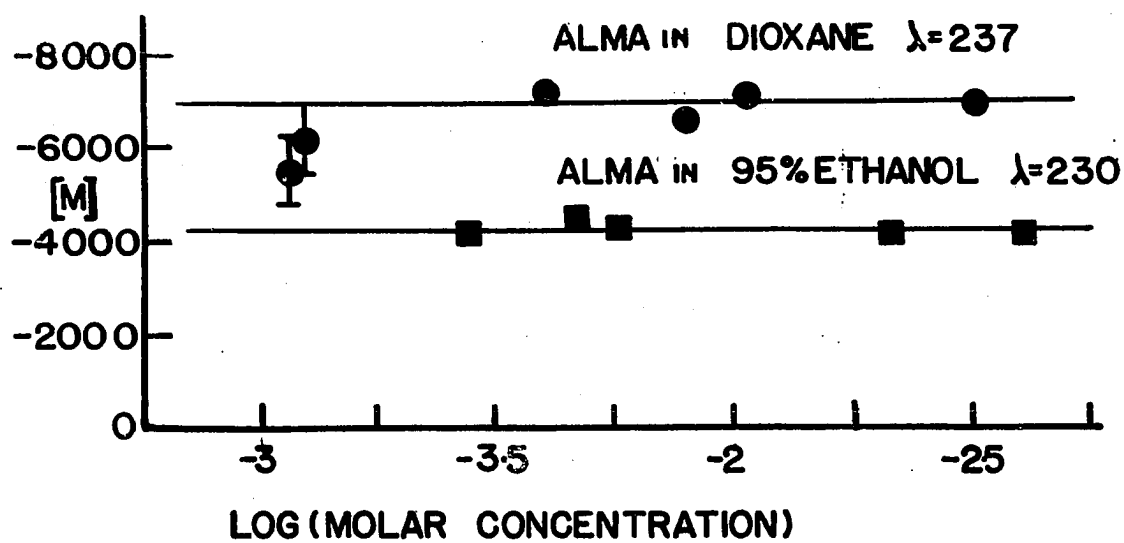The absorbance at 2960 cm^{-1} is a linear function of concentration.

Table 15. The optical rotatory dispersion and circular dichroism of
ALMA, AAMA and ALyMA in solution

Solute and solvent	ORD			CD	
	Trough	$[m]^a$	Crossover	Minimum	$\Delta\varepsilon^a$
ALMA in					
1-4 Dioxane	236 nm	6650	220 nm	215 nm	
Chloroform	237 nm				
n-Octanol	230 nm	4500	220 nm	218 nm	
Ethanol-Hexane	230 nm		220 nm	217 nm	1.47
Ethanol (95%)	230 nm	4000	210 nm	214 nm	
Water	210 nm			200 nm	
AAMA in					
n-Octanol	230 nm	5400	220 nm		
Deuterochloroform	236 nm	7500	222 nm		
Water	210 nm				
ALyMA in					
n-Octanol	230 nm	2940			
Ethanol (95%)	230 nm		210 nm		

^{a}Molar rotation and molar dichroism are not corrected for refractive
index.

In octanol a slight shift of the amide I band to a lower frequency indi-
cates the formation of weak hydrogen bonds probably between the solvent
and the carbonyl groups of the diamide. In deuterochloroform a similar
shift in the amide I band is observed. Hydrogen bonds between deutero-
chloroform and AAMA can not account for this shift, therefore, it must
be attributed to intra- or intermolecular hydrogen bonds involving only
AAMA. The NH stretching vibration at 3350 cm^{-1} also indicates the pre-
sence of inter- or intramolecular hydrogen bound AAMA. In order to
distinguish between inter- and intramolecular hydrogen bonding in the
AAMA deuterochloroform solution, the concentration dependence of hydro-

gen bonding was determined. Molar absorbance near 3350 cm^{-1} and near 3450 cm^{-1} are strongly dependent on concentration (Figures 46 and 47), demonstrating as in the case of ALMA that the hydrogen bonding involves intermolecularly associated diamides.

The ORD of AAMA in organic solvents is also similar to the ORD of ALMA (Table 15). The dependence of the ORD in deuterochloroform upon intermolecular hydrogen bonding between diamides is shown in Figure 48. Over a concentration range in which AAMA went from primarily monomer to trimer, no significant change occurred in the near UV ORD.

ALyMA when dissolved in DMSO exhibits IR absorption bands at 1670, 1600 (NH$_2$ absorption), 1555, 3330 and 3480 cm^{-1} (Figure 40)(Table 14). The interpretation of four of these bands is identical to the interpretation for the similar bands in AGMA-DMSO, ALMA-DMSO and AAMA-DMSO solutions. The absorption band near 1600 cm^{-1} is due to the primary amino group in the lysine side chain. The IR absorption spectrum was also investigated in ethanol. In ethanol a slight shift of the amide I band to lower frequency indicates the formation of weak hydrogen bonds between the solvent and the carbonyl groups of the diamide. The ORD of the ALyMA was determined in n-octanol (Table 15).

Discussion of diamides

When ALMA aggregates and then crystallizes, it forms a hydrogen bonded structure which resembles the parallel or antiparallel β structure of polypeptides. In the x-ray diffraction pattern of ALMA the absence of a 9.5 Å spacing, which when present indicates antiparallel β structure, might be explained by reasoning similar to that used by Arnott

AAMA in CDCl₃

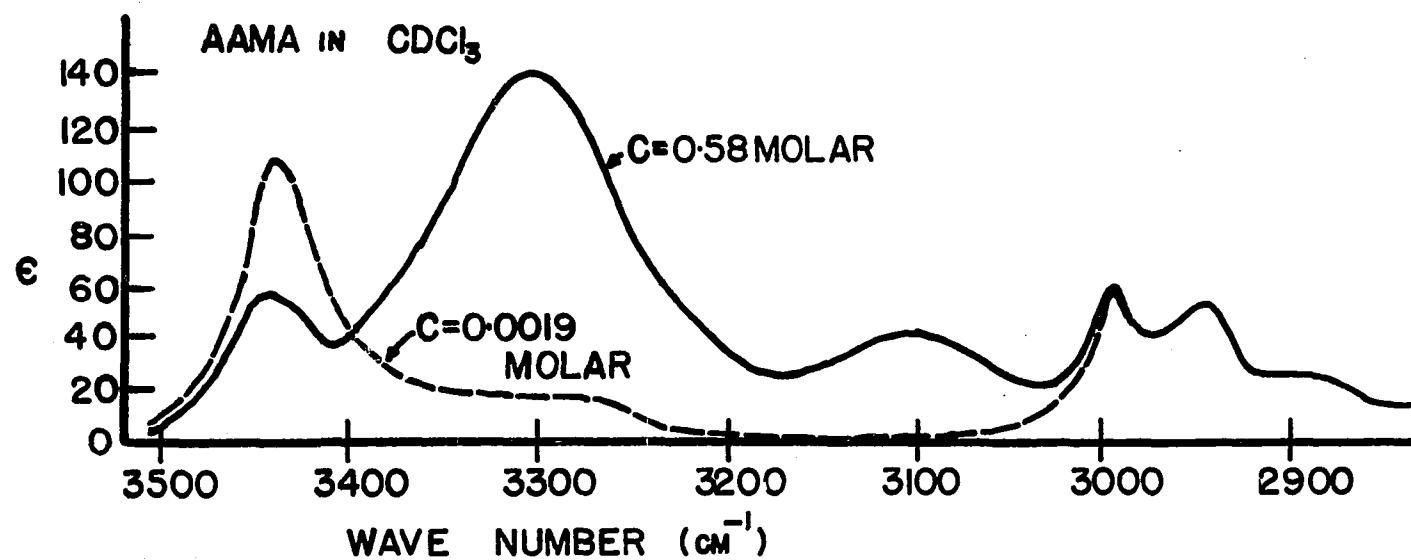Figure 46. The concentration dependence of the infrared absorption bands near 3350 and 3450 cm⁻¹

The absorption at 3350 and 3450 cm⁻¹ are due to hydrogen bound and free amide hydrogens respectively. ε is the molar absorbance.

Figure 47. The concentration dependence of the infrared absorption
bands near 3350 and 3450 cm^{-1}

Absorption at 3350 and 3450 cm^{-1} is due to hydrogen bound
and free amide hydrogens respectively. ε is the molar ab-
sorbance.

Figure 48. The concentration dependence of the minimum optical rotation
in deuterochloroform
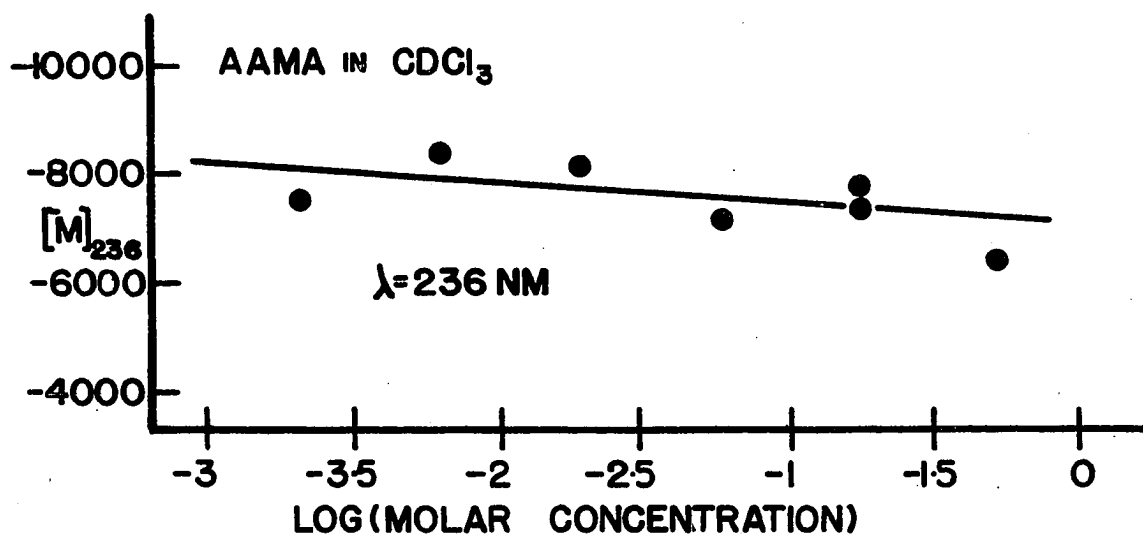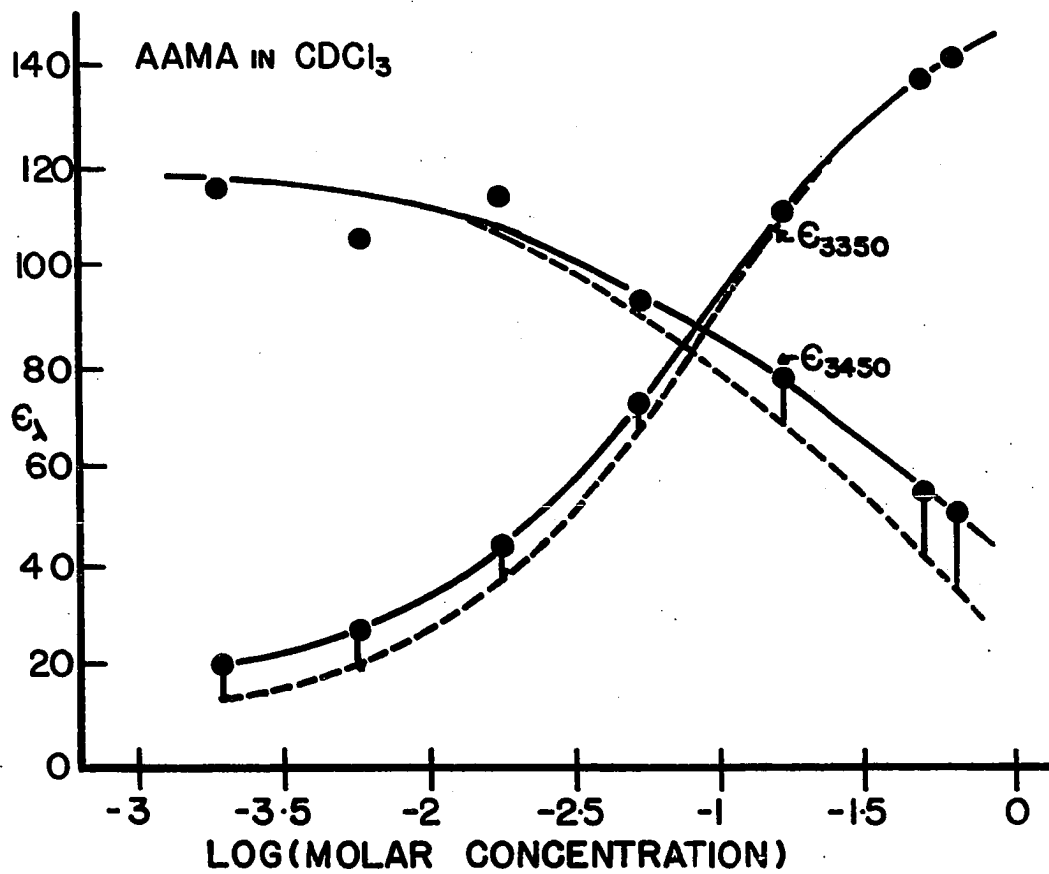
et al. (1967) to explain the diffraction pattern of poly-L-alanine. This was discussed in a previous section. A complete crystallographic analysis of ALMA was attempted; however, suitable single crystals were not available. Crystalline AGMA and one of the crystalline forms of AAMA are probably arranged in a similar fashion. In solution, depending on solvent and concentration, the diamides aggregate due to hydrogen bonding. The intermolecular hydrogen bond formation is easily followed by infrared absorption spectroscopy. It is reasonable to assume that the diamide molecules aggregated in solution are associated through hydrogen bonding in a manner similar to their association in the crystalline form. Based on this assumption the diamides fulfill the requirements of structural models for β polypeptides.

The optical properties of the diamides above 210 nm are surprisingly similar to those of β polypeptides. Although the molar rotation and dichroism of the diamide solutions are smaller in magnitude than in the comparable polypeptide solutions, the sign and position of the cotton effects are similar. Therefore, on the surface, the diamides appear to be excellent models for polypeptide optical properties. One question arises; the ORD seems to depend only on the dielectric constant of solvent and not on the state of aggregation of the diamides. From the concentration dependent ORD experiments, it appears that the monomer and trimer diamides have nearly identical ORD's. There are two possible explanations for the optical activity of monomer. One is that a small fraction (less than 10%) of the monomer is intramolecularly hydrogen bound. Acetyl-L-proline amide which has this configuration has a large rotational trough at 240 nm in dioxane. If the intramolecularly hydro-

gen bound monomer has similar rotational properties to the acetyl-L-proline amide, this might explain the optical activity of the monomer. A more likely explanation is that nonhydrogen bound monomer is optically active with a cotton effect near 220 nm, a result of conformational restrictions discussed by Leach et al. (1966) and Ramachandran et al. (1965). If this latter explanation is correct, the optical activity of the peptide group in diamides does not significantly depend on interactions across hydrogen bonds. If these results can be extrapolated to polypeptides or to the peptide group buried in a hydrophobic interior of a protein molecule, it would seem that ORD or CD above 210 or 220 nm would have little value in structural evaluation. It would appear that the magnitude of this dichroic band is more sensitive to local dielectric constant than to structure.

SUMMARY

The purpose of this study was to determine the structure of fibril-
lar proteins which originate from two distinctly different types of
protein, soluble feather keratin and native insulin. It was thought
that if these proteins could generate similar fibrillar structures, this
process might be generalized to many other dissimilar proteins. In this
study it was shown that the physical properties of the fibrillar systems
were nearly identical.

When solutions of oxidized or reduced and S-carboxy-methylated
feather keratin are maintained under unfavorable conditions of pH and
ionic strength, or when insulin in acidic solution is heat denatured,
fibril formation occurs which does not involve the formation or disrup-
tion of covalent bonds. Electron microscopy and low angle x-ray diffrac-
tion indicate that the feather keratin fibrils have cross sectional di-
mensions of 60 and 90 $\overset{o}{A}$ and the insulin fibrils have them between 30 and
40 $\overset{o}{A}$. Wide angle x-ray diffraction and infrared dichroism studies of
the fibrils show that they have cross-β structures in which individual
molecules are probably confined to single 4.7 $\overset{o}{A}$ thick layers (one mole-
cule per layer in insulin fibrils and two molecules per layer in feath-
er keratin fibrils). These data also suggest that the interlayer inter-
actions are most likely to be of the parallel rather than the antiparal-
lel type. Steric considerations with respect to the internally disulfide
bonded, and therefore conformationally restricted, insulin molecules also
support the parallel structure. Ultraviolet absorption and rotatory
characteristics of the fibrils are consistent with a cross-β structure,

but are similar to those of synthetic polypeptides reported to have the antiparallel structure. Extensive studies using diamides as model compounds for the cross-β interaction suggest, in fact, that these optical properties are more characteristic of the dielectric constant of the amide environment than on the nature of the hydrogen bond interactions. For this reason, and since it is difficult to demonstrate that the synthetic polypeptide systems are indeed purely antiparallel in nature, the apparent conflict in results may not be real.

The conclusions derived from these studies concerning the structure of insulin fibrils have clearly resolved the conflicting reports of Ambrose and Elliott (1951) and of Koltun et al. (1954) in favor of the former.

Since the conclusion of this work, two more fibrillar systems having the cross-β structure have been uncovered in this laboratory. These systems originate from the protein glucagon (Rougvie[1]) and the β chain of insulin (Rougvie and Shriver[2]).

---

[1]Rougvie, M. A., Department of Biochemistry and Biophysics, Iowa State University, Ames, Iowa. An investigation of the cross-β structure of glucagon. Private communication. 1969.

[2]Rougvie, M. A. and C. N. Shriver, Department of Biochemistry and Biophysics, Iowa State University, Ames, Iowa. An investigation of the cross-β structure of the β chain of insulin. Private communication. 1969.

ACKNOWLEDGMENTS

LITERATURE CITED

Ambrose, E. J. and A. Elliott. 1951. Infra-red spectroscopic studies of globular protein structure. Roy. Soc. London Proc., Series A, 208: 75.

Arnott, S., S. D. Dover and A. Elliott. 1967. Structure of β-poly-L-alanine: refined atomic coordinates for an antiparallel beta-pleated sheet. J. Mol. Biol. 30: 201.

Astbury, W. T. 1945. Artificial protein fibres: their conception and preparation. Nature 155: 501.

Astbury, W. T., E. Beighton and C. Weibull. 1955. The structure of bacterial flagella. Symp. Soc. Exp. Biol. 9: 282.

Astbury, W. T. and S. Dickinson. 1935. α-β intramolecular transformation of myosin. Nature 135: 95.

Astbury, W. T., S. Dickinson and K. Bailey. 1935. The x-ray interpretation of denaturation and the structure of the seed globulins. Biochem. J. 29: 2351.

Bamford, C. H., A. Elliott and W. E. Hanby. 1956. Synthetic polypeptides. New York, New York, Academic Press, Inc.

Blout, E. R., I. Schimer and N. S. Simmons. 1962. New cotton effects in polypeptides and proteins. J. Amer. Chem. Soc. 84: 3193.

Bovey, F. A. and F. P. Hood. 1967. Circular dichroism spectrum of poly-L-proline. Biopolymers 67: 325.

Bradbury, E. M., L. Brown, A. R. Downie, A. Elliott, R. Fraser, W. E. Hanby and T. R. R. McDonald. 1960. The cross-β structure in polypeptides of low molecular weight. J. Mol. Biol. 2: 276.

Bradbury, E. M. and A. Elliott. 1963. Infrared spectra and chain arrangement in some polyamides, polypeptides and fibrous proteins. Polymer 4: 47.

Brant, D. A., W. G. Miller and P. J. Flory. 1967. Conformational energy estimates for statistically coiling polypeptide chains. J. Mol. Biol. 23: 47.

Condon, E. U., W. Altar and H. Eyring. 1937. One-electron rotatory power. J. Chem. Phys. 5: 753.

Davidson, B., N. Tooney and J. D. Fasman. 1966. The optical rotatory dispersion of the β structure of poly-L-lysine and poly-L-serine. Biochem. Biophys. Res. Comm. 23: 156.

Davydav, A. S. 1962. The theory ot molecular excitations. New York, New York, McGraw-Hill Co., Inc.

Elliott, A., R. Fraser, T. MacRae, I. Stapleton and E. Suzuki. 1964. An investigation of the structure of poly-S-carbobenzoxy-L-cysteine. J. Mol. Biol. 9: 10.

Eyring, H., J. Walter and G. E. Kimball. 1944. Quantum chemistry. New York, New York, John Wiley and Sons, Inc.

Farrant, J. L. and E. H. Mercer. 1952. Electron microscopical observations of fibrous insulin. Biochim. Biophys. Acta 8: 355.

Filshie, B. K., R. Fraser, T. P. MacRae and G. E. Rogers. 1964. X-ray diffraction and electron microscope observations on soluble derivatives of feather keratin. Biochem. J. 92: 19.

Flory, P. J. and T. G. Fox. 1951. Treatment of intrinsic viscosities. J. Amer. Chem. Soc. 73: 1904.

Foss, J. G. and M. E. McCarville. 1965. Magnetic circular dichroism and magnetic optical rotatory dispersion. J. Amer. Chem. Soc. 87: 228.

Fraser, R., T. P. MacRae, F. H. C. Stewart and E. Suzuki. 1965. Poly-L-alanylglycine. J. Mol. Biol. 11: 706.

Geddes, A. J., K. D. Parker, E. D. Atkins and E. Beighton. 1968. "Cross-β" conformation in proteins. J. Mol. Biol. 32: 343.

Gratzer, W. B. 1967. Ultraviolet absorption spectra of polypeptides. In Fasman, G. D., ed. Poly-α-amino acids. Pp. 177-238. New York, New York, Marcel Dekker, Inc.

Greenspan, F. P. 1947. Oxidation reactions with aliphatic peracids. Indust. Eng. Chem. 39: 847.

Hail, J. D. 1964. Fractionation and characterization of a polymer of soluble feather keratin. Unpublished M. S. thesis. Ames, Iowa, Library, Iowa State University of Science and Technology.

Harrap, B. S. and E. F. Woods. 1964a. Soluble derivatives of feather keratin: isolation, fractionation and amino acid composition. Biochem. J. 92: 8.

Harrap, B. S. and E. F. Woods. 1964b. Soluble derivatives of feather keratin. II. Molecular weight and conformation. Biochem. J. 92: 19.

Holzwarth, G. and P. Doty. 1965. The ultraviolet circular dichroism of polypeptides. J. Amer. Chem. Soc. 87: 221.

Iizuka, E. and J. T. Yang. 1966. Optical rotatory dispersion and circular dichroism of the β form of silk fibroin in solution. Natl. Acad. Sci. Proc. 55: 1175.

Ikeda, S. 1967. Molecular conformation of poly-S-carboxymethyl-L-cysteine in aqueous solutions. Biopolymers 5: 359.

Kirkwood, J. G. 1937. On the theory of optical rotatory power. J. Chem. Phys. 5: 479.

Koltun, W. L., D. F. Waugh and R. S. Bear. 1954. X-ray diffraction investigation of selected types of insulin fibrils. J. Amer. Chem. Soc. 76: 413.

Kung, T. and T. Tsao. 1964. The ultrastructure of insulin fibrils. Biochim. Biophys. Acta Sinica 3: 395.

Leach, S. J., G. Nemethy and H. A. Scheraga. 1966. Computation of the sterically allowed conformations of peptides. Biopolymers 4: 369.

Litman, B. J. and J. A. Schellman. 1964. The $n \rightarrow \pi^*$ cotton effect of the peptide linkage. J. Phys. Chem. 69: 978.

Mandelkern, D. and P. J. Flory. 1952. The frictional coefficient for flexible chain molecules in dilute solution. J. Chem. Phys. 20: 212.

Marsh, R. E., R. B. Corey and L. Pauling. 1955. An investigation of the structure of silk fibroin. Biochim. Biophys. Acta 16: 1.

Miyazawa, T. 1960. Perturbation treatment of the characteristic vibrations of polypeptide chains in various configurations. J. Chem. Phys. 32: 1647.

Miyazawa, T. and E. Blout. 1961. The infrared spectra of polypeptides in various conformations: amide I and II bands. J. Amer. Chem. Soc. 83: 712.

Mizushima, S., T. Masamichi, T. Shimanouchi, T. Sugita and T. Yoshimoto. 1954. Near infrared spectra of compounds with two peptide bands and the configuration of a polypeptide chain. IV. J. Amer. Chem. Soc. 76: 2479.

Moriwaki, T., T. Masamichi, T. Shimanouchi and S. Mizashima. 1959. Infrared spectra of acetylglycine-N-methyl amide and the assignment. J. Amer. Chem. Soc. 81: 5914.

Palmer, K. J. and J. A. Galvin. 1943. The molecular structure of fibers made from native egg albumin. J. Amer. Chem. Soc. 65: 2187.

Parker, K. D. and K. M. Rudall. 1957. The silk of the eggstalk of the green lace-wing fly. Nature 179: 905.

Pauling, L. and R. B. Corey. 1951. Configurations of polypeptide chains with favored orientations around single bonds: two new pleated sheets. Natl. Acad. Sci. Proc. 37: 729.

Pysh, E. S. 1966. The calculated ultraviolet optical properties of polypeptide β-configurations. Natl. Acad. Sci. Proc. 56: 825.

Pysh, E. S. 1967. The calculated ultraviolet optical properties of poly-L-proline I and II. J. Mol. Biol. 23: 587.

Ramachandran, G. N., C. Ramakrishnan and C. M. Venkatachalam. 1965. Determination of the possible conformations of the residues linked in a polypeptide chain. Biopolymers 3: 591.

Ramachandran, G. N., C. Ramakrishnan and V. Sasisekharan. 1963. Stereochemistry of polypeptide chain configurations. J. Mol. Biol. 7: 95.

Rosenheck, K. and B. Sommer. 1967. Theory of the far-ultraviolet spectra of polypeptides in the β configuration. J. Chem. Phys. 46: 532.

Rougvie, M. A. 1954. Studies on a monomer of feather keratin. Unpublished Ph. D. thesis. Boston, Mass., Library, Massachussets Institute of Technology.

Rudall, K. M. 1950. Fundamental structures in biological systems. Progress in Biophys. and Mol. Biol. 1: 39.

Ryle, A. P., F. Sanger, L. F. Smith and R. Kitai. 1955. The disulphide bonds of insulin. Biochem. J. 60: 541.

Sanger, F. and E. O Thompson. 1953. The amino-acid sequence in the chain of insulin. Biochem. J. 53: 366.

Sanger, F. and H. Tuppy. 1951. The amino-acid sequence in the phenylalanyl chain of insulin. Biochem. J. 49: 463.

Sarkar, P. K. and P. Doty. 1966. The optical rotatory properties of the β-configuration in polypeptides and proteins. Natl. Acad. Sci. Proc. 55: 982.

Schellman, J. A. 1966. Symmetry rules for optical rotation. J. Chem. Phys. 44: 55.

Schellman, J. A. 1968. Symmetry rules for optical rotation. Accounts of Chemical Research 1: 144.

Schellman, J. A. and E. B. Nielsen. 1967. Optical rotation and conformation studies on diamide models. In Ramachandran, G. N., ed. Conformation of biopolymers. Pp. 109-122. New York, New York, Academic Press, Inc.

Schellman, J. A. and P. Oriel. 1962. Origin of the cotton effect of helical polypeptides. J. Chem. Phys. 37: 2114.

Scheraga, H. A. 1961. Protein structure. New York, New York, Academic Press, Inc.

Schor, R. and S. Krimm. 1961. Studies on the structure of feather keratin. Biophys. J. 1: 467.

Senti, F. R., C. R. Eddy and G. C. Nutting. 1943. Conversion of globular to oriented fibrous proteins. I. By heat and mechanical working. J. Amer. Chem. Soc. 65: 2472.

Tanford, C., K. Kawahara and S. Lapanje. 1967. Proteins as random coils. I. Intrinsic viscosities and sedimentation coefficients in concentrated guanidine hydrochloride. J. Amer. Chem. Soc. 89: 729.

Timasheff, S. N., H. Susi, R. Townend, L. Stevens, M. J. Gorbunoff and T. F. Kumosinski. 1967. Application of circular dichroism and infrared spectroscopy to the conformation of proteins in solution. In Ramachandran, G. N., ed. Conformation of Biopolymers. Pp. 173-196. New York, New York, Academic Press, Inc.

Tinoco, I. 1962. Optical activity in polymers. Advances Chem. Phys. 4: 113.

Tinoco, I., R. W. Woody and D. F. Bradley. 1963. Absorption and rotation of light by helical polymers: the effect of chain length. J. Chem. Phys. 38: 1317.

Townend, R., T. F. Kumosinski, S. N. Timasheff, G. D. Fasman and B. Davidson. 1966. The circular dichroism of the β structure of poly-L-lysine. Biochem. Biophys. Res. Comm. 23: 163.

Tsuboi, M., T. Shimanouchi and S. Mizushima. 1959. Near infrared spectra of compounds with two peptide bonds and the configuration of a polypeptide chain. VII. On the extended forms of polypeptide chains. J. Amer. Chem. Soc. 81: 1406.

Vaurnakis, J. N., J. K. Yan and H. A. Scheraga. 1968. Effect of side chains on the conformational energy and rotational strength of the $n \to \pi^*$ transition for some helical poly-α-amino acids. Biopolymers 6: 1531.

Waugh, D. F. 1944. The linkage of corpuscular protein molecules. I. A fibrous modification of insulin. J. Amer. Chem. Soc. 66: 663.

Waugh, D. F. 1957. A mechanism for the formation of fibrils from protein molecules. J. Cell. Comp. Physiology 49: 145.

Woodin, A. M. 1954. Molecular size, shape and aggregation of soluble feather keratin. Biochem. J. 57: 99.

Woody, R. W. and I. Tinoco. 1967. The optical rotation of oriented helices III. J. Chem. Phys. 46: 4927.

Yang, J. T. 1967. Optical activity of the α, β and coiled conformations in polypeptides and proteins. In Ramachandran, G. N., ed. Conformation of biopolymers. Pp. 157-172. New York, New York, Academic Press, Inc.